Materials Today • Volume xxx, Number xx • xxxx 2023



ELSEVIER



# Recent approaches for enhancing the performance of dissolving microneedles in drug delivery applications

**Tomás Bauleth-Ramos [1,2,3,#], Nesma El-Sayed [1,4,#], Flavia Fontana [3], Maria Lobita [1,2], Mohammad-Ali Shahbazi [1,2], Hélder A. Santos [1,2,3,*]**

[1] Department of Biomedical Engineering, University Medical Center Groningen / University of Groningen, 9713 AV Groningen, The Netherlands
[2] W.J. Kolff Institute for Biomedical Engineering and Materials Science, University Medical Center Groningen / University of Groningen, 9713 AV Groningen, The Netherlands
[3] Drug Research Program, Division of Pharmaceutical Chemistry and Technology, Faculty of Pharmacy, P.O. Box 56 (Viikinkaari 5 E), University of Helsinki, FI-00014 Helsinki, Finland
[4] Department of Pharmaceutics, Faculty of Pharmacy, Alexandria University, 21521 Alexandria, Egypt

**Dissolving microneedles (dMNs) are promising versatile drug delivery systems for the transdermal delivery of numerous drugs, enabling their use in a wide range of biomedical and pharmaceutical applications. Being made of water-soluble polymers, dMNs own several advantages, including fast dissolution and short application time which enhance patients' compliance and minimize the damage to skin tissue. Moreover, they possess no biohazard risk as they leave no sharp waste behind. For these reasons, the research on dMNs has increased dramatically in recent years. The formulation of successful dMNs requires a well-defined pre-set design, considering the goal and the payloads that will be used. Every aspect of formulation as patch design, needles geometry, polymer composition, method of formation and payloads, has a direct effect on the mechanical properties of the MNs, affecting their administration and efficacy. Thus, there is the need to understand how each factor affects the final formulation and how to optimize each MN. Taking this into consideration, this review serves as a guide for dMN formulation, discussing the different setbacks of each step and possible strategies to overcome them, improving their administration, and enhancing the loading of various molecules and their controlled release.**

**Keywords: Dissolving Microneedles; Drug delivery; Controlled release; Transdermal delivery; Patch**

## Introduction

Transdermal administration of various drugs and biomacromolecules is a promising pathway for efficient therapy, which avoids several hurdles, such as the first pass metabolism effect observed in the case of oral delivery [1]. However, transdermal administration is not easily achievable due to the presence of the stratum corneum (SC), the skin's main barrier, which regulates the diffusion of molecules from and into the skin [2]. The SC forms out of corneocytes with an intercellular lipid matrix arranged in a brick–mortar structure. Overcoming the SC and reaching the viable epidermis or dermis is then a prerequisite for efficient drug delivery [3]. Microneedles (MNs) technology has been developed to provide patches with micron-sized projections (up to 1000 μm long) able to pierce the skin and overcome the SC barrier [4]. MNs can be engineered as solid MNs in dermarollers [5,6] or patches for cosmetics [6]. Solid MNs are commonly fabricated by laser cutting or micromachining [7]. They can be prepared using different materials, including stainless steel [8], silicon [9], and titanium [10]. Solid MNs rely on a 'poke and patch' approach, where the MNs poke the skin to create

* Corresponding author.
*E-mail address:* Santos, H.A. (h.a.santos@umcg.nl)
# Both authors contributed equally.





Please cite this article in press as: T. Bauleth-Ramos et al., Materials Today, (2023), https://doi.org/10.1016/j.mattod.2022.12.007

micro-channels followed by the application of drug loaded formulations such as patches, solutions, creams or gels, to allow the drug diffusion into the skin [11]. As a further development, coating of MNs with antigens and even viruses was introduced arising wide interest in vaccination development [11,12]. However, there are limitations to using solid MNs, including the safety concerns about the biohazardous sharp waste left after use [12]. In addition, the biocompatibility of silicon MNs is questionable, especially if they break and accumulate inside the skin tissue [13]. Furthermore, fast healing of the microchannels formed with the application is essential to avoid the permeation of pathogens [14]. Dissolving microneedles (dMNs) were further developed to avoid leaving any waste behind as they are made of water-soluble polymers that dissolve in the interstitial fluid of the skin to deliver drug molecules. This type of MN-patch follows the strategy of 'poke and patch' a one-step application, which increases patient compliance [15]. For these reasons, dMNs are replacing solid MNs in most of the current research for drug delivery applications. As a new generation of MNs, certain desired characteristics, such as easy and rapid administration and detachment, retention, enhanced stability of the payload its controlled release, should be fulfilled during the development of dMNs for a successful application and drug delivery.

In this review, we provide an expert guide for researchers with checkpoints and the current techniques for the successful development of MNs as transcutaneous devices for drug delivery.

## Physicochemical/mechanical characteristics of MNs

Typically, and on one hand, dMNs have low mechanical properties due to the nature of the water-soluble polymers used, which may hinder the consistent and reliable penetration into the skin. On the other hand, the softening and dissolution of MNs in tissue can prevent tissue damage caused by the mechanical force applied during application [16]. Furthermore, skin inherent elasticity is an opposing factor to the complete insertion of the MNs, presenting a challenge that may require specific MN-designs to overcome. So, different aspects should be considered to develop dMNs with optimized and sufficient mechanical strength for penetration of the SC without mechanical failure. For example, MNs shape, height, diameter and aspect ratio, and tip diameter and angle, together with the materials used for fabrication, affect the penetration efficiency of the MNs patch. Moreover, the MNs' array density and the applied force can also influence the MNs' insertion and fracture properties. Therefore, a balance between the fast disintegration and robust mechanical strength of the needles is important for the successful penetration of the MNs in the skin and their detachment from the base.

### *Geometry*

Various typical designs of dMNs, such as pyramidal and conical shape, have been used in different studies. In fact, the needle geometry is a determinant factor in drug loading, stress distribution, and mechanical properties, influencing the penetration and dissolution of the MNs in the skin. Li *et al.* [17] developed ovalbumin-loaded dextran-based MNs of different geometries (cone, cone-cylinder, rectangular pyramid, and hexagonal pyramid), to study the effect of needle-geometry on the abovementioned properties (Fig. 1**A**). In this study, all designs had the same apex angle of 21°, except for the cone-cylinder with an angle of 37°. This apex angle was designed to be higher than other designs to increase the volume of the MNs without increasing the height, while maintaining the drug loading capacity. The volume ratio of the cone, hexagonal pyramid, and rectangular pyramid was 100: 83: 64, respectively. This meant the cone was more advantageous in drug loading capacity than the other designs. The cone-cylinder with a smaller diameter was designed to reduce the resistance of skin during MNs insertion. However, it showed poor mechanical properties compared to other designs, after the application of 100 N pressure for 5 s. While cone, rectangular pyramid, and hexagonal pyramid maintained $\geq$ 75% of the original height, the cone-cylinder MNs height decreased to 30% of the height. The mechanical properties were consistent with the penetration efficiency, where the highest penetration was achieved by cone MNs, and the lowest was by cone-cylinder MNs. Skin insertion ratios were 97.8%, 76.2%, 49.6%, 38.8% for cone-cylinder, rectangular pyramid, hexagonal pyramid and cone-cylinder, respectively (Fig. 1**B**). *In vivo* studies showed the influence of geometry on the dissolution of MNs. Cone MNs had the highest dissolution ratio of 80%, while the lowest was 40% for cone-cylindrical MNs (Fig. 1**C**). Altogether, cone-shaped MNs presented the best properties compared to the other geometries.

In another recent study, Sillankorva *et al.* [18] have also studied the influence of the MNs geometry in the administration and distribution of bacteriophages (phages) into biofilms for the treatment of topical biofilm-related skin infections. In this study, to form the MNs, a phage loaded PVA solution was casted in PDMS molds with different geometries followed by vacuum and centrifugation. The formed MNs had a cylinder shape with conical tip, with height *ca.* 518 nm and base diameter *ca.* 205 nm or a conical shape with height of *ca.* 515 nm and base diameter of *ca.* 295 nm. The different geometry played a crucial role in the mechanical properties as the force for needle failure of the conical MNs (0.3 N) was 3x higher than for the cylinder shape with conical tip MNs (0.1 N). Moreover, this translated into a higher insertion efficiency in Parafilm® M of the conical MNs comparably to the cylinder MNs. However, the authors did not find a significant influence of the geometry on both the release profiles or on the antimicrobial efficacy *in vitro*.

Micromolding is the most common fabrication technique for dMNs. In this technique, negative elastomeric polydimethylsiloxane (PDMS) molds are used for polymer casting to prepare MNs. So, by producing positive master molds of different designs, it is possible to produce different PDMS molds and consequently dMNs with different geometries. For example, computer-aided additive manufacturing (3D printing), specifically digital light processing (DLP) was used to design master molds of sharper geometries for effective skin insertion. El-Sayed *et al.* [19] introduced new designs of MNs inspired by the 'tanto blade', which is a Japanese Samurai sword with two bevels for enhanced stab or penetration. In this study, two MNs master molds of different tip diameters and angles were designed using OpenSCAD open-source computer-aided design software (Fig. 2-**A**-**B**). The two designs had a height (Z) of 800 μm and a triangle base of X = 300 μm and Y = 200 μm. Furthermore, they had a dif-



Please cite this article in press as: T. Bauleth-Ramos et al., Materials Today, (2023), https://doi.org/10.1016/j.mattod.2022.12.007

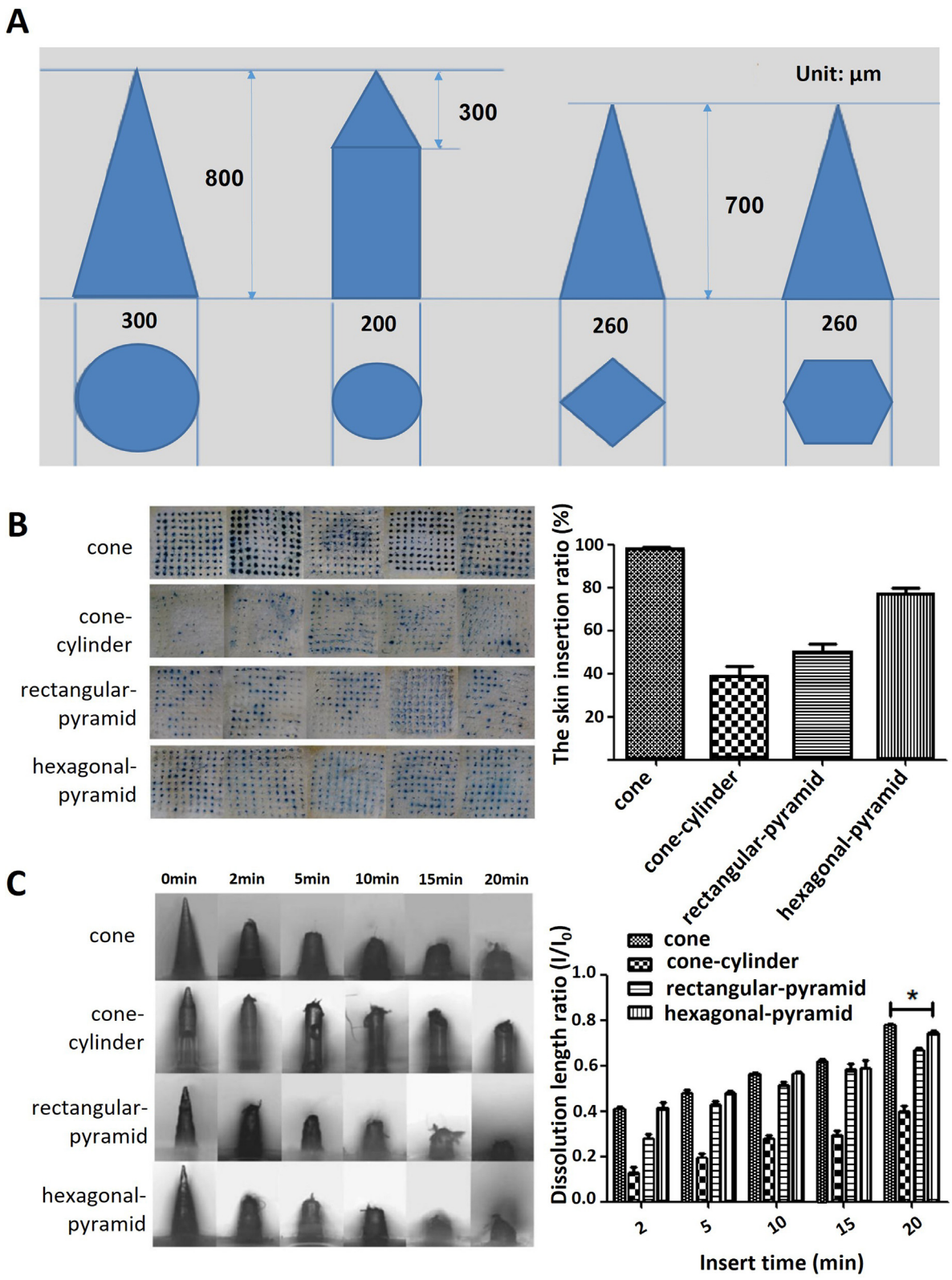


**FIGURE 1**

**(**A) Design of the master molds for the dMNs array: from left to right (cone, cone-cylinder, rectangular pyramid, hexagonal pyramid). (B) *In vitro* skin insertion tests; optical microscopy images of the skin after MNs insertion (upper panel) and the skin insertion ratio (lower panel). (C) Dissolution of the MNs *in vivo*; optical microscopy images of the MNs after insertion in the skin (upper panel) and dissolution length ratio (lower panel) ($I_0$ represent the initial length of the MNs; I represents the dissolution length of the MNs). All data shown are mean ± standard error of the mean (SEM). (n = 5, *p < 0.05). Adapted and reprinted with permission from ref. [17]; Copyright 2020, Elsevier B.V.



Please cite this article in press as: T. Bauleth-Ramos et al., Materials Today, (2023), https://doi.org/10.1016/j.mattod.2022.12.007

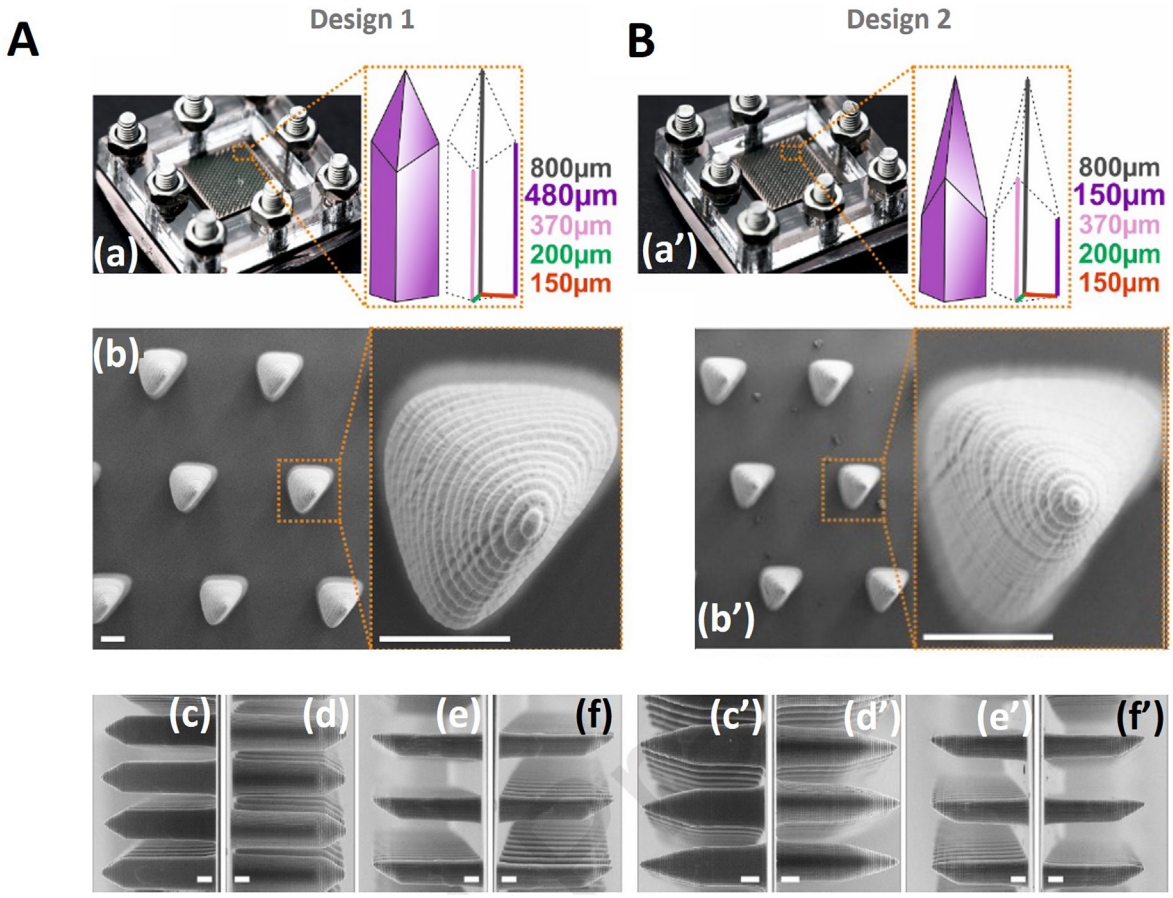


**FIGURE 2**

Positive master molds of 2 potential tanto blade-inspired MNs designs: design 1 (A) and design 2 (B): (Aa, Ba') Photograph of the 3D-printed MNs positive master mold in the final housing to be further used for PDMS casting of the negative mold and illustration of the 3D design of the MNs; (Ab-Af, Bb'-Bf') SEM micrographs of the 3D-printed MNs showing top (Ab, Bb'), back (Ac, Bc'), front (Ad, Bd'), and sides (Ae, Af, Be', Bf'). All scale bars correspond to 100 μm. Adapted and reprinted with permission from ref. [19]; Copyright 2020, Elsevier B.V.

ferent height ratio of the two bevels that varies the tip angles. However, the 3D printing method presented resolution limits, with a horizontal resolution of 30 μm (pixel size), and a layer height of 15 μm, which impacted the final mold. Thus, the final 3D printed masters showed final dimensions that differed according to the design's slimness. The molds had height of 759 μm and 660 μm, tip diameter of 23 μm and 9 μm and the tip angle of 66° and 39° for design 1 (M1, the less slim) and design 2 (M2, the slimmer), respectively. Despite this drawback, this process had the advantage to be cost-effective, as it was possible to fabricate master molds in the lab using a bench-top 3D printer. Furthermore, dMNs were prepared using polyvinyl alcohol (PVA)/sucrose (1:1) via PDMS negative molds. Both MNs showed insertion forces lower than 20 N (the average pressing force by thumb) and lower than their respective fracture forces, which is crucial to avoid premature failure of the MNs during insertion into the skin. Scanning electron microscope (SEM) images of MNs retrieved after insertion in skin substitute (agarose gel-covered by Parafilm®) to mimic skin elasticity showed robust MNs in the case of MN2, while MN1 showed some broken MNs at the base. In general, the sharper design of MN2 revealed better mechanical properties (insertion and fracture) compared to MN1. Additionally, MN2 resulted in deeper penetration in human skin *in vitro* (550 μm) compared to MN1 (300 μm).

Bediz *et al.* [20] used mechanical micromilling for the fabrication of master molds of different designs as a pyramid, straight obelisk, and negative-beveled obelisk with different geometric parameters (width, height, and apex angle). dMNs were then prepared using carboxymethyl cellulose (CMC)) and combinations with polyvinylpyrrolidone (PVP) or maltodextrin. After insertion into the skin, a larger portion of the obelisk MNs dissolved, and so allowed four times higher skin deposition of the cargo as detected by fluorescent image analysis compared to pyramidal MNs. This was attributed to the obelisk shape, which was designed to allow complete insertion of the needles into the skin by minimizing the insertion force and skin resistance. It is worth noting that the experiment was done by comparing the same array configuration and MN-height for both the obelisk and pyramidal arrays. In addition, for the obelisk MNs geometry, the authors designed a round corner around the base of the MNs to act as a fillet to support the mechanical strength of the MNs during insertion.

To prevent incomplete insertion of dMNs, due to skin deformation and resistance, Hou *et al.* [21] developed elongated



Please cite this article in press as: T. Bauleth-Ramos et al., Materials Today, (2023), https://doi.org/10.1016/j.mattod.2022.12.007

rapidly separating dMNs. The MNs' tips were pyramidal in shape (470 μm in height, made of dextran/ PVA) and were loaded with the drug molecules (Fig. 3**A-D**). The needles were separated from the base (made of PVP k90) with blank pillars (640 μm in height, made of hyaluronic acid (HA)/sucrose complex), which were designed to dissolve faster after insertion into the skin, leaving the MNs tips deposited inside the skin tissue, ensuring their complete insertion and avoiding drug wastage. The developed MNs showed an insertion depth of more than 500 μm in Parafilm® and more than 550 μm in rat dorsal skin (Fig. 3**E-F**). This designed ensured that the drug-loaded MNs tips were fully inserted into the skin tissue, as the separating part of the MNs could overcome the elastic deformation of skin and dissolve fast at the same time.

In a different strategy, Lahiji *et al.* [22] developed MNs of interlocking geometry with a narrow neck and wide-body for complete insertion into the skin and prevention of detachment of MNs after insertion in the skin. The developed MNs, with a height of 600 μm, had a wine glass-shaped layer with a sharp tip. The needles consisted of three main parts: neck, body, and tip with a diameter of 120 μm, 250 μm, and 10 μm, respectively. The wine glass-shaped MNs were compared to conventional MNs of the same height and a tip diameter of 24 μm, concerning the mechanical properties, interlocking efficiency, and efficiency of drug delivery (Fig. 4**A**). The breakage force of both types of MNs was comparable and around 0.38 N/needle. However, the conventional MNs broke in the middle section, while the wine glass-shaped MNs broke in the neck region. The minimum forces required for skin penetration were 0.1 and 0.9 N/needle for wine glass-shaped and conventional MNs, respectively. Therefore, both MNs showed similar mechanical properties and skin penetration capabilities. The wine glass-shaped MNs showed a higher interlocking effect after insertion into the skin compared to the conventional ones (Fig. 4**B**), where the detachment force was 0.2 N and 0.08 N, respectively. Moreover, although both MNs were inserted to the same depth in the skin, the new design enhanced the attachment efficiency as after insertion into the skin and upon 10 cycles of bending motion at 120° angle, the gap between the skin tissue and the wine glass-shaped MNs was 86 μm compared to 237 μm for the conventional MNs. This was attributed to the interlocking properties of the new design. An important factor for efficient delivery of the drug dose is the volume distribution, especially in case of incomplete insertion. It was found that 48% of the drug was encapsulated up to 120 μm from the base for the conventional MNs, compared to 17.3% for the new design (Fig. 4**C**). Thus, in case of incomplete insertion of the MNs, the new design was capable of delivering a higher amount of the drug into the skin as most of the drug was concentrated in the mid part of the MNs. Also, the permeation through the skin was higher for the new design 4.56 ± 0.19 μg/cm$^2$ compared to 2.85 ± 0.29 μg/cm$^2$ for the conventional MNs. The higher permeation efficiency was attributed to the interlocking properties and the volume distribution of the newly designed MNs.

### *Patch design*

Fast dissolution, disintegration, or separation of dMNs in the skin is a crucial prerequisite for efficient delivery of drugs and minimizing the administration time, which is essential for patient compliance, especially in the case of self-administration. The fast administration is also important for efficient clinical practice, especially when targeting large populations as in mass vaccination. For enhanced skin insertion and fast dissolution of MNs, Chu and Prausnitz [23] developed arrowhead MNs, which consist of drug-loaded dMNs arrowheads mounted on mechanically strong metal shafts. The arrowheads were made of PVP/PVA with a height of 600 μm on a metal shaft of 600 μm, with an overlap of 100 μm. In another design, the arrowheads were made out of PVP/sucrose and loaded with inactivated influenza virus, with a height of 600 μm, and mounted on a 700 μm metal shaft with 150 μm overlap. These MNs were designed to allow for complete insertion in the skin, in addition to enhancing the mechanical properties by combining both the dMNs and the solid shaft, compared to conventional dMNs. The authors tested the effect of the shaft height on the penetration depth of the arrowhead. For 300, 600, and 900 μm shafts, when keeping the height of the arrowhead constant at 600 μm, the penetration depth of the arrowhead was 600 μm less than the total height of the MNs, *i.e.*, 300-μm penetration depth in case of 900 μm total height of the MNs (600 μm arrowhead + 300 μm shaft). The shaft height was important to avoid incomplete insertion of a 600 μm arrowhead due to the skin deflection effect. Therefore, using shafts with a height of 600 and 900 μm was enough for the complete insertion of the arrowhead into the skin. Moreover, fast separation of the arrowhead was achieved after seconds from insertion into the skin due to the presence of highly water-soluble excipients such as PVP and sucrose and the mechanical separation of the arrowheads from the shafts. The insertion of the MNs for 5 sec in the skin resulted in the delivery of 70% of the 9 μg sulforhodamine encapsulated in the arrowheads, while 90% was delivered after 60 sec. Moreover, by applying mechanical perturbation after insertion of the MNs in the skin, to facilitate the separation of the arrowhead, there was an increase in the drug delivery to more than 80% and 90% after 1 and 5 sec, respectively.

As seen, the fabrication of MNs over micropillars is a strategy that can be applied to achieve the complete insertion of the MNs in the skin. Taking this into consideration, a combination of 3D printing and micro-molding can be used to develop these MNs. However, if the micropillars have a diameter similar or smaller than the diameter of the MNs themselves, they can accidentally be inserted into the skin, causing possible skin injury or inflammation. In order to avoid this, Jung *et al.* [24] developed dMNs with modified micropillars of 45° curved edge and larger diameter (500 μm) than the MNs (300 μm), creating a safety ring of 200 μm around the MNs. The micropillars were fabricated out of polymethyl methacrylate, which is proved not to cause skin irritation, while the MNs were fabricated from the fast-dissolving HA. While the height of the micropillars was 300 μm, the MNs' height was 500 μm (Fig. 5**A-B**). Upon skin insertion, the safety ring allowed only the penetration of dMNs without the micropillars. Another important aspect to consider in this type of design, is the adhesion force between the MNs and micropillars. In this case, the adhesion force was adjusted to be enough for sufficient mechanical properties and efficient insertion in the skin upon application of vertical force. In addi-



Please cite this article in press as: T. Bauleth-Ramos et al., Materials Today, (2023), https://doi.org/10.1016/j.mattod.2022.12.007

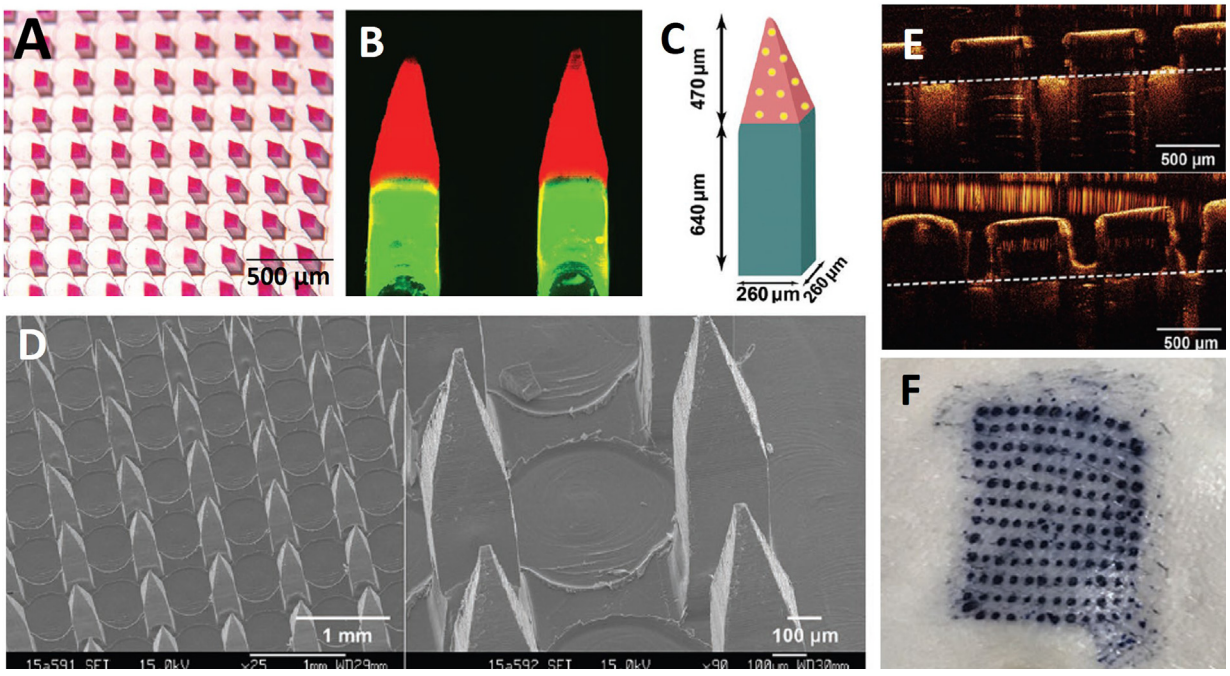


**FIGURE 3**

(A) Micrographs of rhodamine B loaded elongated dMNs. (B) Rhodamine B (red) and FTIC (green) loaded MNs under a fluorescence microscope. (C) Design of MNs structure with dimensions. (D) SEM images of the MNs. (E) Non-invasive optical imaging tomography (OCT) images after insertion of 8 layers of Parafilm M (top row) and full-thickness rat dorsal skin (bottom row), the dashed line represented the surface of the Parafilm M/skin. (F) Photograph of the rat skin after insertion. Adapted and reprinted with permission from ref. [21]; Copyright 2019, John Wiley & Sons, Inc.

tion, the application of lateral force by the finger was enough for fast separation of the MNs after insertion into the skin (Fig. 5**C**). Fig. 5**D** shows the preparation method of the MNs, while the morphology of different MNs is shown in Fig. 5**E** and the fracture and separation analysis is shown in Fig. 5**F**-G.

Another design for dissolving HA MNs on the top of pillar or base arrays was developed by Jun *et al.* [25] The base arrays were truncated square pyramid stands made from polycaprolactone (PCL) with two different designs: one without a wall (no-walled stand, NWS) and another with a wall on one side of the stand (single-walled stand, SWS). The presence of a wall in the base arrays enhanced the mechanical stability of the MNs and increased the adhesion between the tip and the base. This adhesion was necessary to prevent tip breaking upon insertion but to allow the tip separation upon removal. The SWS MNs showed 9.3 times higher mechanical resistance to axial compression compared to NWS. Skin insertion tests in porcine skin were performed and both types of MNs showed successful separation from the base array. While the tips from SWS MNs showed deep insertion in the skin, most of the tips from NWS were not fully inserted in the skin and were lying on the skin surface. The authors also tested double-walled stand (DWS) MNs for insertion into the skin. The results showed that only 42% of the tips were inserted in the skin and the rest were not separated from the base after patch removal. This indicated that the SWS was the optimum design to achieve higher mechanical properties while allowing for fast separation of the MNs' tips and deep insertion into the skin. Another model of fast-separating MNs was developed by El-Sayed *et al.* [19]. They modified the PVA-based MNs patch to accelerate the separation of MNs in the skin. Four channels were carved in the corners of the square patch, where a small volume of buffer solution can be applied after skin insertion (Fig. 6**A**). The liquid diffused due to the capillary force and resulted in the fast separation of MNs after 1 min of skin insertion to deposit the loaded nanoparticles inside the skin (Fig. 6**B**).

### *Needles composition*

Table 1 collects the most common materials used for dMNs preparation. Material selection is crucial to achieve the required properties for functional dMNs. In fact, the material properties play a crucial role to control the mechanical properties, penetration efficiency, and fast dissolution/disintegration. MNs should be robust enough to pierce the skin and then soften when coming in contact with the interstitial fluid to later dissolve and release the loaded drug cargo [13]. Two important parameters that control the ability of the MNs to pierce skin, a sharp tip and the mechanical strength, are controlled by the material properties. Enhancing the mechanical properties of dMNs is then an essential factor to consider, knowing that some polymers used for the fabrication of these MNs do not provide sufficient mechanical properties. For example, MNs formed from unmixed silk fibroin break easily [26]. Bonfante *et al.* [27] compared three different polymers for the preparation of MNs; HA, CMC, and alginate in a low concentration range (1–5% w/v). In this study, the authors compared the effect of the polymer on the shrinkage of the MNs upon drying, which affected the final dimensions of the MNs, the morphology, the piercing capabilities, and the dissolution of the MNs. Well-defined and flexible MNs were produced by using HA or CMC. However, the use of alginate yielded brittle and blunt MNs. Additionally, alginate showed



Please cite this article in press as: T. Bauleth-Ramos et al., Materials Today, (2023), https://doi.org/10.1016/j.mattod.2022.12.007

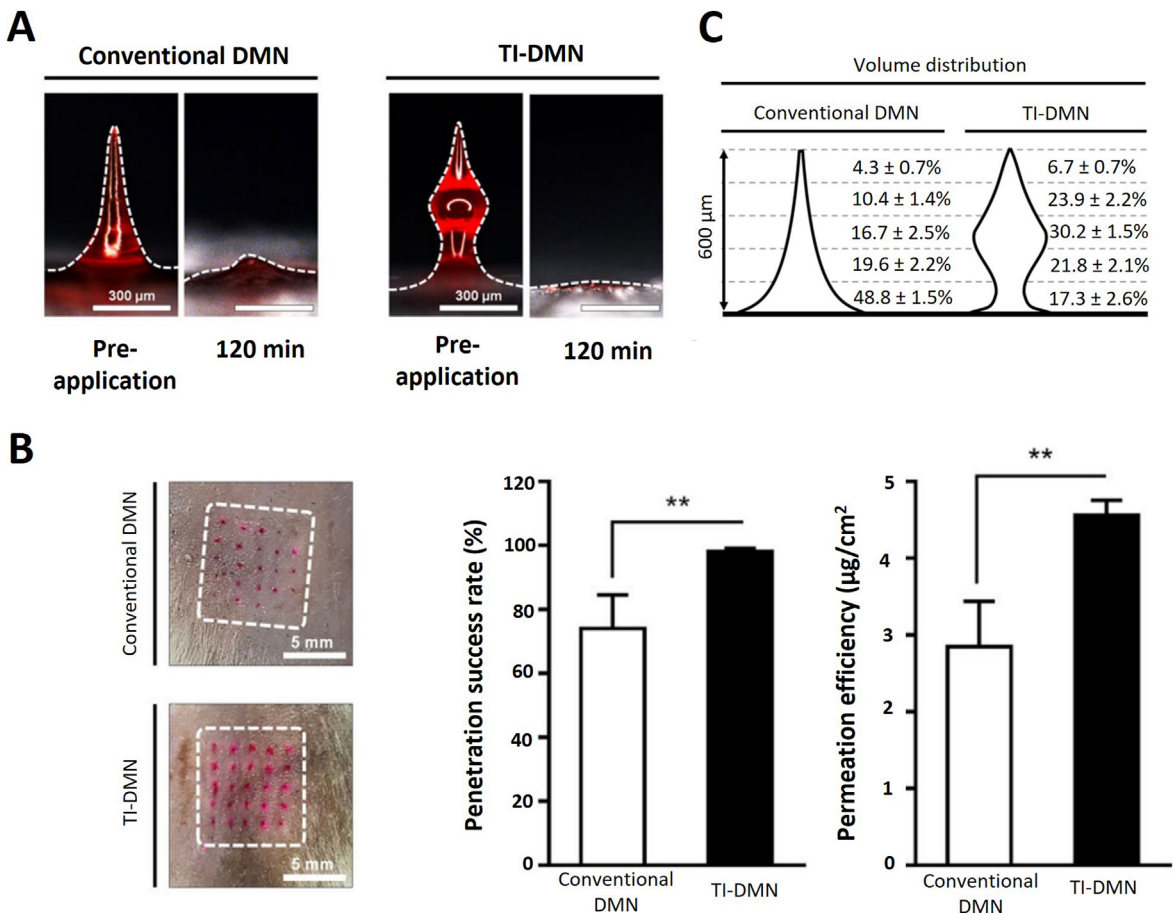


**FIGURE 4**

(A) Shape and dissolution of conventional and interlocking MNs (TI-DMN) (right). (B) Images of skin after MNs insertion; conventional MNs and interlocking MNs and the skin penetration success rate. (C) The volume distribution of both types of MNs. Adapted and reprinted with permission from ref. [22]; Copyright 2019, Nature Portfolio.

the highest shrinkage, 21.8%, compared to 8.9% and 7.2% for HA and CMC, respectively. HA MNs showed the best piercing properties, and the fastest dissolution (1.5 min) compared to CMC and alginate MNs. The chemical structure of the polymer plays the main role in controlling the properties of the MNs. Thus, since the polymer chain of HA has fewer inter-H bonds, it is not sterically hindered allowing the penetration of the water and faster dissolution of the polymer. While CMC has longer branched groups, showing more connection between the chains of the polymer, and alginate has higher stability due to the higher frequency of H bonds. Additionally, the shrinkage of the polymer can hinder the penetration of water.

In another recent study, Shah *et al.* [28] compared the mechanical properties of MNs made from polymers of different origins and with low or high molecular weights: extracellular matrix polymers (gelatin and HA), naturally-derived polymers (CMC and dextran) and synthetic polymers (PVA and PVP). The produced MNs were formed by casting a solution of 5% (w/w) of each polymer into PDMS molds, followed by centrifugation and drying. All prepared MNs were conically shaped and had a height of 500 to 520 µm and base diameter of 200 to 220 µm. From the prepared MNs, only gelatin (low MW) and PVP MNs had fracture forces lower than 4 N, which is considered the minimum force required to penetrate skin in conical MNs [29]. However, despite some polymers (e.g. CMC) having high fracture forces at both MWs, the MW highly impacted their stiffness and flexibility, which might facilitate their insertion in non-flat skin.

One strategy to enhance and accelerate the dissolution of MNs is mixing the polymer with fast-dissolving additives such as sugars and polymers as PVP. While sugars are biocompatible and dissolve fast, most small molecular sugars are hard and brittle with a high modulus. An appropriate complexation of sugar with polymer, and a ratio and concentration adjustment are necessary to get intact robust MNs while preserving the fast dissolution properties. It was noticed that the fracture force of polymer-sugar complex systems was higher than pure HA [21]. This was attributed to the hydrogen bonds formed between the polymer and sucrose molecules, as confirmed by Fourier transform infrared (FTIR). Adding a small amount of sucrose can improve the elastic modulus. Furthermore, sucrose facilitates water uptake into the matrix which results in acceleration of disintegration. A HA/sucrose ratio of 4:1 was selected as the optimum ratio for robust and fast dissolving separating parts of the MNs. A higher sucrose ratio would sacrifice the mechanical strength and result in brittle MNs and failure of demolding [21].



Please cite this article in press as: T. Bauleth-Ramos et al., Materials Today, (2023), https://doi.org/10.1016/j.mattod.2022.12.007

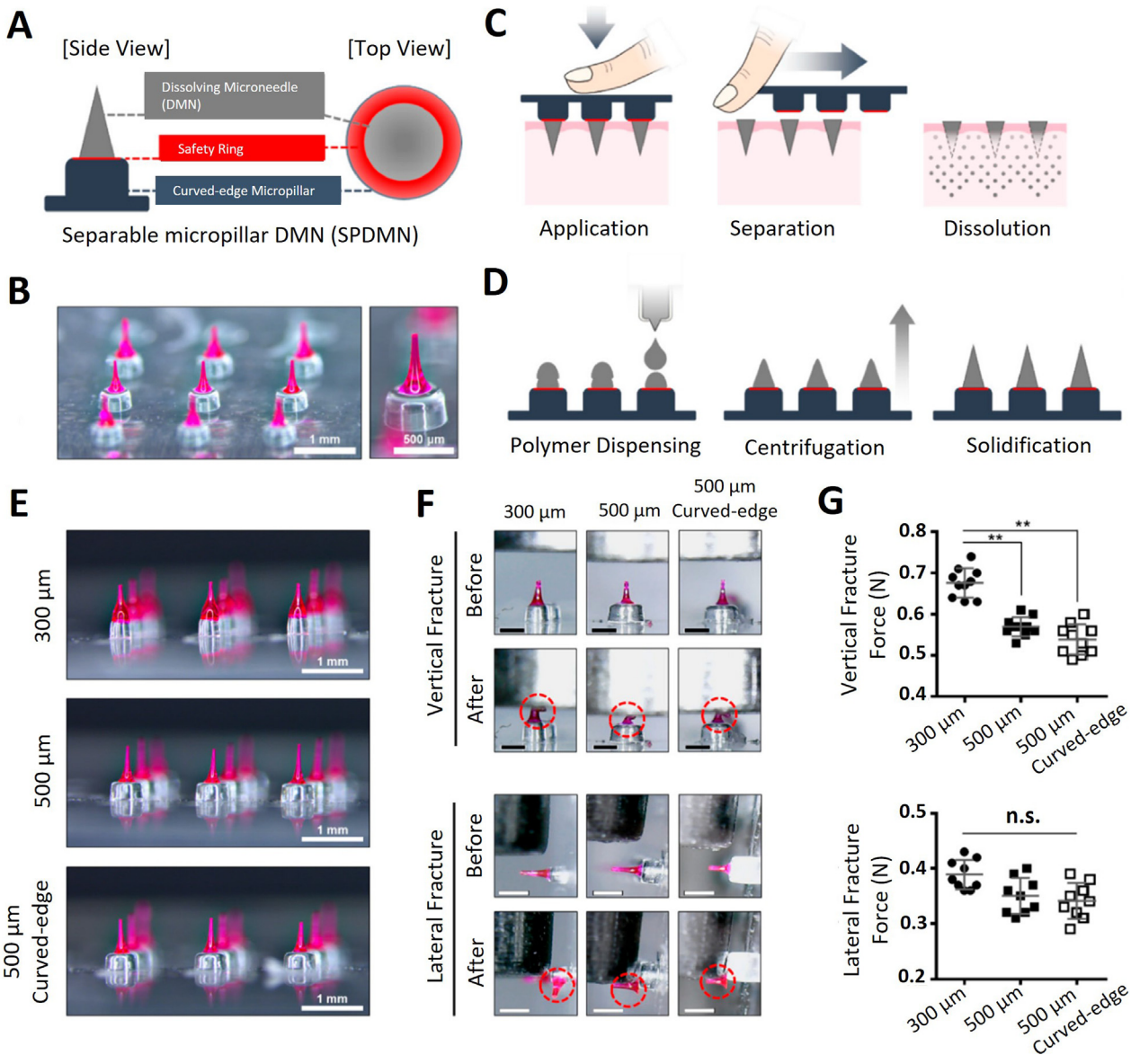


**FIGURE 5**

(A) Design of the MNs over micropillars (side and top view). (B) Morphology of MNs over micropillars. (C) Mechanism of MNs separation from the micropillars after lateral force application. (D) preparation of method of MNs. (E) Morphology of MNs fabricated over 300 µm, 500 µm, and curved-edge 500 µm micropillars. (F-G) Fracture and separation force analysis. Adapted and reprinted with permission from ref. [24]; Copyright 2020, MDPI.

## Drug loading

Drug loading represents one of the main challenges in the fabrication of MNs for drug delivery applications as it is affected by multiple variants. Owing to the small size and volume of the MNs tips, the loading capacity of the MNs is very limited, with loadings that can go up to 10 mg per patch, but are usually lower than 1 mg [72–74]. This can become problematic for drugs with higher dosing range [75]. Also, since numerous drugs can diffuse through the water-soluble MN matrix, it is difficult to control their encapsulation and localization within the MNs [12,76]. Furthermore, as MNs are mainly produced from one single material, the co-encapsulation of different drugs based on drug-matrix interactions is also restricted [73,77]. Another major limitation in the drug loading process stems from the conditions to which the MNs are subjected during their preparation and manipulation. Mainly, the use of different solvents, temperature, and pressure during the fabrication process, can lead to the degradation of the payload [78–81]. Hence, during the development process, it is crucial to consider the physicochemical characteristics of the payload and the materials used to produce the MNs, the method of production, and the potency and stability of the molecules, as they all affect and might limit the loading. Herein, we will discuss the limitations inherent to different types of payloads and give an overview of the main strategies to overcome these hurdles. A summary of the different payloads and strategies applied to enhance their loading in dMNs can be found in Table 2.

### *Hydrophobic drugs*

Hydrophobic drugs represent a considerable share of the currently marketed drugs and of the new chemical entities under



Please cite this article in press as: T. Bauleth-Ramos et al., Materials Today, (2023), https://doi.org/10.1016/j.mattod.2022.12.007

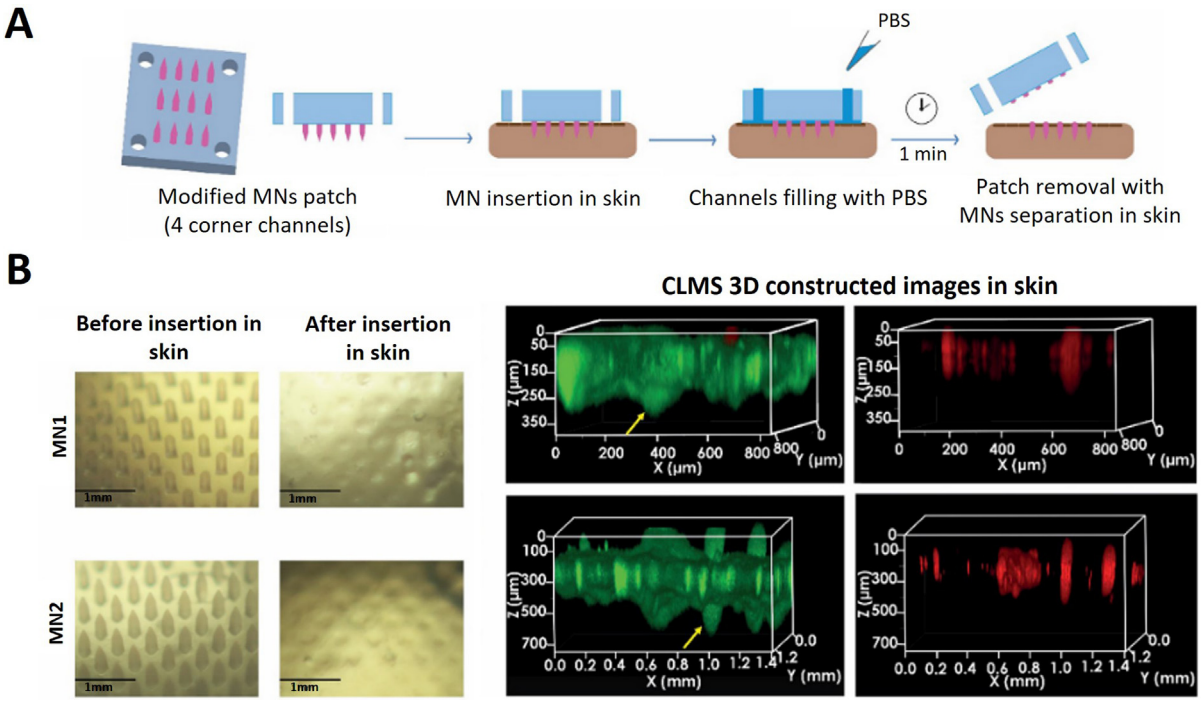


**FIGURE 6**

(A) A scheme shows the modification of the gold nanoclusters-gelatin nanoparticles-loaded MNs patch by forming channels at the 4 corners, then applied to human skin followed by adding Phosphate-buffered saline (PBS) through the channels to induce fast solubilization of the MNs and detachment from the patch base. (B) The effect of MNs morphology and modifying the MNs patches on skin penetration of two different designs of MNs, showing the separation of the MNs from the base (left panels) after insertion for 1 min in the skin. The inserted MNs have been imaged in the skin by confocal laser scanning microscopy (CLSM) (right panels) gold nanocluster-gelatin nanoparticles signal (red) separated from skin and PVA signals (green). The intrinsic fluorescence of PVA cannot be separated from that of skin, due to their similar fingerprint. The MNs can be distinguished from the skin by their obvious morphology (referred to by yellow arrows). MN1 and MN2 penetrated the skin to about 300 and 550 μm from the skin surface, respectively. Adapted and reprinted with permission from ref. [19]; Copyright 2020, Elsevier B.V.

development [82–84]. Thereby, the need to develop efficient drug delivery methods for these molecules is of utmost importance. One of the biggest obstacles faced in the development of drug delivery systems for these drugs is the need for organic solvents for their dissolution, which can impair their use due to health concerns [85,86]. Moreover, the use of organic solvents can also affect the production of the MNs leading to the heterogeneity of the hydrophilic polymers and/or to the formation of pores in the polymeric matrix [4]. Also, the loading of hydrophobic drugs *per se* can be challenging due to aggregation and consequent heterogeneous distribution within the MNs [86,87]. Over the years, different approaches to enhance the delivery of hydrophobic drugs through MNs have been designed to overcome these adversities. These strategies are discussed in this section.

*Nano/Micro-particles*

Nanoparticles (NPs) and microparticles (MPs) are versatile and powerful drug delivery devices [88]. These small particles can be produced with a wide array of materials (*e.g.*, polymers, lipids, silicon) and be precisely tailored for different purposes. In fact, by altering their physicochemical properties it is possible to encapsulate payloads with different physicochemical characteristics (*e.g.,* hydrophilic, hydrophobic, lipophilic), to increase and control their drug loading and release, protect them from degradation, and target them to different cells/tissues [82,89–95]. Thus, due to their many advantages, NPs and MPs represent powerful solutions to surpass the different obstacles related to the administration of hydrophobic molecules by dMNs.

For example, in a proof of concept study, Vora *et al.* [96] developed a method to produce double-layered PVP MNs loaded with poly lactic-co-glycolic acid (PLGA) NPs-MPs to improve the intradermal delivery of hydrophobic molecules. In this study, vitamin $D_3$ ($VD_3$), a liposoluble and potent molecule, was used as a model drug and encapsulated by a single emulsion technique into PLGA NPs-MPs. The formed particles, with sizes between 400 nm to 3.6 μm, successfully encapsulated $VD_3$ with an efficiency of 72.8%, corresponding to 133 ± 24 μg/ mg of particles. The double-layered MNs were then produced by mixing the PLGA particles with PVP (20%, w/v), and casting the resulting solution into a master-templated pyramidal mold (14 × 14 arrays), followed by centrifugation, and drying (Fig. 7**A**). The resulting needles measured 600 μm (height) and had two different layers (Fig. 7**B**). As a result of the wide size distribution of the particles, the tip had a porous, rough structure. The second layer, made of PVP only, presented a smoother structure. Moreover, after dissolution in PBS, the particle size remained the same and no aggregation was observed. These MNs were able to penetrate to a depth of *ca.* 380 μm using Parafilm M® membrane as a skin model, and to a depth of 250 to 300 μm in neonatal porcine skin [97]. To evaluate the effect of the developed system on the deposition in the skin, an *ex vivo* study in neonatal porcine skin was



Please cite this article in press as: T. Bauleth-Ramos et al., Materials Today, (2023), https://doi.org/10.1016/j.mattod.2022.12.007

**TABLE 1**

**Common polymers for the preparation of dissolving MNs.**[a]

| Polymer | Other compositions | Loaded bioactive agent | MNs application | Ref. |
|---|---|---|---|---|
| **HA** | | Magnesium ascorbyl phosphate | | [30] |
| | | Methotrexate | Treatment of psoriasis | [31] |
| | MN-combined with bacterial nanocellulose as the back layer. | Rutin (model drug) | | [32] |
| | | Green tea extract | Wound healing | [33] |
| | | Adenosine | Improve skin wrinkles, dermal density, and elasticity | [34] |
| | Sodium hyaluronate/chitosan composite MNs | Ovalbumin (model antigen) | Intradermal immunization | [35] |
| | MNs containing curcumin-loaded micelles | Curcumin | | [36] |
| | | Insulin | Diabetes | [37] |
| | MNs loaded with near-infrared responsive PEGylated gold nanorod | Doxorubicin | Human epidermoid cancer therapy | [38] |
| | | 5-Aminolevulinic Acid | Photodynamic therapy of superficial tumors | [39] |
| | | Sumatriptan Succinate | Migraine | [40] |
| | | Gentamicin | Neonatal sepsis | [41] |
| | Alginate and hyaluronate | Insulin | Diabetes | [42] |
| | | Insulin | Diabetes | [43] |
| | | IgG | Intradermal protein delivery | [44] |
| **PVP** | Copolymer polyvinylpyrrolidone-co-methacrylic acid (PVP-MAA) | Allergen extracts | Skin allergy test | [45] |
| | | mRNA | | [46] |
| | | Sinomenine hydrochloride | Anti-inflammatory | [47] |
| | | Fluorescein sodium and fluorescein isothiocyanate–dextrans (model drugs) | Intraocular drug delivery | [16] |
| | Chitosan nanoparticles-loaded MNs | A model antigen, ovalbumin (OVA), and an adjuvant, CpG oligodeoxynucleotides (CpG). | | [48] |
| **Cellulose derivatives** | CMC | Ovalbumin | Vaccination | [49] |
| | CMC | Lidocaine | Anesthesia | [50] |
| | CMC /powder-carrying MNs | Finasteride | Androgenetic alopecia | [51] |
| | HPC | Cyclosporin A | | [52] |
| | HPMC/PVP | Alpha-Arbutin | | [53] |
| **Chitosan** | | Bovine serum albumin | Transdermal Delivery of Macromolecules | [54] |
| | | Vascular endothelial growth factor (VEGF) | Wound healing | [55] |
| | Chitosan MNs and a poly(l-lactide-co-d, l-lactide) (PLA) supporting array | Ovalbumin | Vaccination | [56] |
| | Thiolated chitosan MNs | Tacrolimus | Immunosuppression | [57] |
| | | Meloxicam | Pain management in cattle | [58] |
| | | Ovalbumin | Vaccination | [59] |
| | | Luteinizing Hormone-releasing Hormone | Androgen Deprivation Therapy for lethal prostate cancer | [60] |
| **Alginate** | Alginate and maltose | Insulin | Diabetes | [61] |
| | | Bovine Serum Albumin | | [62] |
| | Glucose-responsive gold nanocluster-loaded MNs | Insulin | Diabetes | [63] |
| **silk fibroin** | | Insulin | Diabetes | [64] |
| | | Chemotherapeutic agents (thrombin and temozolomide) and targeted drug (bevacizumab) | | [65] |
| | | Influenza vaccine | Vaccination | [66] |
| **PVA** | | Doxorubicin | Cancer | [67] |
| | PVA/PVP | Bovine serum albumin | Macromolecules delivery | [68] |
| | PVA/PVP | Insulin | Diabetes | [69] |
| | Cholecalciferol nanosuspension-loaded MNs (PVA or PVP) | Cholecalciferol | Loading of hydrophobic drug | [70] |
| | PVA/maltose microneedle | Sinomenine hydrochloride | Rheumatoid arthritis | [71] |

[a] Abbreviations: HA: hyaluronic acid, PVP: polyvinylpyrrolidone, CMC: carboxymethyl cellulose, HPC: hydroxypropyl cellulose (HPC), HPMC: hydroxypropyl methylcellulose, PVA: polyvinyl alcohol.

performed. The results showed a significant deposition of $VD_3$ using the MNs when compared to patches without needles (Fig. 7**C**). Furthermore, higher accumulation was shown around 400 μm depth, which is in accordance with the insertion studies. While this study has shown the ability of these MNs to deliver particles and hydrophobic drugs, further studies would be



Please cite this article in press as: T. Bauleth-Ramos et al., Materials Today, (2023), https://doi.org/10.1016/j.mattod.2022.12.007

**TABLE 2**

**Dissolving MNs for the delivery of different types of drug molecules.**

| Microneedles | | | | | | | | Ref. |
|---|---|---|---|---|---|---|---|---|
| Loading | | | | | Method of Production | Material | | |
| | Drug/Molecule | Type of Formulation | Composition/ Characteristics | Loading/Encapsulation efficiency% (EE) per patch | | Needles | Backing layer | |
| **Hydrophobic drugs** | Vitamin $D_3$/ Cholecalciferol | Nano-microparticles | PLGA, 400 nm to 3.6 μm | 265 ± 32 μg | Micromolding | -PVP (360 kDa; 20%, w/v) | | [96] |
| | | Nanosuspension | 305 nm | 10% ± 2% w/w | | -PVP (360 kDa; 30% w/v) | | [70] |
| | Nile Red | Colloidal nanoparticles | HA and PVP (ratio 1:1), 157 ± 6 nm | EE- 99.9 % | Drawing lithography | -HA (29 kDa):PVP (30–60 kDa) ratio 1:1 | -CMC (90 kDa) | [86] |
| | Capsaicin | Colloidal nanoparticles | HA and PVP (ratio 1:1), 167 ± 4 nm | EE- 99.9 % | Drawing lithography | -HA (29 kDa):PVP (30–60 kDa) ratio 1:1 | -CMC (90 kDa) | [86] |
| | | Nanomicelles | α-lactalbumin, 30 nm | – | Micromolding | -Water:HA:PVA mass ratio 17:2:1 | | [98] |
| | Paclitaxel | Solid lipid nanoparticles (SLNs) | Cetyl Palmitate and tricaprin, 230 nm | 54.13 μg | Micromolding | -HA (<10 kDa; 40%, w/v) | -PVP K90 ethanol solution (31.25%, w/v) | [100] |
| | IR-780 | SLNs | Cetyl Palmitate and tricaprin, 230 nm | – | | -HA (<10 kDa; 40%, w/v) | -PVP K90 ethanol solution (31.25%, w/v) | [100] |
| | Albendazole | SLNs | 100 nm | 0.94 ± 0.03 mg | – | -PVA (31–50 kDa)-PVP (58 kDa) | -PVP (360 kDa; 15% w/w)-Glycerol (1.5%, w/w) | [101] |
| | | Nanosuspension | 96.53 ± 8.43 nm | 0.87 ± 0.09 mg | – | -PVP or PVA | -PVP (360 kDa; 15% w/w)-Glycerol (1.5% w/w) | [112] |
| | Doxycycline | SLNs | 100 nm | 0.84 ± 0.02 mg | – | -PVA (31–50 kDa)-PVP (58 kDa) | -PVP (360 kDa; 15% w/w)-Glycerol (1.5%, w/w) | [101] |
| | | Nanosuspension | 98.87 ± 9.77 nm | 1.00 ± 0.15 mg | – | -PVP or PVA | -PVP (360 kDa; 15% w/w) -Glycerol (1.5% w/w) | [112] |
| | Cisplatin | Lipid NPs | DOTAP, cholesterol, and DSPE − PEG − AA | – | Micromolding | -Sodium CMC (8%) | -SCMC | [102] |
| | | Lipid NPs | DOTAP, cholesterol, and DSPE − PEG − AA | – | | -PVP (360 kDa; 15% w/w) | | [175] |
| | Rilpivirine | Nanosuspension | | 4 mg | – | -PVA (9–10 kDa, 15% w/w) | -PVP (360 kDa; 20% w/w)-Glycerol (1.5% w/w) | [108] |
| | Itraconazole | Nanosuspension | 300 nm | 3.3 mg | Micromolding | -PVA (31–50 kDa; 15% w/w)-PVP (58 kDa; 25% w/w) | -PVP (90 kDa; 30% w/w)-Glycerol (1.5% w/w) | [109] |
| | Methotrexate (free acid) | Nanosuspension | 680 nm | 2.48 mg | | -PVA (31–50 kDa; 15% w/w)-PVP (58 kDa; 20% w/w) | | [113] |

(continued on next page)



Please cite this article in press as: T. Bauleth-Ramos et al., Materials Today, (2023), https://doi.org/10.1016/j.mattod.2022.12.007

Please cite this article in press as: T. Bauleth-Ramos et al., Materials Today, (2023), https://doi.org/10.1016/j.mattod.2022.12.007

**TABLE 2 (*CONTINUED*)**

| Microneedles | | | | | | | Ref. |
|---|---|---|---|---|---|---|---|
| Loading | | | | Method of Production | Material | | |
| | Drug/Molecule | Type of Formulation | Composition/ Characteristics | Loading/Encapsulation efficiency% (EE) per patch | | Needles | Backing layer | |
| | Ivermectin | Nanosuspension | 98.12 ± 7.76 nm | 0.86 ± 0.07 mg | – | -PVP or PVA | -PVP (360 kDa; 15% w/w)-Glycerol (1.5% w/w) | [112] |
| | Curcumin | Nanosuspension | 520 ± 40 nm | 10.9 ± 1.1 μg | – | -PVA (9–10 kDa) | -PVA (9–10 kDa; 20% w/w) | [114] |
| | | Inclusion complexes with cyclodextrins | Carboxymethyl-$\beta$-cyclodextrin sodium salt (CM-$\beta$-CD) | – | Micromolding and UV crosslinking | -Gelatin methacryloyl-$\beta$-CD | | [176] |
| | Dutasteride | Nanosuspension | – | 11/12% (w/w) | – | -CMC (5% w/w)-Trehalose (1.5% or 5% w/w)-Tween 80 (1% w/w) | | [115] |
| | Triamcinolone acetonide | Inclusion complexes with cyclodextrins | Hydroxypropyl-β-cyclodextrin (HP-β-CD) | 80.28 to 92.52 μg | Micromolding | -HA(<10 kDa):HP-β-CD at ratio 1:2 (w/v) | -PVP K90: ethanol (ratio 1:2.7, w/v) | [120] |
| | | Nanosuspension | 264 nm | 117.06 ± 9.07 μg | | -100 mg NS in 150 μL deionized water | -PVA (31–50 kDa 15% w/v)-PVP (58 kDa 20% w/v) | .[177] |
| | Levonorgestrel | Inclusion complexes with cyclodextrins | HP-β-CD | 66.94 μg | Micromolding | -Dextran (40 kDa) -Chitosan -beta-sodium -Glycerophosphate-HP-β-CD (1:1:1) | -PVP K90 (in ethanol) | [74] |
| | Leuprolide acetate | Solid dispersion | – | 14.3 μg | Micromolding | -Sodium chondroitin sulfate | | [178] |
| | Aspirin | Solid dispersion | – | 6 to 6.7 mg | | -PVP (40 kDa)-PMVE/MA (1500 kDa) | | [179] |
| | Atorvastatin calcium trihydrate | Solid dispersion | – | 1.9 to 3.4 mg | | -PVP (40 kDa)-PMVE/MA (1500 kDa) | | [179] |
| | Cyclosporin A | Co-solvency | – | 625 μg | | -HPC (80 kDa) in methanol | | |
| | Etonogestrel | Microcrystal particles/Powder | 10–30 μm | 550 μg | | -HPMC (10% w/w) | -PVA (35% w/w) | [52] |
| | Artemether | Nanosuspension | 148.10 ± 4.27 nm | 30,027 ± 69.5 μg | | -PVP (K-90 30% w/w) | | [111] |
| | Lumefantrine | Nanosuspension | 321.00 ± 16.50 nm | 8806 ± 461 μg | | -Sodium hyaluronate (3.3% w/w) | -PVP (MW 90 kDa, 15% w/w) | |

TABLE 2 (*CONTINUED*)

| Microneedles | | | | | | | | Ref. |
|---|---|---|---|---|---|---|---|---|
| Loading | | | | | Method of Production | Material | | |
| | Drug/Molecule | Type of Formulation | Composition/ Characteristics | Loading/Encapsulation efficiency% (EE) per patch | | Needles | Backing layer | |
| | Finasteride | Lipid NPs | Glyceryl monostearate and squalene. 180 nm | 47.36 ± 0.92 μg | Micromolding | -HA (34 kDa, 40% w/v) | -Dextran 40 (10% w/v)-HA (34 kDa, 10% w/v)-HA (200–400 kDa, 10% w/v) | [180] |
| | Shikonin | Micelles | 130 ± 8 nm | 0.805 ± 0.017 μg/mg | | -Karaya gum (40 % w/v)-PVA (10% w/v)-PVP (20 % w/v) | | [181] |
| **Hydrophilic drugs** | Diethylcarbamazine | SLNs | 100 nm | 0.55 ± 0.00 mg | – | -PVA (31–50 kDa)-PVP (58 kDa) | -PVP (360 kDa; 15% w/w)-Glycerol (1.5%, w/w) | [101] |
| | Methotrexate | Matrix interaction | | Up to 65.3 ± 2.9 μg | Micromolding | -HA (10 kDa; 25% w/v) | | [31] |
| | Lidocaine hydrochloride | Matrix interaction | – | 3.43 ± 0.12 mg | | -HPMC (3% w/w)-Gantrez S-97 (12% w/w)-Water (50% w/w) -Lidocaine hydrochloride (35% w/w) | -HPMC (3% w/w)-Gantrez S-97 (12% w/w)-Water (50% w/w) | [122] |
| | | Matrix interaction | – | 2.11 mg | Centrifugal lithography | -HA | -Solvent Casting Polyurethane (SPU) | [123] |
| | 5-aminolevulinic acid | Matrix interaction | – | 69.38 ± 4.89 μg | Micromolding | -CMC-Na (20 mg/mL)-PVP K30 (380 mg/mL)-Deionized water (DI) | -PVP K90M (0.31 mg/mL) | [124] |
| | Hyaluronidase | | – | 109.81 ± 6.73 μg | | | | |
| | Metformin | Matrix Interaction | – | 98.5 ± 1.3 | | -PLGA (50:50) | -PLGA (75:25) | [126] |
| **Peptides and proteins** | aPD1 | Lipid NPs | DOTAP, cholesterol, and DSPE − PEG − AA, | – | | -PVP (360 kDa; 15% w/w) | | [175] |
| | | Dextran NPs | pH sensitive, 250 nm | – | Micromolding and UV crosslinking | -Acylated HA (300 kDa; 4 wt%)-MBA (4 wt%)-Photoinitiator (0.05 wt%) | | [139] |
| | | 1-methyl-DL-tryptophan-Acylated HA NPs | 151 nm | – | Micromolding | -Acylated HA (50 kDa; 4 wt%) | | [140] |
| | aCTLA4 | Dextran NPs | pH sensitive, 250 nm | – | Micromolding and UV crosslinking | -Acylated HA (300 kDa; 4 wt%)-MBA | | [139] |

(continued on next page)



Please cite this article in press as: T. Bauleth-Ramos et al., Materials Today, (2023), https://doi.org/10.1016/j.mattod.2022.12.007

**TABLE 2 (*CONTINUED*)**

| Microneedles | | | | | | | Ref. |
|---|---|---|---|---|---|---|---|
| Loading | | | | Method of Production | Material | | |
| | Drug/Molecule | Type of Formulation | Composition/ Characteristics | Loading/Encapsulation efficiency% (EE) per patch | Needles | Backing layer | |
| | | | | | (4 wt%)-Photo initiator (0.05 wt%) | | |
| | ScaA88-300 | – | – | 5 μg | DAB or CL | -CMC (90 kDa; 12% w/v) | -CMC | [128] |
| | Lysozyme | Protein-matrix interaction | – | – | Micromolding | -PVP K30 (50% w/v)-PVA (50% w/v) | | [132] |
| | Bleomycin | Protein-matrix interaction | – | 100 μg | | -HA (10 kDa; 30% w/v) | -HA (10 kDa; 30% w/v) | [133] |
| | Recombinant Staphylococcal enterotoxin B protein | Protein-matrix interaction | – | 13 ± 1 μg | | -Chondroitin sulfate (2% w/v)-Trehalose (0.8% w/v) | | [135] |
| | Proteolipid protein (PLP) fragment – $PLP_{139-151}$ | Protein-matrix interaction | – | ~40 μg | | -Chitosan-PVA (130 kDa; 10% w/v) -PVP (10 kDa; 15% w/v) | | [136] |
| | | PLGA NPs | 200 nm | – | Micromolding | -PVA (130 kDa; 10% w/v):PVP (10 kDa; 15% w/v) ratio 3:2 (v:v) | | [142] |
| | BSA | Protein-matrix interaction | – | – | | -Chitosan-PVA (130 kDa; 10% w/v)-PVP (10 kDa; 15% w/v) | | [136] |
| | Ovalbumin (OVA) | Protein-matrix interaction | – | – | DAB | -HA | – | [137] |
| | | Protein-matrix interaction | – | 652 ± 57 μg (delivered only 0.16%) | Micromolding | -HA (150 kDa; 1, 2 or 5% w/v) | -HA (150 kDa; 5% w/v) | [143] |
| | | Protein-matrix interaction | – | – | – | -PVP (20% w/t)-PVA (15% w/t) | | [134] |
| | | PLGA NPs | 358 nm | 10 μg | Micromolding | -PMVE/MA (20% w/w) | | [141] |
| | | PLGA NPs | 170 nm | 4.15 ± 1.93 μg (delivered 24%) | | -HA (150 kDa; 1, 2 or 5% w/v) | -HA (150 kDa; 5% w/v) | [143] |
| | Flu-MH | Protein-matrix interaction | – | 15 μg | | -HA:Dextran: Povidone (ratio 11:8:1) | | [138] |
| | Insulin | Powder | – | 225.5 ± 8.6 μg | | -CMC (5 to 20% w/v) | -CMC film | [147] |
| | | Protein-matrix interaction | – | 90.4 ± 3.1 μg | | -CMC (20% w/v) | | [147] |
| | | | – | ~5 IU (173.5 μg) | | -Silk fibroin | -Silk fibroin -Proline | [64] |
| | | | – | ~0.25 IU (8.7 μg) | Micromolding | -Gelatin (10%) | -CMC (90 kDa; 10%) | [182] |

TABLE 2 (*CONTINUED*)

| Microneedles | | | | | | | Ref. |
|---|---|---|---|---|---|---|---|
| Loading | | | | | Method of Production | Material | |
| | Drug/Molecule | Type of Formulation | Composition/ Characteristics | Loading/Encapsulation efficiency% (EE) per patch | | Needles | Backing layer | |
| | | | – | 0.20 ± 0.02 IU (∼7 μg) | | -γ-PGA (1000 kDa; 30 wt.%) | -PVA (6 kDa; 50% w/v)-PVP (10 kDa; 50% w/v) | [183] |
| | Hemagglutinin | Additives/ Stabilizers | - | ∼12 μg | Micromolding | -NaCMC (1% w/v)-Stabilizer (10% w/v in ammonium acetate buffer) | -PVA:sucrose:water (mass ratio of 8:6:15) | [81,151] |
| | Lixisenatide | Protein-matrix interaction | – | 4.25 ± 0.07 μg | | -PVP K29/32 (10% w/w) | -PVP K29/32 (50% w/w) | [184] |
| | Ovalbumin fused with hepatitis B core | Mesoporous silica NPs | 33.4 ± 2.5 nm | – | | -Chitosan 8 wt%, -Trehalose 0.4 wt% | -Chitosan 8 wt% | [144] |
| | Matrix 2 peptide – model influenza antigen | Polymeric NPs | 342 ± 32 nm | 44 | | -Trehalose dihydrate -Sodium Hyaluronate (150 kDa, 450 kDa and 1000 kDa) | -Sodium Hyaluronate | [185] |
| | Collagen type III | Matrix Interaction | – | 97.24 ± 5.42 | Micromolding | -HA (200 mg/mL) | – | [186] |
| | bFGF | PLGA microspheres | 120 nm | – | | -PVP (Mw = 250 000) | - | [187] |
| **DNA/RNA** | Poly:IC (synthetic dsRNA) | PLGA NPs | 170 nm | 3.9 ± 1.8 μg | | -HA (150 kDa; 1, 2 or 5% w/v) | -HA (150 kDa; 5% w/v) | [143] |
| | | Matrix interaction | – | – | | -HA (150 kDa; 1, 2 or 5% w/v) | -HA (150 kDa; 5% w/v) | [143] |
| | Ebola DNA (EboDNA) | PLGA-PLL/γPGA NPs | 87 nm | 44.7 ± 1.5 μg | | -PVA (2000 da; 10% w/w) | -PVA (2000 da; 35% w/v)-PVP (10% w/v) | [160] |
| | | Matrix interaction | – | 13.8 ± 0.8 μg | | -PVA (2000 da; 10% w/v) | -PVA (2000 da; 35% w/v)-PVP (10% w/v) | [160] |
| | siRNA targeting transforming growth factor-beta type I receptor (TGF-βRI) | Mesoporous silica-coated upconversion NPs (UCNPs@$mSiO_2$) | 60 nm | – | | -HA (50% w/v) | | [161] |
| | pDNA | Cationic NPs (using acid cationic peptide - RALA) | RALA-DNA complex, < 100 nm | 30.2 ± 1.29 μg | Micromolding | -PVP (360 kDa; 20% w/v) | | [165] |
| | | Cationic NPs (using acid cationic peptide - RALA) | RALA-DNA complex, < 100 nm | PVA (9–10 kDa) – 17.7 μg; PVA (13–23 kDa) – 15.4 μg; PVP (58 kDa) – 14.2 μg; PVP (360 kDa) – 12.6 μg; | | -PVP (360 kDa; 20% w/w)-PVP (58 kDa; 30% w/w)-PVA (13–23 kDa; 20% w/w)-PVA (9–10 kDa; 20% w/ | | [166] |

(continued on next page)

Please cite this article in press as: T. Bauleth-Ramos et al., Materials Today, (2023), https://doi.org/10.1016/j.mattod.2022.12.007

Please cite this article in press as: T. Bauleth-Ramos et al., Materials Today, (2023), https://doi.org/10.1016/j.mattod.2022.12.007

**TABLE 2 (*CONTINUED*)**

| Microneedles | | | | | | | | Ref. |
|---|---|---|---|---|---|---|---|---|
| Loading | | | | | Method of Production | Material | | |
| | Drug/Molecule | Type of Formulation | Composition/ Characteristics | Loading/Encapsulation efficiency% (EE) per patch | | Needles | Backing layer | |
| | | | | | | w) | | |
| | | Cationic NPs (using acid cationic peptide - RALA) – Lyophilized | 75 nm | 57.3 μg | | -PVA (9–10 kDa; 20% w/w) | | [168] |
| | | Cationic NPs (using acid cationic peptide - RALA) | 38 nm | 17.7 μg | | -PVA (9–10 kDa; 20% w/w) | | [168] |
| | pcDNA4-PCV2 (DNA vaccine for porcine circovirus Type 2) | Polyplexes | 56.1 ± 2.7 nm | 20.3 ± 1.3 μg | | -PVA (6000 Da; 10%)-bPEI (10 kDa; 2.5%) | -PVA (6000 Da; 30%)-PVP (10 kDa; 10%) | [169] |
| | pVAX1 (DNA plasmid vector encoding the secreted protein Ag85B of Mycobacterium tuberculosis) | Matrix interaction | – | 4.2 μg | Micromolding | -HA (750–1000 kDa; 15%) | | [188] |
| | Anti-VEGF DNA aptamer | Matrix interaction | – | – | | -PVA (10 kDa)-PVP (10 kDa) at 20% w/v | -PVA (10 kDa)-PVP (10 kDa) at 50% w/v | [189] |
| | mRNA (naked luciferase mRNA, mLuc; OVA mRNA) | Matrix interaction | – | Up to 5 μg | | -PVP (10 kDa) | | [46] |
| | Lucifrase mRNA | Matrix interaction | – | – | | -HA (50 mg/mL) | | [170] |
| EVs | Human adipose stem cell-derived EV | Matrix interaction | 138.1 nm | – | | -HA (MW = 30–50 kDa) | | [174] |

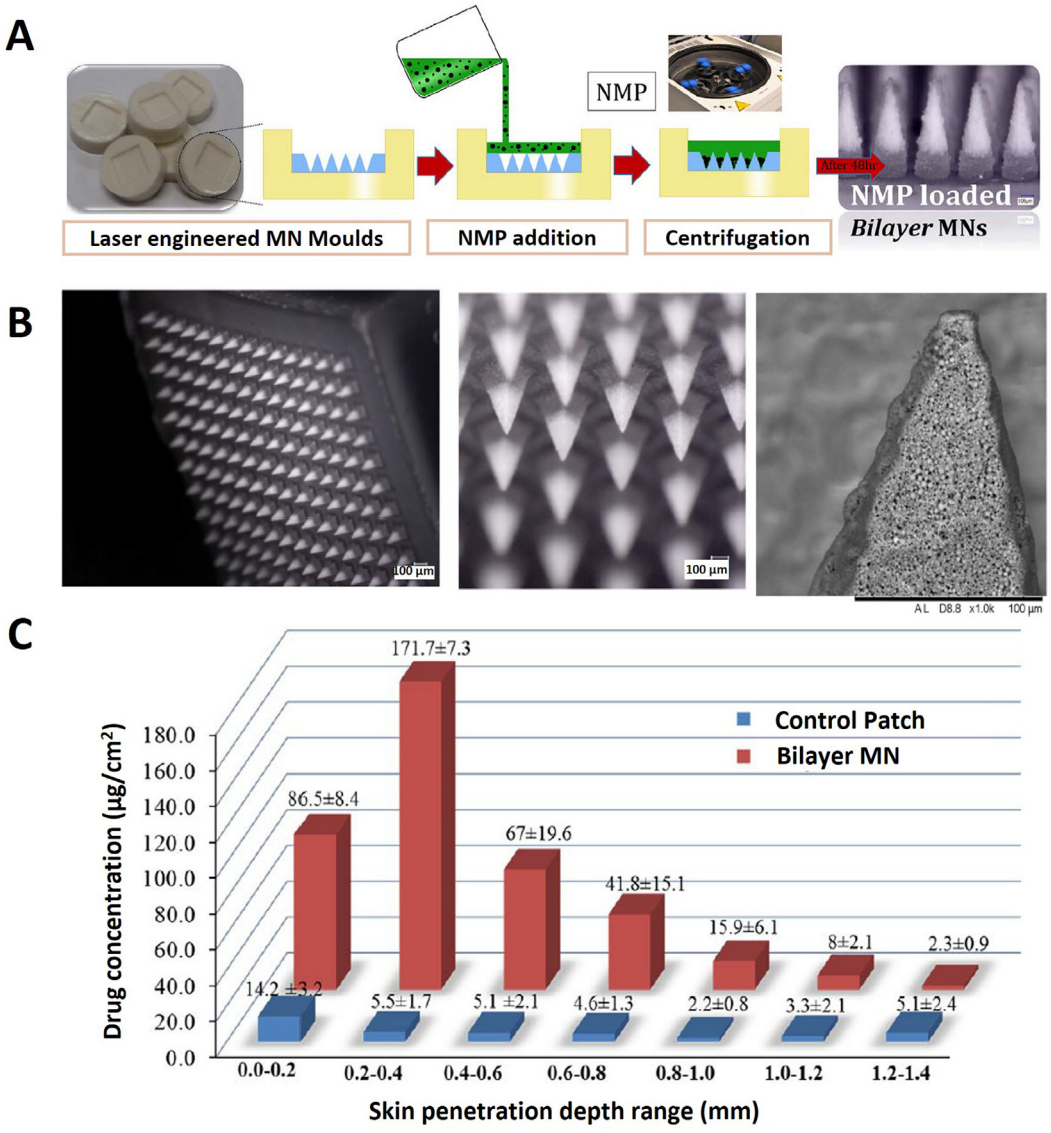


**FIGURE 7**

(A) Scheme of double-layered PLGA-loaded PVP MNs. (B) Digital microscopic and SEM images of PLGA-loaded PVP MNs. (C) Concentration of VD3 in different depths after administration with MNs or control patch. Adapted and reprinted with permission from ref. [96]; Copyright 2017, Elsevier B.V.

needed to compare the advantages of using particles in comparison to free drugs and to better assess the release profile *ex vivo* and *in vivo*.

Using an alternative and innovative strategy, Dangol *et al*. [86] have prepared colloids of lipophilic drugs with polymeric combinations, to prepare nanosized drug particles that can be homogeneously loaded in MNs without the use of organic solvents. To do this, the authors used Nile Red (NR) dye, and the anti-inflammatory drug capsaicin (Cap), used for rheumatoid arthritis, both highly lipophilic compounds. By homogenizing these compounds with HA and PVP at 1:1 ratio, colloidal NPs were formed with 157 ± 6 nm of diameter for NR and 167 ± 4 nm for Cap. Furthermore, this combination led to a transition of the drugs to an amorphous form, which was important for the uniform distribution of the drugs within the MNs. The dMNs were fabricated by drawing lithography, using plates coated with CMC into which droplets of HA and PVP 1:1 ratio polymer combination with NR and Cap were dispensed and blow dried. The resulting cylindrical MNs had a height of approximately 600 µm, tip diameter of 35 µm, and successfully encapsulated both payloads. The efficacy of drug delivery was assessed using the Franz cell diffusion test on pig cadaver skin comparing the produced MNs with topical formulations of the drugs. After 24 h, the MNs had permeated *ca*. 93% and 96% of NR and Cap, respectively, compared to only 32% and 42% release achieved by the topical solutions. Type II collagen-induced arthritic mice were treated with MNs loaded with Cap or its topical solution. By measuring the serum concentration of Cap for 72 h after treatment, it was possible to observe that the maximum serum concentration using the MNs was 47 µg/mL compared to only 21 µg/mL applying the topical solution, corresponding respectively to 95% and 41% delivery efficiency. Moreover, the MN treatment led to a reduction in the swelling of the hind paws, preservation of bone integrity, and a signifi-



Please cite this article in press as: T. Bauleth-Ramos et al., Materials Today, (2023), https://doi.org/10.1016/j.mattod.2022.12.007

cant reduction of the inflammation observed by the downregulation of the expression of inflammatory cytokines (tumor necrosis factor (TNF)-α, interleukin (IL)-6, IL-1β).

In another relevant recent study, Bao *et al*. [98] used nanomicelles (M) combined with dMNs to improve the loading and bioavailability of Cap for anti-obesity treatment. In this study, Cap was successfully loaded into α-lactalbumin nanomicelles (M-Cap) with an approximate average size of 30 nm, enhancing its solubility. The M-Cap loaded MNs were prepared by micromolding technique, by casting a mixture of HA and PVA with the M-Cap into PDMS molds followed by centrifugation and vacuum. This technique produced robust MNs with a rectangular pyramid shape and 600 μm height (Fig. 8**Aa**). By using Cy5 (hydrophobic dye) as a model drug, the authors showed that encapsulation of the hydrophobic compounds in the micelles allowed for its homogenous distribution in the needles contrariwise to their incorporation alone (Fig. 8**Ab-c**), surpassing one of the limitations of the combination of hydrophobic drugs with dMNs. Furthermore, *in vivo* biodistribution studies in high-fat diet (HFD)-induced obese mice, have shown longer-lasting retention of the hydrophobic compounds in inguinal white adipose tissue (iWAT) when administered by micelle-loaded MNs (96 h), compared to free compound loaded MNs (72 h) and subcutaneous injection of micelles (48 h) or free compound (12 h) (Fig. 8**B**). Anti-obesity efficacy *in vivo* studies were also performed in HFD-induced obese mice comparing the mice bodyweight after treating them every other day for 28 days with, MNs loaded with either M-Cap (MP-M-Cap), empty micelles (MP-M), or free Cap (MP-Cap) and subcutaneous injection of M-Cap (IN-J-M-Cap). Despite every treatment inducing a significant reduction of body weight compared to day 0, MP-M-Cap led to the largest weight loss (77.6% of starting weight), followed by MP-M (82%), IN-J-M-Cap (89%), and MP-Cap (97.2%) (Fig. 8**C**). Additionally, the maximum Cap concentration in blood was also significantly higher after treatment of MP-M-Cap compared to MP-Cap. In sum, these results showed a significantly higher bioavailability of the drug when encapsulated in micelles and combined with dMNs, proving the advantage of using NPs as carriers for hydrophobic drugs in combination with dMNs.

Jing *et al*. [99] have used also nanomicelles combined with dMNs to enhance the delivery of a hydrophobic drug (shikonin, SKN) to treat psoriasis. In this study, nanomicelles were prepared of HA and acid-sensitive histidine to create pH-sensitive NPs. Moreover, the NPs were further coated with human normal immortalized keratinocyte (HaCaT cell) membranes to actively target keratinocytes. The produced NPs were spherical, had an average diameter of *ca*. 130 nm, PDI of 0.2 and a surface charge of *ca*. −24 mV. SKN was highly encapsulated (encapsulation efficiency of 93% and loading degree of 4%) and its release was demonstrated to be pH dependent in *in vitro* settings. Furthermore, coated NPs showed higher uptake efficiency and targeting ability, *in vitro*, compared to non-coated NPs, which translated into an enhancement of the treatment, by inducing higher degrees of apoptosis in abnormal proliferative cells. The dMNs were produced by micromolding technique, by casting a NPs dispersion with 40% (w/v) karaya gum, 10% PVA and 20% PVP, into molds followed by vacuum and drying in a desiccator at RT. The produced MNs had pyramidal shape, with a height *ca*. 526 nm and homogeneously distributed NPs. Moreover, these MNs totally dissolved within 15 min both in aqueous medium and skin tissue. When tested in *ex vivo* mouse skin, the MNs showed a significantly higher skin retention and transdermal delivery of SKN compared both to SKN loaded NPs and free SKN. In addition, when applied in a mouse psoriasis *in vivo* model, the developed MN system combined with the coated NPs loaded with SKN, showed higher curative effects than the other groups, reducing the activation of JAK/STAT3 signaling pathway and downregulating pro-inflammatory factors expression. Hence, in this study the use of both NPs and MNs was crucial to enhance the effect of the treatment.

Other types of NPs, such as lipid-based NPs, have also been explored to load hydrophobic drugs into dMNs. A recent study performed by Qin *et al*. [100], showed the advantages of combining solid lipid NPs (SLNs) with dMNs. In this study, thermosensitive SLNs loaded with paclitaxel (PTX), a chemotherapeutic, and IR-780, a near-infrared (NIR) dye with photothermal effects, both poorly water-soluble molecules, were combined with dMNs to achieve a chemo-photothermal combined therapy for melanoma. PTX and IR-780 were successfully encapsulated into the SLNs (PTX/IR-780 SLNs) with high encapsulation efficiencies, 97%, and 63%, respectively. Furthermore, due to the thermolabile properties of the prepared SLNs, a controlled pulsatile release profile of PTX was achieved by applying a NIR laser (Fig. 9**A**). When exposed to the NIR laser, the IR-780 absorbed the energy and converted it into heat, leading to the phase transition of the SLNs and consequent release of the payloads. When turned OFF, the SLNs cooled down and re-solidified, decreasing the drug release rate. Additionally, by exposing both IR-780 solution and IR-780 loaded SLNs to a NIR laser for different time points and intensities, the authors verified that the encapsulation of IR-780 greatly improved its stability in water solution while maintaining its photothermal properties (Fig. 9**B-C**). *In vitro* experiments showed higher payload release within the cells after laser irradiation due to the photothermal effect or IR-780 under NIR laser. This translated to a higher antiproliferative effect of the paclitaxel/IR-780 loaded SLNs compared to paclitaxel SLNs, IR-780 SLNs, and paclitaxel/IR-780 solution. The dMNs were produced by micromolding using centrifugation. SLNs were successfully encapsulated into the dMNs, being mostly concentrated in the tips, and their physicochemical characteristics remained unchanged (Fig. 9**D-E**). The developed MNs had sufficient mechanical strength to pierce the skin to a depth of approximately 700 μm and were quickly dissolved. When applied in melanoma-bearing mice, the SLNs-loaded MNs induced a higher accumulation of SLNs in the tumor site compared to intravenous or intratumoral administration. In addition, mice treated with the paclitaxel/IR-780 SLNs loaded MNs plus laser irradiation completely eradicated the tumors and no tumor recurrence was observed (Fig. 9**F**). Contrariwise, in mice treated with paclitaxel/IR-780 loaded MNs (without the use of SLNs), the tumor volume kept increasing (Fig. 9**F**) and the survival rate was 0% before day 30. The authors explain this result is a direct consequence of the low stability of IR-780 in an aqueous solution. Thus, in this study, the use of SLNs and MNs was crucial to increase the stability of the payloads and control their release and accumulation in the therapeutic area.



Please cite this article in press as: T. Bauleth-Ramos et al., Materials Today, (2023), https://doi.org/10.1016/j.mattod.2022.12.007

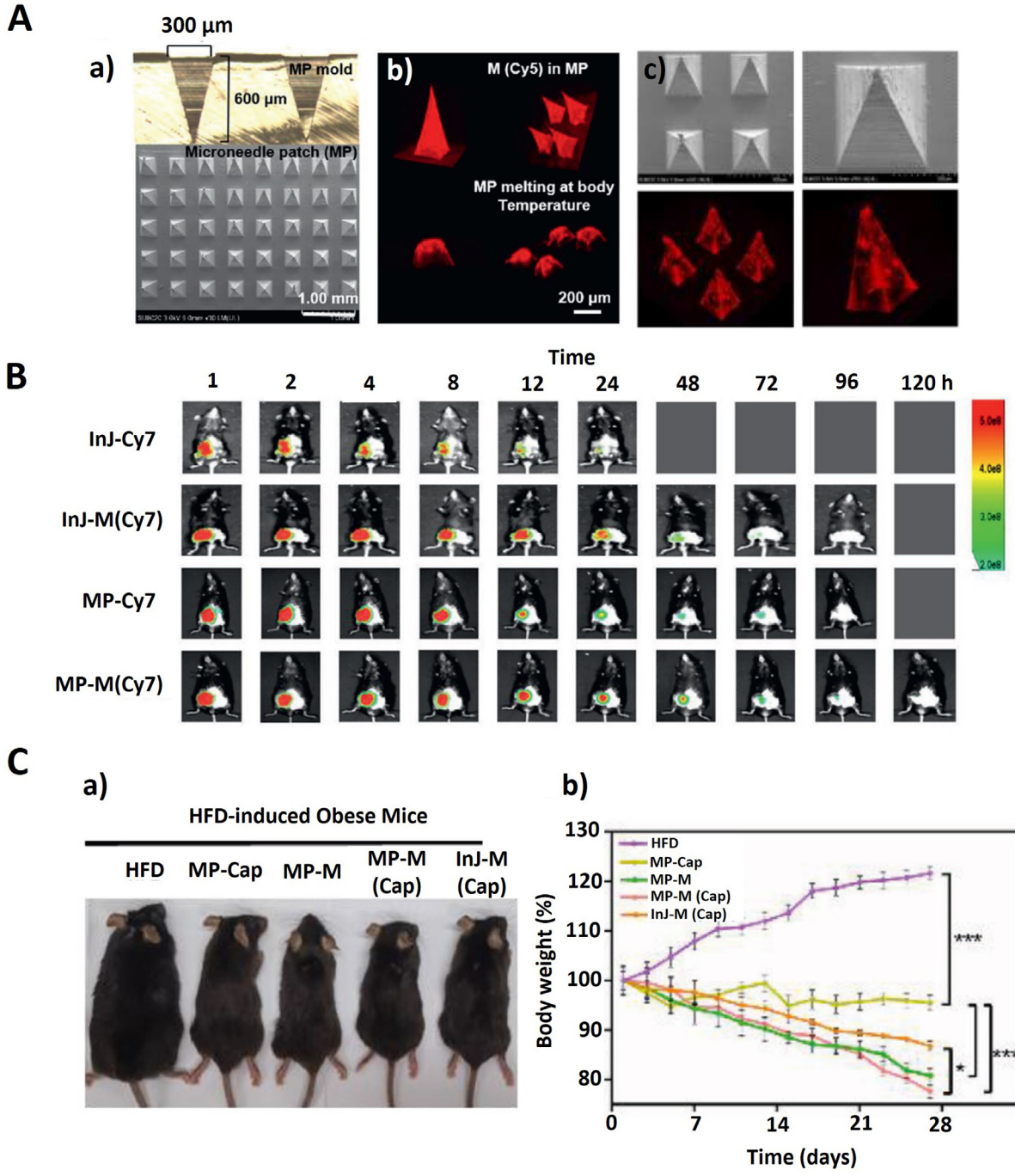


**FIGURE 8**

(A) Characterization of the developed micelle-loaded MNs; (a) SEM images of the MNS. Scale bar: 1 mm; (b) Confocal microscopy image of MP-M-Cy5 before and after being inserted into mice skin. Scale bar: 200 µm; (c) SEM and confocal microscopy images of free Cy5 loaded MNs. (B) *In vivo* fluorescence image of biodistribution study. (C) Anti-obesity efficacy study; (a) Photograph of HFD-induced mice after treatment with the different formulations; (b) HFD-induced mice bodyweight time curve after treatment with the different formulations. Adapted and reprinted with permission from ref. [98]; Copyright 2021, John Wiley & Sons, Inc.

In another study, Permana *et al.* [101], combined SLNs with dMNs to enhance the delivery and lymphatic uptake of different molecules, including the hydrophobic drugs albendazole and doxycycline, for the treatment of human lymphatic filariasis. In this study, both albendazole and doxycycline were successfully encapsulated into spherical SLNs with encapsulation efficiencies of *ca.* 90% and 55%, respectively. Moreover, the formed NPs, with a size of *ca.* 100 nm and polydispersity index (PDI) of *ca.* 0.3, were able to sustain the release of the payloads. To prepare the dMNs, a homogenous mixture of lyophilized SLNs and PVA and PVP polymers was firstly casted into a silicone mold, a pre-cast dry baseplate was placed behind the formulation, and vacuum was applied. Importantly, it was found that the formulation process did not affect the properties of the drug-loaded NPs. The resulting dMNs could successfully be inserted into the skin up to a depth of *ca.* 370 µm, improving



Please cite this article in press as: T. Bauleth-Ramos et al., Materials Today, (2023), https://doi.org/10.1016/j.mattod.2022.12.007

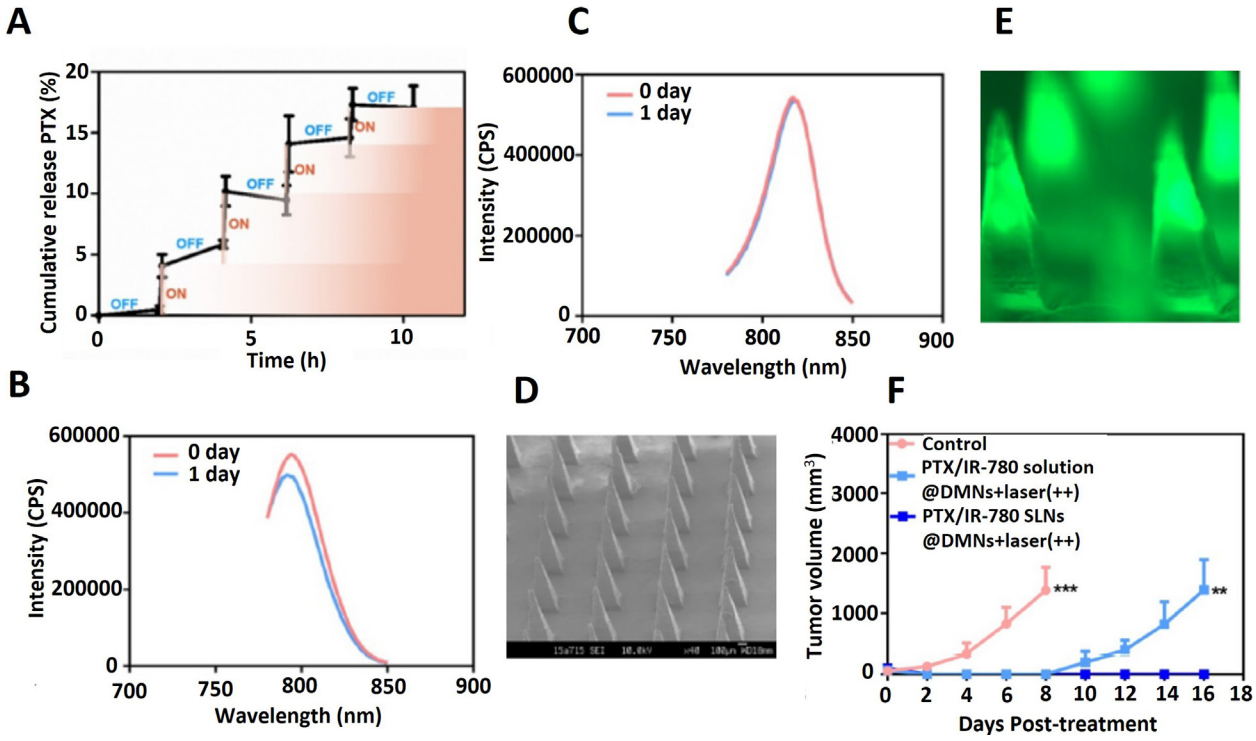


**FIGURE 9**

(A) Paclitaxel release profile from PTX/IR-780 SLNs. (B) Fluorescence spectrum of IR-780 solution after being stored 1 day in the light. (C) Fluorescence spectrum of PTX/IR-780 SLNs after being stored 1 day in the light. (D) SEM image of PTX/IR-780 SLNs. (E) Fluorescence microscopy image of PTX/IR-780 SLNs. (F) Tumor volume after treatment with MNs loaded with either PTX/IR-780 solution or PTX/IR-780 SLNs and laser. Adapted and reprinted with permission from ref. [100]; Copyright 2020, Ivyspring International Publisher.

the delivery and retention of the drugs in the dermis layer of the skin. Additionally, the *in vivo* pharmacokinetic profiles and biodistributions of both drugs after either oral administration or transdermal administration via the prepared dMNs were analyzed in rats. The results showed a significantly higher bioavailability and concentration in the lymphatic system after administration by dMNs, and a diminished biodistribution in the liver, kidney, and spleen.

Another interesting study using lipid NPs combined with dMNs was performed by Lan *et al.* [102]. In this study, pH-responsive lipid NPs loaded with cisplatin (CDDP), a first-line chemotherapeutic drug with poor solubility either in water or organic solvents, were incorporated into CMC-based MNs to enhance the efficacy and safety of anticancer therapy. CDDP was highly encapsulated into lipid NPs containing 1,2-dioleoyl-3-trimethy-lammonium-propane (DOTAP), cholesterol and 1,2-distearoyl-sn-glycero-3-phosphoethanolamine-N-[amino(polye thylene glycol)-2000] (ammonium salt) (DSPE−PEG−AA), which induce endosomal escape, cancer targeting and acid labile properties. The fabrication of the dMNs and encapsulation of the CDPP@NPs was done by a molding method. Confocal fluorescence microscopy studies have shown a uniform distribution of the NPs within the MNs tips. Additionally, the formed MNs were able to penetrate skin tissue and rapidly dissolve, depositing the particles in the tissue. *In vivo* studies in a xenograft tumor model have shown that CDDP@NPs-loaded MNs had a significantly enhanced anticancer effect when compared to intravenous or subcutaneous injection of free CDDP and CDDP@NPs. Moreover, CDDP@NPs loaded MNs also had an improved effect when compared to free CDDP-loaded MNs (despite the difference was not statistically significant). CDDP@NPs-loaded MNs increased the safety of the treatment by reducing the toxicity and side effects of CDDP. Taking into consideration the positive results of this study, the same group produced a follow-up study combining the previously developed CDDP@NPs with aPD-1 and loading them into dMNs to synergistically combine chemo and immunotherapy strategies for immunotherapy-unresponsive cancers treatment [103]. Firstly, anti-PD-1 antibody (aPD-1), an immune checkpoint inhibitor, was loaded into the outer layers of the CDDP@NPs, through hydrophobic and electrostatic interactions between the NPs and aPD-1, forming aPD-1/CDDP@NPs. Next, the NPs loaded MNs were formed by the molding method, through the casting of a NPs/PVP solution into a PDMS mold followed by centrifugation and drying. The formed aPD-1/CDDP@NPs MNs could successfully penetrate the skin and deliver the payloads, having shown an enhanced tumor regression in comparison with free CDDP, free aPD-1, aPD-1+CDDP, aPD-1/CDDP@NPs, CDDP@NPs loaded MNs and aPD-1@NPs loaded MNs, in an immunocompetent tumor-bearing mouse model. Furthermore, aPD-1/CDDP@NPs MNs led to high T-cell infiltration (*ca.* 76% of $CD8^+$ T-cells), elevated IFN-γ expression, and a decrease of regulatory T-cells, which directly correlated with the enhanced tumor regression efficiency compared to the other groups.



Please cite this article in press as: T. Bauleth-Ramos et al., Materials Today, (2023), https://doi.org/10.1016/j.mattod.2022.12.007

These studies highlight the several advantages of NPs to improve hydrophobic drug delivery using dMNs and the versatility of materials that can be explored for this purpose.

*Nanocrystals/Nanosuspension*

Nanosuspensions (NSs) are colloidal dispersions of submicron-sized hydrophobic drug particles, prepared without matrix, and stabilized with surfactants and polymers [103–105]. Reducing a micro-sized drug to submicron size increases its surface-to-volume ratio leading to an enhanced dissolution rate and consequently higher bioavailability [106]. Thus, the application of NSs to MNs is another viable strategy to improve the transdermal delivery of hydrophobic drugs [107].

Taking this into account, Vora *et al*. [70] developed dMNs loaded with NS of $VD_3$ to improve its transdermal delivery. The NS was prepared by a sonoprecipitation solvent evaporation method, which involved dropping the $VD_3$ solution into a stabilizer solution under probe sonication, followed by evaporation. In order to optimize the conditions of the NS formation, the authors performed a systematic study applying diverse stabilizers (PVA or PVP of different molecular weights, MWs) with different concentrations, different solvents (ethanol or acetone), and different sonication amplitudes. The MW of PVA and PVP was found to have a direct correlation with the formed particles' size, with lower MWs producing smaller particles. Furthermore, contrary to $VD_3$ concentration, increments in both the stabilizer's concentration and sonication amplitudes led to smaller particles. Therefore, $VD_3$-NS prepared with PVA (10 kDa) was chosen as it formed particles with *ca*. 305 nm size and PdI of 0.27. To fabricate the MNs, a micromolding method was applied. $VD_3$-NS prepared with PVA (10 kDa) was mixed with PVP (360 kDa) and casted into a PDMS mold template, followed by centrifugation and drying at RT, producing MNs with approximately 10% (w/w) loading of $VD_3$-NS. While $VD_3$-NS loaded MNs produced homogenous MNs with no observed significant aggregation or changes in particle size after dissolution, the same was not observed for plain $VD_3$ loaded MNs. These findings reinforced the utility of using NSs to load hydrophobic drugs for MNs development. The fabricated MNs were also shown to have adequate mechanical properties, being able to penetrate both Parafilm M® and neonatal porcine skin to a depth between 350 to 400 μm. To assess the permeation efficiency of the $VD_3$-NS loaded MNs, an *ex vivo* study in neonatal porcine skin using Franz cells was performed. After 24 h of applying the developed MNs into the skin, *ca*. 500 μg were delivered compared to only 73 μg when using a film of $VD_3$-NS without the needles.

In one interesting study done in collaboration with Janssen Pharmaceutica, Mc Crudden *et al*. [108] have also combined NS with dMNs to improve the delivery of a hydrophobic drug, rilpivirine (RPV) for human immunodeficiency virus prophylaxis. In this proof of concept study, a two-step needle casting process of RPV-NS and PVA(9–10 kDa) followed by the application of a solid baseplate made of PVP and glycerol was applied to form the RPV-NS loaded dMNs. The produced MNs were able to successfully penetrate a commercially available synthetic tissue model, which emulated the mechanical characteristics of vaginal tissue. *Ex vivo* studies in bovine vaginal tissue have confirmed the ability of the developed MNs to penetrate the tissue, and more importantly, to deliver RPV into the tissue. Moreover, *in vivo* studies in rats confirmed the *in vitro* results as RPV was detected in plasma, lymph nodes, and vaginal tissue.

In another successful example, a NS of itraconazole (ITZ-NS) was loaded in PVA/PVP dMNs to improve its solubility and enhance the treatment of cutaneous candidiasis [109]. ITZ-NS was prepared using a media milling technique [110], which after optimization, produced particles with *ca*. 300 nm. An *in vitro* release study comparing ITZ to ITZ-NS has shown that the release from ITZ-NS (*ca*. 90%) was *ca*. 3-fold higher than for ITZ (*ca*. 32%), proving its ability to enhance the solubility of ITZ. Furthermore, the enhanced solubility also translated into enhanced antifungal activity. In fact, ITZ-NS had the same minimal inhibitory concentrations (MIC) and minimal fungicidal concentrations (MFC), (MIC = 2.5 μg/mL and MFC = 5 μg/mL) as a solution of ITZ in DMSO, but significantly higher when compared to a solution of ITZ in water (MIC > 2560 μg/mL and MFC > 2560 μg/mL). The authors then prepared two layered MNs containing different concentrations of ITZ-NS (10, 20, 30, 40 and 50 %) with PVA/PVP polymer mix on the tips and a pre-casted dry base plate of PVP and glycerol. By analyzing their mechanical properties through height reduction and depth of penetration after insertion into Parafilm M®, it was found that only the condition with 50% of ITZ-NS had poor mechanical properties (*ca*. 31% height reduction) while all the others showed similar results among them, with height reduction of only *ca*. 11% and depth of penetration of 500 μm. Furthermore, MNs with 40% ITZ-NS (equivalent to *ca*. 3.3 mg of ITZ per MN) could also penetrate porcine skin to a depth of 500 μm and were totally dissolved after 30 min inserted into the skin. The developed MNs after *ex vivo* application in porcine skin showed higher distribution in the skin compared to a patch without needles and to a conventional cream. The enhanced distribution by the MNs further translated into a higher antifungal activity in an ex vivo fungal infection model on porcine skin, compared to the controls. These results showed a significant benefit of ITZ-NS incorporation in the dMNs.

Recently, dMNs were produced to deliver artemether (ART) and lumefantrine (LUM), anti-malaria hydrophobic drugs usually administered by oral route, in order to improve their bioavailability and absorption.[111]. To do so, NS of each drug were firstly prepared by anti-solvent precipitation technique [112], rendering particles with size *ca*. 148 nm and 321 nm for ART and LUM, respectively, and enhanced water solubility. The dMNs were prepared by micromolding technique (Fig. 10**A**-**B**), by casting a mixture of ART-NS (20% w/w) and PVP K-90 (30% w/w) or of LUM-NS (20% w/w) with sodium hyaluronate (SHA; 3% w/w) into silicone molds. The formed MNs were successfully inserted into 3 layers of Parafilm® (equivalent to 378 μm), with a height reduction of *ca*. 2.7% and 1.4% for MNs with ART and LUM, respectively. Moreover, the developed MNs improved the deposition of both drugs into *ex vivo* porcine skin (Fig. 9**C**), when compared to polymeric films (without needles) of the same formulation. *In vivo* bioavailability studies, comparing the delivery of the drugs by MNs or by oral treatment, proved that MNs with LUM have higher efficacy than the oral treatment and that MNs with ART can deliver ART in a high therapeutic dosage that would be effective for treatment (Fig. 10**D**). In fact, the drug



Please cite this article in press as: T. Bauleth-Ramos et al., Materials Today, (2023), https://doi.org/10.1016/j.mattod.2022.12.007

loaded MNs were able to significantly inhibit parasitemia of treated animals compared to untreated group.

NS can also be applied to deliver hydrophobic forms of drugs usually employed in their hydrophilic forms, improving their delivery, and diminishing their secondary effects. For example, methotrexate (MTX), a folic acid antagonist with anti-inflammatory and immune-modulatory effects, is used as first-line treatment for psoriasis. This drug is mostly used in its sodium salt (MTX Na), which is highly hydrophilic and has a very short life. Thus, MTX NA needs to be administered frequently leading to severe secondary effects. However, MTX also exists as a free acid which is characterized by poor water solubility. Taking this into consideration, Tekko *et al*. [113] prepared dMNs loaded with poorly water-soluble NS of MTX to enhance its loading and sustain its delivery. The MTX NS was prepared using PVA as a stabilizer, and acid-base neutralization for precipitation and sonication, yielding homogenous MTX particles with a size of *ca*. 680 nm. The dMNs were then prepared by the micromolding method using a mixture of PVA (50 kDa) and PVP (58 kDa) with different concentrations of MTX NS. The produced NS-MNs were able to load up to 2.48 mg of MTX per patch and maintain its stability. However, the mechanical properties were affected by the NS as higher concentrations of MTX-NS led to higher needle height reduction after an insertion study in Parafilm M®. Nonetheless, the MNs were able to successfully penetrate the skin. Comparative e*x vivo* release studies in porcine skin have proven the capacity of the MTX NS-MNs to sustain the release as after 24 h only *ca*. 39% was released compared to *ca*. 85% release from MTX NA-MNs. Furthermore, *in vivo*, the MTX NS-MNs were able to improve the delivery of MTX to the skin and diminish its systemic exposure. Despite these positive results, the authors underline a limitation in the delivery efficiency as only 25% of the loaded dose was delivered. The use of NS combined with MNs has been also applied with several other drugs such as doxycycline, albendazole and ivermectin [112], curcumin [114], and dutasteride [115] highlighting its versatility.

### *Cyclodextrins*

Cyclodextrins (CD) are a class of cyclic oligosaccharides formed by the linkage of D-(+)-glucopyranoses via six (α-CD), seven (β-CD) or eight (γ-CDs) 1,4-α-glucosidic bonds. The resulting structure forms a truncated conical shape with a hydrophobic cavity with ether and carbon-hydrogen bonds and a hydrophilic outer rim with hydroxyl groups [116]. This makes CDs hydrophilic and biocompatible macrocyclic hosts, capable of interacting with poorly water-soluble molecules via host–guest inclusion complexes and increasing this way their solubility [117]. Thus, CDs have been used to enhance the solubility of hydrophobic drugs and improve their delivery [118,119].

Considering this, Lin *et al*. [120] have fabricated HA dMNs containing hydroxypropyl-β-cyclodextrin (HP-β-CD) to deliver triamcinolone acetonide (TA), a hydrophobic glucocorticoid, for hypertrophic scar (HS) therapy. HP-β-CD was mixed with HA to reinforce the MNs' mechanical strength and to improve drug loading. To prepare the MNs, a triple centrifugation molding method was applied. Briefly, a HA/HP-β-CD solution was casted over a PDMS mold and centrifuged. After, the excess was removed, and the mold was centrifuged again to concentrate the polymer in the tips before adding a PVP solution to form the back layer. Finally, the mold was centrifuged again and dried for 72 h before peeling. Due to its hydrophobicity, TA was firstly solubilized in HP-β-CD solution increasing its solubility by forming inclusion complexes with HP-β-CD. By testing different ratios HA:HP-β-CD, it was found that the mechanical strength of the MNs increased in a proportional manner to the amount of HP-β-CD. These enhanced mechanical properties stem from the breaking of intramolecular hydrogen bonds and the formation of intermolecular hydrogen bonds between HA and HP-β-CD, as proved by XRD and FTIR. Moreover, the higher molar ratio of HP-β-CD to TA also led to higher TA loading. *Ex vivo* studies in rabbit skin with HS were performed, showing the ability of the MNs to penetrate to a depth of approximately 500 μm, and to enhance the delivery and retention of TA in HS tissue during 12 h, when compared to TA cream or TA injection. In addition, *in vivo* studies in rabbit ear HS model, have further confirmed these results as after administration of TA loaded MNs, HS tissue disappeared, showed signs of histological recovery, and the expression of collagen I and TGF-β1 mRNA and proteins significantly diminished.

Another successful example of using CDs to improve the delivery of hydrophobic drugs using MNs was done by Yao *et al*. [74]. In this study, the dMNs were fabricated by a two-step molding method using dextran combined with HP-β-CD to enhance the loading of the levonorgestrel (LNG), a poorly water-soluble contraception drug. Furthermore, chitosan and beta-sodium glycerophosphate (β-GP), thermosensitive compounds, were also added into the polymer mix to improve the release of LNG. The prepared MNs had adequate mechanical properties for skin penetration and displayed high solubility, as *ca*. 40% of the MNs were dissolved after 10 min in contact with PBS at 34 °C. The addition of HP-β-CD to the MNs highly impacted the LNG loading, increasing it *ca*. 30-fold, from 1.73 μg to 66.94 μg. Additionally, the developed NPs were shown to successfully deliver *in vitro* (75.62 ± 22.79 %) LNG across the skin and had a similar *in vivo* pharmacokinetic profile compared to oral administration of suspension with the same LNG amount.

Recently, in another study, β-CD were combined with gelatin methacryloyl (GelMA) to prepare MNs with enhanced loading of the hydrophobic drug curcumin for cancer treatment [121]. To fabricate the matrix to produce the MNs, β-CD were firstly conjugated to GelMA via N′-ethylcarbodiimide hydrochloride (EDC)/N-hydroxysuccinimide (NHS) coupling, with a yield of *ca*. 40 wt-% (Fig. 11**A**). An aqueous suspension of curcumin was used to compare the loading between unmodified and modified GelMA. The modification of GelMA with β-CD increased the loading capacity by 5.5-fold, from *ca*. 85 to 466 μg/mL, and improved its stability. Comparing the FTIR spectrums and differential scanning calorimetry (DCS) thermograms of GelMA-β-CD-curcumin and the physical mixture of GelMA-β-CD+curcumin, the authors verified the existence of host–guest interactions within GelMA-β-CD-curcumin and their absence in the physical mixture, confirming the formation of inclusion complexes. To produce the MNs, a GelMA-β-CD−curcumin solution was casted into a PDMS mold, followed by centrifugation and crosslinking with UV-light (Fig. 11**A**). The formed MNs had a height of *ca*. 600 μm, a base with a width of 300 μm and curcumin was suc-



Please cite this article in press as: T. Bauleth-Ramos et al., Materials Today, (2023), https://doi.org/10.1016/j.mattod.2022.12.007

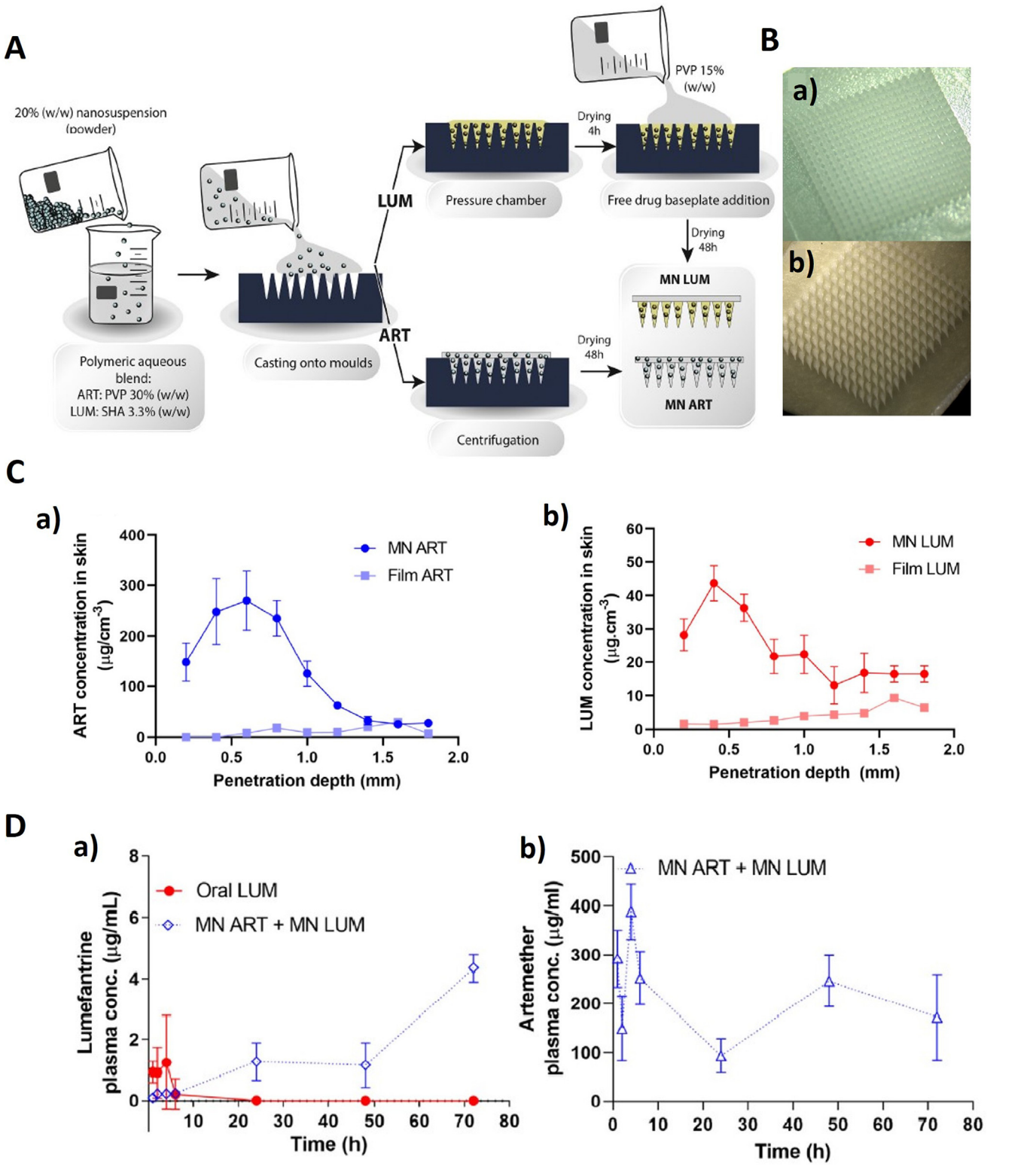


**FIGURE 10**

(A) MN patch fabrication using micromolding. (B) MNs arrays: (a) PVP k-90 30% ART NS-T 20%; (b) 3.3% w/w SHA + 20% LUM NS-T. (C) *Ex vivo* porcine skin insertions: (a) ART concentration within different penetration depths (mm) after 24 h application of MN ART or drug containing film; (b) LUM concentration within different penetration depths (mm) after 24 h application of MN LUM or drug containing film. (D) Pharmacokinetic analysis: (a) LUM and (b) ART employed in mice as a comparator of WHO recommended oral treatment. Adapted and reprinted with permission from ref. [111]; Copyright 2021, Elsevier B. V.



Please cite this article in press as: T. Bauleth-Ramos et al., Materials Today, (2023), https://doi.org/10.1016/j.mattod.2022.12.007

cessfully located in the needles (Fig. 11**B**). *Ex vivo* and *in vivo* studies have shown the ability of the MNs to successfully penetrate the skin. Additionally, due to the presence of methacrylate groups, the mechanical properties, and the drug release profile was tuned. In fact, higher degrees of crosslinking led to increased mechanical strength and to a longer release profile (Fig. 11**C**). To test the efficacy of the developed MNs to deliver curcumin, an *in vitro* experiment was designed using melanoma cells spheroids embedded into a GelMA hydrogel to mimic the extracellular matrix. One day after the application of either the developed MNs or a non-transdermal patch (same constitution of the MN patch but without the needles) into the gel containing the spheroid, it was possible to observe an improved anticancer efficacy of the MNs (Fig. 11**D**). *In vivo* experiments in mice have attested to the biocompatibility of the developed MNs as no significant inflammation was observed by histological analysis and there were no significant changes in the immune cell populations (CD3+ T-cells, CD68+ macrophages, and CD79A+ B-cells), as confirmed by immunofluorescence staining. These studies have shown that CDs can be used to improve the loading of hydrophobic drugs and simultaneously play an important role in tuning and enhancing the mechanical properties of the MNs.

### *Hydrophilic molecules*

MNs, due to their ability to surpass the SC, significantly enhance the transdermal delivery of hydrophilic and macromolecular molecules. Using this route, it is possible to surpass the skin barrier, increasing the bioavailability of the drug while avoiding high systemic levels of drug exposure, first-hepatic metabolism, and rapid clearance of drugs. Consequently, it leads to the need for lower and less frequent dosages and consequently diminished side effects, higher patient compliance, and higher therapeutic efficacy.

dMNs, made of hydrophilic matrices, facilitate the dispersion and loading of hydrophilic drugs, making them extremely attractive drug delivery systems for this type of molecule. For example, several dMNs have been developed to deliver the hydrophilic local anesthetic drug lidocaine and MTX [31,122,123]. However, some challenges remain as for instance due to the high hydrophilicity the drug molecules can diffuse during production or have rapid clearance from the application site. For example, Du *et al*. [31] produced HA dMNs loaded with MTX. In this study, the MNs were prepared by a micromolding approach in which MTX solutions with different drug concentrations were firstly casted into PDMS molds, under vacuum, followed by the addition of HA solution (250 mg/mL). Despite adding firstly the drug into the molds, MTX was also found in the baseplate of the MNs. The authors suggested this occurred due to its diffusion within the polymeric matrix. Moreover, notwithstanding the fact that the MTX-MNs had a higher antipsoriatic effect than a topical cream with the same amount of MTX in a mouse model, frequent doses had to be applied. This can be linked to a rapid clearance of the application site.

Other hydrophilic drugs, as for example 5-aminolevulinic acid (ALA) and metformin (MET) have also been loaded within dMNs for a combination therapy against HS [124]. In this study, the MNs were produced by micromolding, by casting a polymeric solution of PVP, CMC-Na and hyaluronidase together with ALA and MET, into PDMS molds, followed by centrifugation and drying. Hyaluronidase was included in the formulation to both increase the mechanical strength of the MNs and as a penetration enhancer by promoting the degradation of HA. In fact, the mechanical strength of MNs with hyaluronidase was significantly higher than MNs without it. The authors attributed this phenomenon to the interactions between the hyaluronidase and the polymers [125]. Moreover, hyaluronidase containing MNs induced an enhanced drug permeation (*ca*. 100%) in a Franz diffusion cell test, compared to MNs without it (*ca*. 50%). The same results were also observed *in vivo*, in rabbits with HS. The presence of MET led to a higher cytotoxicity and decreased collagen deposition, enhancing the treatment.

In another recent study [126], MET was loaded in PLGA MNs for obesity treatment. In this study, MET was mixed with PLGA solution (200 mg/mL) in dimethylformamide, and casted into PDMS molds by vacuum and centrifugation, followed by drying (Fig. 12**A**). The produced MNs had pyramidal shape and a height of *ca*.700 μm (Fig. 12**B**). Moreover, MET was successfully loaded with *ca*. 90 μg of MET per patch and released overtime in *in vitro* settings (*ca*. 89% release after 8 h). When applied in high fat diet-induced obese mice, the MNs enhanced the delivery of MET, leading to higher decrease in body weight and visceral fat and enhanced metabolic health (Fig. 12**C**). To avoid drug diffusion and concentrate it in the tips, several techniques, for example, the use of a bubble separating the backing layer from the needles, separable arrowheads, patchless MNs, etc., can be pursued [23,56,76,127]. Also, to circumvent the fast release of the drug molecules, different strategies can be applied to control their release profile. These strategies are discussed in the following section.

#### *Biotherapeutics*

*Production method*. During the fabrication process of dMNs, the payloads are exposed to different stress factors (*e.g*., temperature, pH, osmolality, organic solvents, pressure), which can significantly affect their activity. Therefore, when choosing the methods to formulate the biotherapeutics carrying dMNs, it is necessary to consider that different methods, such as micromold-

**FIGURE 11**

(A) Scheme of GelMA-β-CD-curcumin MNs production: (a) Conjugation of GelMA with β-CD using EDC/NHS; (b) Loading with curcumin; (c) UV cross-linking to form GelMA-β-CD-curcumin MNs. (B) Images of GelMA-β-CD-curcumin MNs: (a) Fluorescence image of drug-loaded MNs. Curcumin is represented in green. Scale bar:200 μm; (b)SEM image of MNs. Scale bar:300 μm. (C) MNs characterization: (a) Mechanical strength of the different MNs; (b) *In vitro* release of curcumin from GelMA-β-CD-curcumin MNs. (D) Live/Dead screening of B16F10 spheroids to assess the *in vitro* efficacy of the MNs: (a) Blank MNs; (b) GelMA-β-CD-curcumin nontrasndermal patch; (c) GelMA-β-CD-curcumin MNs. Scale bar: 100 μm; (d) Confocal 3D image of GelMA-β-CD-curcumin MNs. Scale bar: 600 μm; (e) Fluorescent image of GelMA-β-CD-curcumin MNs on spheroids. Scale bar: 100 μm. Adapted and reprinted with permission from ref. [121]; Copyright 2020, John Wiley & Sons, Inc.



Please cite this article in press as: T. Bauleth-Ramos et al., Materials Today, (2023), https://doi.org/10.1016/j.mattod.2022.12.007

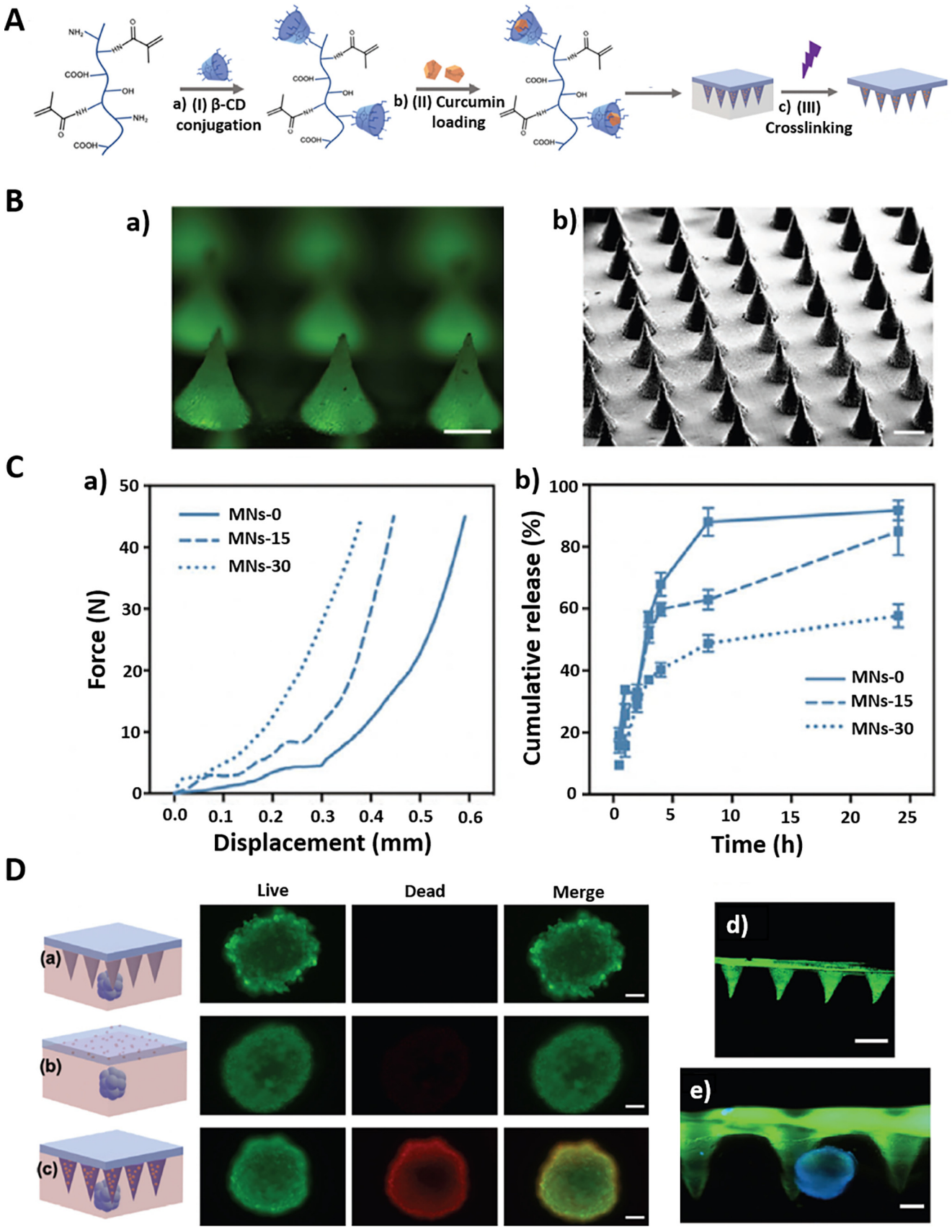




Please cite this article in press as: T. Bauleth-Ramos et al., Materials Today, (2023), https://doi.org/10.1016/j.mattod.2022.12.007

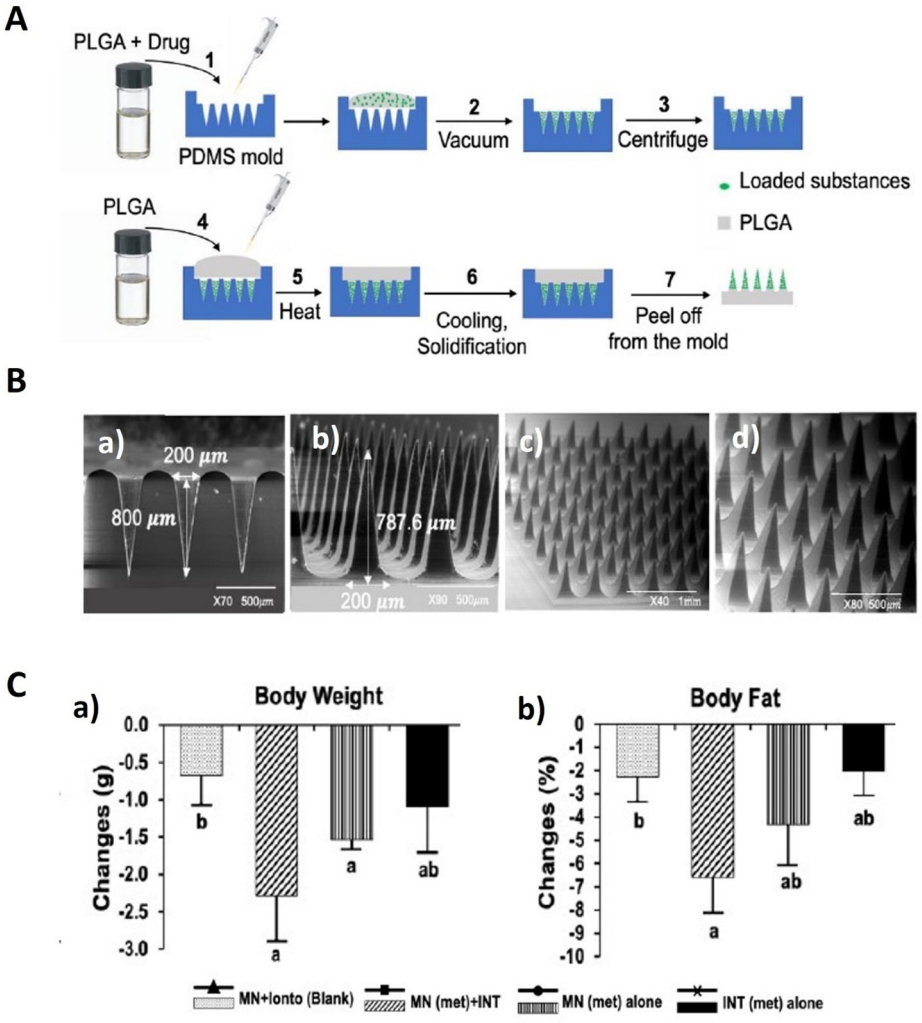


**FIGURE 12**

(A) Fabrication of PLGA dissolving MN patches. (B) Different views of MNs patches: (a) Length and base of the mold; (b) Needles length and base; (c-d) MN array with 800 μm. (C) Metabolic effects of metformin: (a) Body weight; (b) Fat%. Adapted and reprinted with permission from ref. [126]; Copyright 2022, MDPI.

ing, droplet-born air blowing (DAB), and centrifugal lithography (CL), possess different stress factors. While micromolding is based on casting a polymer into PDMS molds followed by centrifugation/vacuum and drying, DAB and CL are droplet-based methods. In DAB, the solidification occurs via air-blowing process while in CL it happens via centrifugal force conjugated with vacuum [128]. These methods are well described somewhere else [129]. Thus, an appropriate screening must be performed to choose the best production method for each molecule. Bearing this in mind, recently Lee *et al.* [128] performed a comparative study of the functional activity of the antigen ScaA88-300 (ScaA) for scrub typhus, after CMC dMNs production by DAB and CL (Fig. 13**A**). The ScaA-MNs prepared by DAB and CL had an identical conical shape (Fig. 13**B**) with *ca.* tip length of 445 μm and 489 μm, respectively. Moreover, fracture force studies (0.36 ± 0. 02 N for DAB and 0.24 ± 0.02 N for CL) and *in vitro* skin penetration studies in pig cadaver skin demonstrated adequate mechanical strength of both MNs to penetrate the skin. To analyze the activity of ScaA, dissolved ScaA solutions from ScaA-MNs formed by both DAB and CL were incubated with immune splenocytes, and the amount of secreted interferon (IFN)-γ and the % of IFN-γ producing CD4+ and CD8+ T cells were measured (Fig. 13**C**). MNs prepared by CL produced significantly higher amounts of INF-γ and a higher % of IFN-γ producing T cells, indicating a higher antigen activity. The authors suggested the difference in the solidification method (air-blowing by DAB or vacuum drying by CL) was most likely the crucial factor affecting the activity but further studies should be conducted. *In vivo* immunization studies performed in mice comparing IgG antibody levels after injection of ScaA-MN produced by CL and ID injection of ScaA solution with adjuvant, have shown strong responses produced by the MNs but at lower levels than the ones produced by ID injection. These results stem most likely from the absence of adjuvant within the MNs. Nonetheless, ScaA-MNs enhanced the long term stability of ScaA antigen compared to the ScaA solution. MNs stored for 4 weeks at RT were able to maintain their antigenic activity (% of INF-γ CD8 T cells remained the same), while ScaA solution stored for 4 weeks presented a significantly lower % of INF-γ CD8 T cells (Fig. 13**D**).



Please cite this article in press as: T. Bauleth-Ramos et al., Materials Today, (2023), https://doi.org/10.1016/j.mattod.2022.12.007

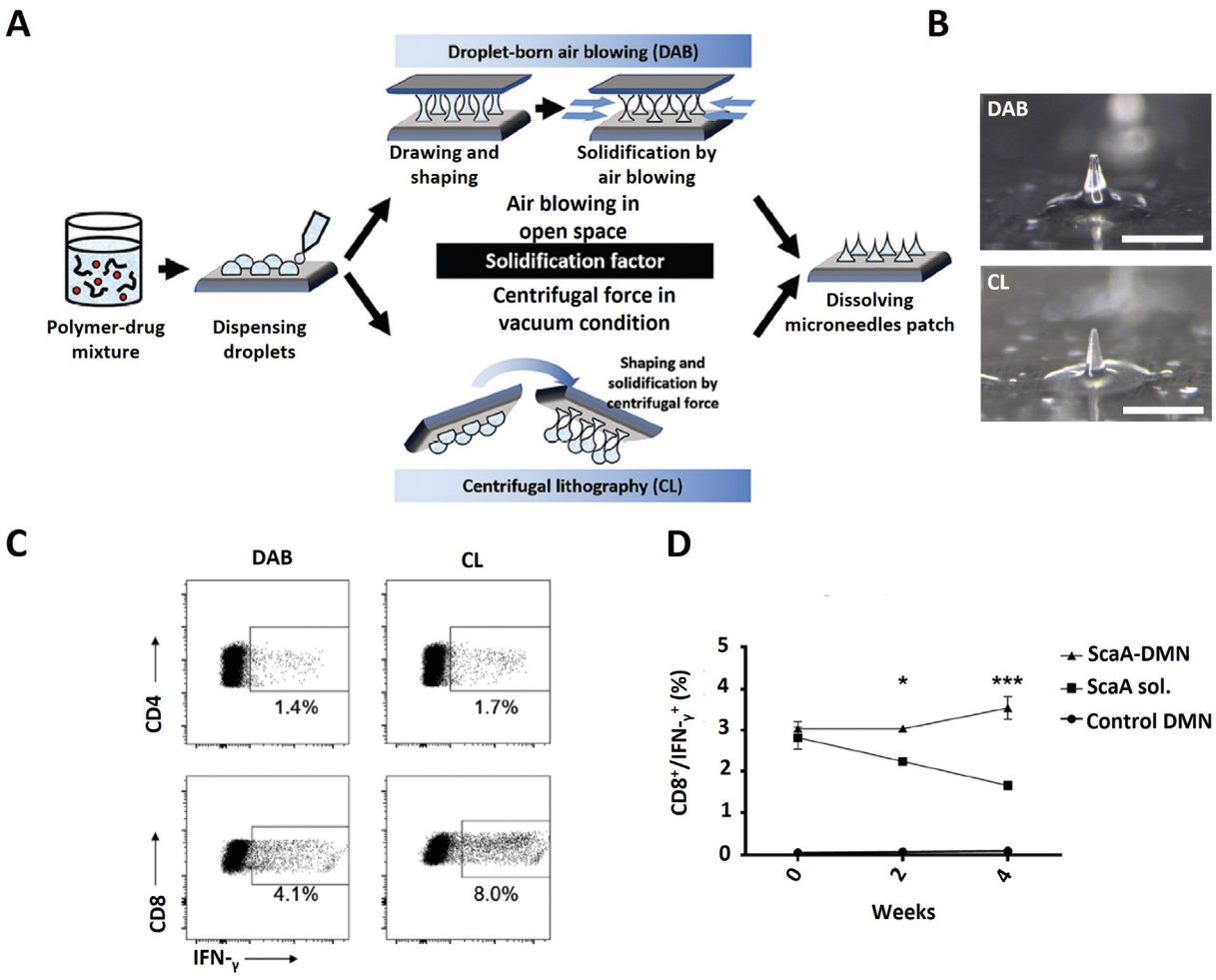


**FIGURE 13**

(A) Scheme of MNs production by DAB and CL. (B) Images of MNs fabricated by DAB and CL. Scale bar: 500 μm. (C) Antigenicity of ScaA from MNs prepared by DAB and CL: Percentage of INF-γ producing CD4+ and CD8+ T cells. (D) Long-term stability of ScaA-loaded MNs. Percentage of INF-γ producing CD8+ T cells after stimulation with MNs, ScaA loaded MNs, and ScaA solution after 0-, 2- and 4-weeks storage. Adapted and reprinted with permission from ref. [128]; Copyright 2018, John Wiley & Sons, Inc.

*Peptides and proteins*. Proteins are among the most important biotherapeutics in the clinical setting due to their high specificity and low toxicity compared with chemical drugs, and the possibility to be applied in the treatment of numerous diseases like cancer, genetic and immune disorders, cardiovascular diseases, infections, and others [130]. Examples of therapeutic proteins include monoclonal antibodies (mAbs), hormones, vaccines, cytokines, fusion proteins, enzymes, anticoagulants, and growth factors [131]. Despite its wide applicability, protein administration faces many challenges due to its physicochemical characteristics. Proteins are large molecules (can reach over 100 kDa), hydrophilic, highly charged, and have a secondary and tertiary structure that needs to be maintained to keep their activity. Therefore, proteins cannot easily cross biological barriers and are subjected to denaturation and degradation by enzymes and different stress factors such as temperature, pH, and osmolarity. In fact, the most common delivery routes for therapeutic protein application, parenteral and oral, are still associated with instability, short half-life, low bioavailability, and poor patient compliance. Transdermal delivery, and specially achieved using MNs, is seen as a viable alternative delivery. Therefore, when formulating dMNs for protein and peptide delivery, it is necessary to take into consideration all the above-mentioned factors. To successfully deliver proteins and peptides dMNs need to completely dissolve upon insertion, as poor dissolution leads to poor bioavailability, to release the payloads from the matrix, and to conserve their physicochemical stability both within the MNs matrix and upon release.

Different strategies can be applied to load proteins into dMNs in order to increase their loading, improve their stability, control their release and consequently enhance their activity. These strategies are discussed in this section to provide an overview for better understanding of possible designs for future delivery of proteins by MNs.

*Protein-matrix interactions*. One advantage of dMNs is that their polymeric matrix can incorporate proteins themselves, keeping their stability and controlling their delivery. Recently, Panda *et al.* [132] have compared lysozyme, an enzyme of size 14 kDa, loaded dMNs made with three different commonly used polymers, PLGA, HA, and PVP. All MNs were prepared by micromolding casting method, in which the tip of the MN was filled with a mix-



Please cite this article in press as: T. Bauleth-Ramos et al., Materials Today, (2023), https://doi.org/10.1016/j.mattod.2022.12.007

ture of lysozyme solution and polymer, and the backing layer constituted of protein-free polymer. As result of the hydrophobic nature of PLGA, an organic solvent was used to dissolve PLGA and the lysozyme in order to prepare PLGA dMNs. All MNs were successfully fabricated, as confirmed by SEM imaging, and can penetrate Parafilm into a depth of *ca*. 160 μm. However, PLGA MNs required higher puncture force compared to PVP and HA. Using sodium dodecyl sulfate–polyacrylamide gel electrophoresis (SDS-PAGE) and circular dichroism, the authors have shown that the enzyme retained its structural integrity after being loaded into the dMNs and stored for 30 days at 25 °C and 60% relative humidity (RH). After 90 days of storage, the lysozyme concentration diminished by *ca*. 10% in all the MNs. *Ex vivo* studies in rat skin have shown a much faster dissolution and lysozyme release of HA and PVP dMNs (50 % in ~20 min) compared to PLGA dMNS (30% in 72 h). The different release profile was ultimately translated into a faster enzymatic activity, measured by lysis of cells, of HA and PVP dMNS compared to PLGA dMNs.

In another study, bleomycin, a glycopeptide antibiotic used for HS treatment, has been loaded into HA dMNs [133]. In this study, HA MNs were produced by the two-step casting micromolding method. A bleomycin and HA solution was firstly casted into a PDMS mold under vacuum, followed by the casting of a HA solution to form the backing layer. The produced MNs, with a height of 650 μm, were able to load approximately 100 μg of bleomycin per patch. However, due to its high solubility, bleomycin diffused through the HA matrix, being only *ca*. 20% present in the needles while the rest accumulated in the base. Bleomycin-loaded MNs were mechanically robust and were inserted into porcine skin, which can simulate HS tissue, to a depth of approximately 330 μm. *In vitro* release studies using Franz-diffusion cells showed a burst release, *ca*. 20%, within the first minute and more than 80% release after 30 min, even if most of the bleomycin was located in the base. Interestingly, bleomycin-loaded MNs stored for 6 weeks have shown similar *in vitro* inhibitory effects on HS fibroblasts compared to freshly prepared MNs, and higher than bleomycin solution. These results showed that HA MNs can preserve the stability of bleomycin and the combination can also mediate a stronger antiproliferative effect.

Recently, a model protein, ovalbumin (OVA), was also incorporated into dMNs to improve the delivery of proteins to the posterior segment of the eye [134]. In this study, the authors prepared MNs with different compositions, PVP 40%, PVA 30%, PVP 20% + PVA 15% and HA 2.5%, in an aqueous drug solution of 50% (%w/w). The base layer was formed separately with PVP and glycerol. To form the patch, the polymer + OVA solution was casted into silicone molds and the pre-formed dry base layer was added on the back of the polymeric solution and the molds placed in positive pressure chamber (5 bar). The MNs were then dried for 24 h at RT. The height of all MNs was *ca*. 750 μm. Moreover, except for the HA MNs, all MNs had a height reduction of less than 15% after application of a force of 3 N/array, indicating sufficient mechanical strength for insertion. Furthermore, all MNs, with exception of the HA MNs, were able to be inserted into porcine sclera up to 75% depth of the MNs height. Also, through SDS-PAGE and ELISA kits, the authors concluded that the incorporation of OVA in the MNs did not affect its bioactivity. *Ex vivo* studies performed in Franz-diffusion cells, have shown that MNs with PVP and PVA could permeate over 80% of OVA after 48 h. Moreover, PVP only MNs showed a significant increase in OVA permeation when compared to eye drops and needle free patches.

Other studies have also shown the applicability of dMNs for the delivery of proteins and proved their use in clinical settings [135–138].

*Nanoparticles*NPs, as a result of their many advantages, have been applied to enhance the delivery of different protein therapeutics to assist in vaccination, control autoimmune diseases, inflammation, *etc*. Thereby, their combination with dMNs is also highly advantageous for the delivery of biotherapeutics.

Recently, immune checkpoint inhibitors have attracted much attention in improving cancer immunotherapy. Considering this, Wang *et al*. [139] encapsulated aPD-1 and glucose oxidase (GOx) in pH-sensitive dextran NPs, which were loaded in HA dMNs for cancer immunotherapy. The MNs were formed by *in situ* polymerization with UV-light due to its mild conditions which avoid the denaturation of the antibodies and preserve their stability. The bioactivity of aPD-1 after MN formation was estimated to be approximately 90%. The formed conical MNs, with 600 μm height and 300 μm diameter base, contained the loaded NPs distributed within the tips (Fig. 14**A-C**). The MNs had good mechanical properties (failure force of 0.38 N/ needle), being successfully inserted into mouse skin to a depth of *ca*. 200 μm. By encapsulating aPD-1 together with GOx inside dextran NPs, an enzymatic-mediated controlled release was promoted as GOx converts glucose into gluconic acid, leading to a more acidic environment and consequent degradation of the NPs. In fact, the formed spherical NPs with a size of 250 nm and aPD-1 loading of 7.1 wt-%, changed conformation and diminished their size when in contact with PBS buffer containing glucose at a normoglycemic level. Consequently, a sustained release profile of aPD-1 from the MNs was observed in the presence of GOx, while there was barely any release in its absence (Fig. 14**D**). Finally, the authors performed *in vivo* studies in a B16F10 mouse model of melanoma, comparing the efficacy of MNs + NPs with aPD-1 + GOx, MNs + NPs with aPD-1, MNs + GOx, and free aPD-1, after single administration in the tumor site. The developed system MNs + NPs with aPD-1 + GOx has shown remarkable efficacy, inhibiting tumor development, improving the survival rate to 40% after 40 days, and inducing high T-cell infiltration (Fig. 14**E-F**). Contrariwise, all the other groups showed poor tumor inhibition and lower T-cell infiltration. These results stem from the fact that the developed system can sustain the release of aPD-1 and induce its accumulation in the tumor area. The authors also tested the co-loading of aPD-1 with aCTLA4 (another checkpoint inhibitor), which had a synergistic effect resulting in disease-free survival of 70% of treated mice for 60 days.

In a follow-up work from the same group, NPs made of a covalently conjugated drug (1-methyl-DL-tryptophan; 1-MT) to HA were prepared to form an amphiphilic structure to load aPD-1 [140]. The formed NPs were then loaded into HA MNs for combinatorial treatment of melanoma. In this study, aPD-1 was also successfully encapsulated into the NPs (4.5%, w/w), and sustainedly released from NP-loaded MNs in the presence of hyalur-



Please cite this article in press as: T. Bauleth-Ramos et al., Materials Today, (2023), https://doi.org/10.1016/j.mattod.2022.12.007

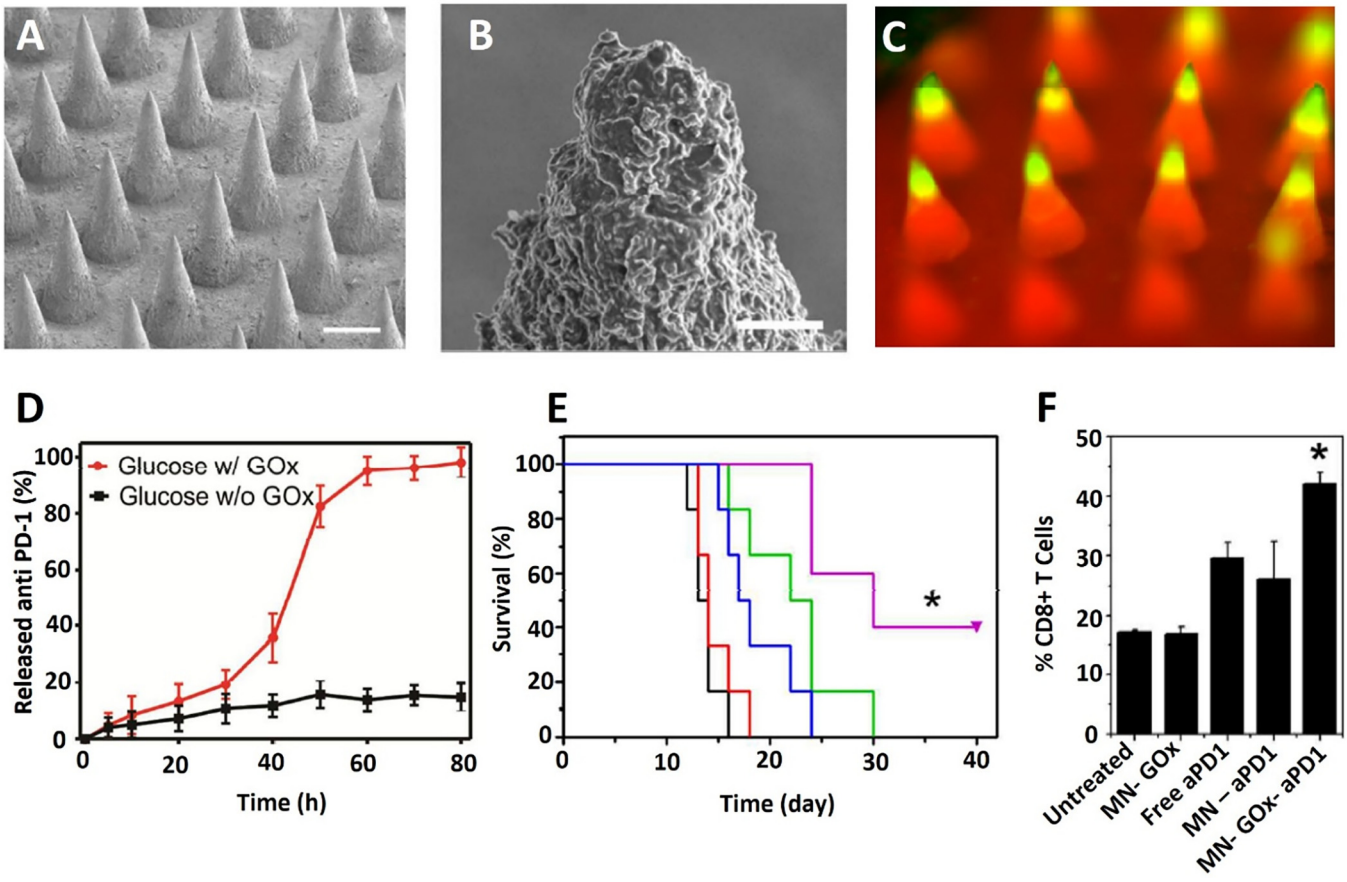


**FIGURE 14**

(A) SEM image of MNs. Scale bar: 200 μm. (B) SEM image with higher magnification to observe the NPs within the MNs. Scale bar: 5 μm. (C) Fluorescence image of MN loaded with FITC. Scale bar: 200 μm. (D) *In vitro* release of aPD-1 from MN in presence of glucose and at 37 °C. (E) Survival curve after treatment with GOx-aPD1-MN (purple), aPD-1-MN (blue), GOx-MN (red), free aPD-1 (green), and untreated (black). (F) Percentage of tumor-infiltrating CD8+ T cells. Adapted and reprinted with permission from ref. [139]; Copyright 2016, American Chemical Society.

onidase. When applied to B16F10 melanoma-bearing mice, the NP-loaded MNs enhanced the accumulation and retention of 1-MT and aPD-1 at the tumor site. This translated into delayed tumor growth, 70% survival at 40 days post-treatment, increased CD8+ T cell recruitment, and a decrease of CD4+FoxP3+ regulatory T cells recruitment.

Antigens are other biotherapeutics being widely used nowadays in immunotherapy for vaccination purposes or to restore immunological tolerance in autoimmune diseases. It is known that drug delivery devices like NPs and MNs can be used to control their release, improve their targeting, protect them from degradation, enhancing their effect. One successful example of the combination of antigens with NPs and dMNs was a study performed by Zaric *et al*. [141]. In this study, antigen-loaded NPs were combined with dMNs to enhance antigen stability and retention in the skin and consequently improve vaccine immunogenicity. The model antigen OVA was loaded in PLGA NPs prepared by a double emulsion technique. The prepared OVA-NPs had an approximate size of 358 nm and 36% of OVA encapsulation efficiency. The OVA-NPs loaded dMNs were produced by micromolding. An OVA-NP suspension was mixed with a solution of Gantrez AN-139 (copolymer of methylvinylether and maleic anhydride, PMVE/MA) and subsequently casted into a silicone mold. After centrifugation and drying, a solution of blank PMVE/MA was casted into the mold to form the base plate. The formed MNs dissolved completely after 15 min of being inserted into mice skin *in vivo*, depositing the NPs in the dermis layer at a depth between 80 and 130 μm. Interestingly, application of blank MNs or MNs loaded with blank NPs into mice ears induced an inflammatory reaction, observed by significant recruitment of monocytes and neutrophils to the area of application. Moreover, 72 h after application of fluorescently labeled NPs loaded MNs, 20% of the dendritic cells (DCs) present on the auricular draining lymph-nodes were fluorescently tagged and corresponded to emigrating skin DCs ($CD11c^{+}MHCII^{high}$), showing the ability of the developed system to deliver the NPs vaccines to DCs. When using OVA-NPs loaded MNs, only the emigrating skin DCs ($CD11c^{+}MHCII^{high}$) isolated from the proximal auricular lymph nodes were able to stimulate OVA-specific T cell proliferation and elevated production of IFN-γ, suggesting a localized delivery of the NPs by the MNs. To analyze the benefits of delivering OVA by NPs loaded MNs, the authors performed several *in vivo* experiments. In the first experiment, $CD11c^{+}$ DCs were isolated from auricular lymph nodes and co-cultured with OVA-specific OT-I T cells after immunization with MNs loaded either with blank NPs, OVA-NPs, or soluble OVA. After



Please cite this article in press as: T. Bauleth-Ramos et al., Materials Today, (2023), https://doi.org/10.1016/j.mattod.2022.12.007

7 days, OVA-NPs induced significant proliferation of $CD8^+$ T cells when compared to soluble OVA. However, after 14 days, there was an equal response among both groups. The authors stipulate that the use of NPs prolonged the retention of the antigen in the skin. In the second experiment, MNs loaded with either OVA-NPs or soluble OVA were prepared and stored at ambient conditions for 4, 6, and 10 weeks before being used to immunize mice. While up to 4 weeks of storage both groups developed comparable $CD8^+$ T cell response, after 4 weeks the response of soluble OVA MNs declined. However, the OVA-NPS MNs response was maintained throughout the duration of the study, which is indicative of an enhancement of antigen stability when loaded within the NPs. Finally, after proving the enhanced retention and stability of OVA when using OVA-NPs loaded MNs, the authors studied their efficacy *in vivo*. In fact, the developed system induced potent vaccination in mice, inhibiting the growth of tumor cells after immunization, and also protecting them from viral challenges.

Although the encapsulation of antigens within NPs and delivery through dMNs can be advantageous due to their increased stability and enhanced antigen retention in the skin, several challenges still need to be taken into consideration and surpassed in their production. For example, recently, Lima *et al*. [142] encapsulated PLP139-151 peptide (PLP) into PLGA NPs which were loaded into dMNs for multiple sclerosis treatment. PLP was successfully loaded (loading of 20%) into spherical PLGA NPs with *ca*. 200 nm diameter. The release profile of PLP from the prepared NPs was characterized by an initial burst release with 60% released in the first minutes, followed by a sustained release over 20 h. PLGA NPs loaded MNs were prepared by micromolding technique, producing needles with an average height of 550 μm and a base width of 180 μm. The loading of NPs into the MNs induced a more sustained release of PLP. Yet, the presence of large amounts of polymer generated by the MNs dissolution hampered the detection of the peptide, with only 2% being quantified. Thus, when designing peptide release studies from dMNs, it is necessary to consider that the release might be limited by peptide-polymer interactions. In another study by Monkare *et al*. [143], different production aspects and their impact on the formulation of antigen-NPs loaded MNs were also addressed. OVA and poly(I:C) (PIC) adjuvant were co-encapsulated within PLGA NPs, which were loaded in HA dMNs for intradermal immunization. OVA-PIC-NPs were prepared by a double emulsion technique, producing NPs with approximately 170 nm diameter, and a similar loading capacity of *ca*. 3% (w/w), for both OVA and PIC, corresponding to a weight ratio of 1:1 of the encapsulated doses. The dMNs were successfully prepared by a micromolding method, casting the NPs and HA polymer mixture into PDMS molds, followed by the application of vacuum, centrifugation, and drying. Different weight ratios of HA to NPs (1:1, 1:4, and 1:10) were tested, and all formed MNs with equal dimensions. However, fluorescent microscopy images have shown that, as a result of the high viscosity of HA, only in the lower ratios (1:1 and 1:4) the NPs were homogeneously distributed and concentrated in the tips. Moreover, to understand how the production of the MNs would affect the stability and release of the NPs, the authors measured the size and PDI of different samples after dissolution in PBS. The tested samples were, NP-loaded MNs, NP suspension, a physical mixture of NPs and HA, and a physical mixture of NPs and HA dried either at 37 °C and ambient pressure or at RT and in a vacuum. While physically mixing HA with the NPs barely affected their size and PDI (Z-average of 169 nm, PDI 0.23), the drying process had a significant impact. Vacuum and RT dried samples showed a small increase in size and PDI (Z-average of 201 nm, PDI 0.27); however, samples dried at 37 °C and ambient pressure were highly aggregated (Z-average > 1000 nm, PDI 0.61). After dissolution from the MNs, both size and PDI presented increased values (Z-average of 287 nm, PDI 0.35), which indicated some aggregation. Taking into consideration the results of this experiment, the observed aggregation after MN dissolution was stipulated to stem from the centrifugation step to concentrate the NPs in the MNs tips during MN production. *Ex vivo* studies in human skin confirmed that despite all, the formulations could successfully penetrate the skin, and the ratio HA:NPs significantly influenced the MNs dissolution, with an increased amount of HA being directly correlated to a higher dissolution. Using the ratio 1:4, which produced better results *ex vivo*, the authors compared the delivery of free OVA-loaded MNs to OVA-loaded NPs-MNs in mice *in vivo*. MNs loaded with NPs showed a significantly increased delivery efficiency, being able to deliver 24% of their dose while free OVA-loaded MNs were only able to deliver 0.16%. *In vivo* immunization studies were also performed to compare the efficacy of the dMNs compared to hollow MNs. IgG1 and IgG2 responses in mice were measured after treatment with OVA-PIC-NPs, free OVA-PIC solution, or a mixture 1:1 of both, delivered either by hollow or dMNs. No major differences were detected when administering free solution or the mixture. However, when administering OVA-PIC-NPs, hollow MNs induced a significantly stronger IgG1 and IgG2 response than dMNs, inducing robust CD8+ and CD4+ T-cell responses while dMNs only induced minimal CD4+ response. The authors suggested that these results stem from the incapacity of the dMNs to deliver NP in non-aggregated form. In another recent study by Guo *et al*. [144]OVA was fused with hepatitis B core (HBc) protein virus like particles and loaded together with mesoporous silica (MSN) NPs in chitosan MNs, to produce a cancer vaccine. In this study, the MNs were prepared by a 2 step micromolding method, by firstly casting a chitosan solution mixed with OVA-HBc and MSN NPs into PDMS molds followed by centrifugation and vacuum, followed by casting a chitosan solution (8 wt%) and drying at 37 °C overnight. The produced MNs had a height of approximately 500 μm and were able to sustain compressive force up to 320 mN/needle before failure, which allow successful skin insertion [145]. Moreover, they were shown to be able to be inserted *in vivo* and released the particles overtime. The used OVA-HBc and MSN particles had size of *ca*. 33 nm and 50 nm, respectively, were biocompatible up to a concentration of 400 μg/mL and were able to induce DC maturation and OVA presentation *in vitro*. Furthermore, the developed MNs enhanced the efficacy of vaccination, as seen by the increment of CD4+ T cells and CD8+ T cells in the lymph nodes and of the level of antigen-specific antibody, when compared to subcutaneous injections of the different formulations. Moreover, the developed MNs were also able to induce higher antitumor therapeutic effect, inhibit-



Please cite this article in press as: T. Bauleth-Ramos et al., Materials Today, (2023), https://doi.org/10.1016/j.mattod.2022.12.007

ing tumor growth and prolonging survival of mice injected with tumor cells after being vaccinated with the MN system.

Overall, these studies show that while NPs can be used to deliver peptides/proteins together with dMNs, different aspects of the formulation process need to be taken into consideration and to be further studied.

*Powder-loaded MNs.* One interesting strategy to improve the stability of biotherapeutics and enhance their loading is to apply them directly in powder form, avoiding the reconstitution process which is known to partially degrade the therapeutics and limit their loading capacity [146]. Taking this into consideration, recently Kim *et al*. [147] loaded insulin powder within dMNs to increase their loading capacity and diminish its activity loss. The dMNs were fabricated by a micromolding method, by adding CMC to PDMS molds followed by centrifugation and drying. This method produced MNs with an average length of *ca*. 800 μm, a base width of *ca*. 451 μm, and concave-shaped microcavities. The microcavities were formed due to the shrinkage of CMC and worked as reservoirs in which insulin powder was loaded, producing powder-carrying MNs (PCMs). Interestingly, by varying the concentration of CMC (5–20%, w/v), the size of the cavities could be controlled without affecting the MNs morphology (Fig. 15**A**). Lowering the CMC concentration increased the size of the cavities and consequently enhanced the insulin loading, observed by testing the loading of calcein as a model drug (Fig. 15**B**). However, only MNs with CMC concentration equal or over 10% displayed adequate mechanical properties, successfully penetrating pig skin *ex vivo*. Furthermore, PCMs have shown an enhanced loading, 2.5-fold higher, compared to CMC MNs in which insulin was loaded in a saturated solution (20 mg/mL in 0.1 M of HCl) (Fig. 15**C**). *In vivo* studies in fasted mice model comparing PCMs with insulin-solution loaded MNs and subcutaneous (s.c.) Injection, have shown a higher $T_{max}$ and lower $C_{max}$ in both MNs compared to the s.c. injection. Bioavailability was also lower for PCMs and insulin-solution MNs (61.51% and 62.22%, respectively) compared to sc. injection (100%). This indicated a partial absorption of insulin, probably derived from metabolism or degradation due to the slow release. The authors suggested that increasing dissolution would most likely also increase the bioavailability. Moreover, after 4 and 8 weeks in storage at 25 °C, PCMs showed higher insulin stability than insulin-solution MNs (Fig. 15**D**).

*Additives/stabilizers.* Another approach to stabilize and enhance protein activities within dMNs is the incorporation of additives in the dMNs formulation. For example, small sugars, such as disaccharide trehalose, which is known to prevent dehydration-induced protein unfolding during lyophilization, have been applied in MNs to preserve the biological activity and improve the pharmacokinetic profile and bioavailability of biotherapeutics [148–150]. In a systematic study, Mistilis *et al*. [81] tested 61 different formulation excipients and their combinations, to develop thermostable dMNs to deliver influenza antigens. The effects of the drying process, buffer salts, surfactants, and stabilizers on the stability of the influenza vaccine were assessed. The antigen-loaded MNs were prepared by micromolding, casting under vacuum a solution of antigen with 1% sodium CMC (NaCMC,w/v) and 10% of stabilizer (w/v) into PDMS molds. After drying, a backing solution constituted of PVA, sucrose, and water was casted into the mold under vacuum, and the MNs left to dry for 2 days before demolding. To study the influence of drying and buffer salts, the vaccine was prepared with NaCMC and trehalose, dissolved in different buffers, and exposed to different temperatures (4 °C, 25 °C, and 40 °C). Interestingly, the used buffers played a crucial role in the activity of the antigen when subjected to different temperatures. When the MNs were prepared in PBS or potassium diphosphate, the increase in temperature led to a significant activity loss. Yet, there were barely any changes when using 4-(2-hydroxyethyl)-1-piperazineethanesulfonic acid (HEPES) or ammonium acetate. Furthermore, the inclusion of surfactants into the formulation also led to remarkable, *ca*. 50%, activity loss. Taking these results into account, the authors performed the rest of the tests using ammonium acetate buffer, no surfactant, and a drying temperature of 25 °C. From 61 different combinations of stabilizers, after sequential stability studies performed from 1 to 4 weeks at 40 °C to narrow the ones which would grant further stability, the best combinations were trehalose/sucrose, sucrose/arginine, and arginine/heptagluconate which have shown no significant activity loss over 1 month. After 3 months at 25 °C, these 3 combinations have not shown a significant loss of activity. However, after 6 months, only arginine/heptagluconate has shown no significant activity loss. These results showed a successful development of a thermostable influenza vaccine using arginine and heptagluconate as stabilizers. In a follow-up study by the same group, the three best formulations (trehalose/sucrose, sucrose/arginine, and arginine/heptagluconate) were further tested for stability at 25 °C and 40 °C over 24 months and after being exposed to different stress factors (*e.g.*, high temperature, multiple freeze–thaw cycles) [151]. In this study, the arginine/heptagluconate combination was again able to provide enhanced stability, with no activity loss and no changes in the appearance detected after 12 months of storage at 25 °C. *In vivo* immunization studies in mice have shown stronger immunization of MN patches both fresh and stored for 13 months at 25 °C when compared to intradermal (ID) injection of fresh vaccine. Additionally, ID injection of vaccine reconstituted from the stored MN patches produced similar immune responses to fresh ID injection. After exposing the developed MN patches to different stresses, 60 °C storage for 4 months, five freeze–thaw cycles in 24 h, and electron beam sterilization no significant losses of activity were observed. These results confirm that the addition of stabilizers is a powerful strategy to enhance the stability and activity of antigens and should be considered when developing MNs.

Overall, MNs can encapsulate and deliver proteins with high efficiency, and enhance their stability without refrigeration [72,151–154].

*DNA and RNA.* Gene therapy is the use of genetic material (DNA and RNA) to correct defective genes or induce gene alterations (*e.g.*, knock down, knock-in, overexpression), to achieve a therapeutic goal [155,156]. Thus, gene therapy represents a powerful tool for the management and treatment of numerous diseases. However, its success has been hampered by the difficulties of its administration and the need to surpass the multiple extra- and intracellular barriers within the body, which contribute to high degradation and clearance of the genetic material, and its



Please cite this article in press as: T. Bauleth-Ramos et al., Materials Today, (2023), https://doi.org/10.1016/j.mattod.2022.12.007

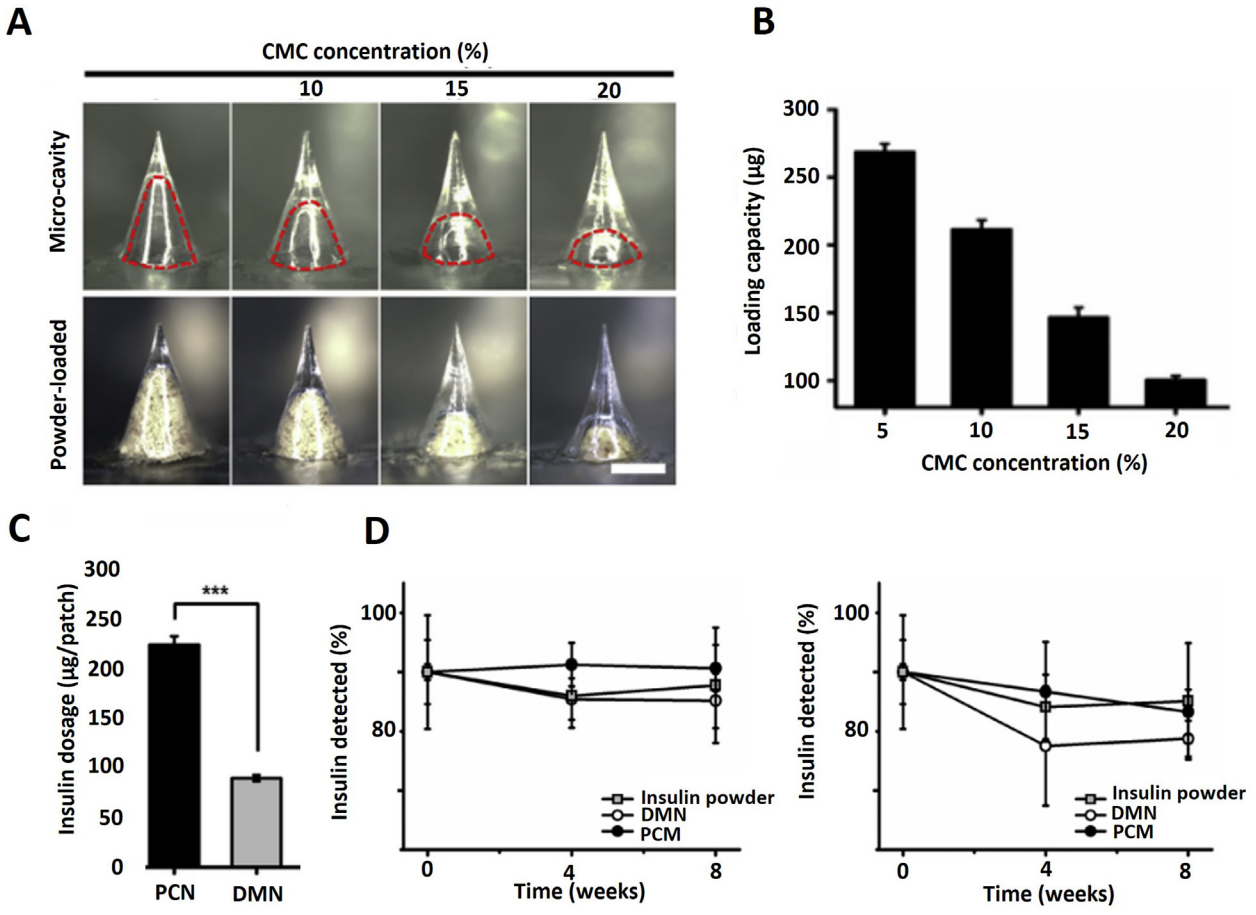


**FIGURE 15**

(A) Microscopic images of PCMs fabricated with different concentrations of CMC, before and after calcein loading. Scale bar: 1 mm. (B) Loading of calcein powder in PCMs fabricated with different concentrations of CMC. (C) Insulin loading of PCMs and insulin-solution MNs. (D) Long-term stability of insulin powder, PCMs, and insulin-loaded MNs after storage at (a) −20 °C and (b) 25 °C. Adapted and reprinted with permission from ref. [147]; Copyright 2020, Elsevier B.V.

consequent poor delivery and efficacy [157,158]. MNs, due to their many advantages can be used to overcome these hurdles surpassing the skin barrier and delivering the genetic material to the immune cell-rich environment of the epidermis, which is of great advantage for example for vaccination purposes. Moreover, since dMNs deliver the genetic material in solid form, it diminishes its use in solution, avoiding degradation by enzymes (DNase and RNase). Nonetheless, due to the labile nature of the genetic material, it is vital to consider the used materials and the manufacturing methods of MNs to guarantee the bioactivity of the DNA/RNA, the maximum loading efficiency, and to ensure a proper release [157].

*Nanoparticles*NPs can increase the stability of DNA/RNA and its applicability by surpassing biological barriers, improving endocytosis, inducing endosomal escape, and ultimately increasing their transfection efficacy [159]. Thus, their combination with dMNs to deliver gene therapies is extremely attractive.

For example, in a recent study, Yang *et al*. [160] compared the preparation of PVA dMNs loaded with naked Ebola DNA (EboDNA) or PLGA-PLL/γPGA NPs coated with EboDNA (EboDNA/NPs) to produce a thermostable vaccine against Ebola. The prepared PLGA-PLL/γPGA NPs, with a diameter of 87 nm, and a surface-charge of 52 mV were able to load 0.24 μg of EboDNA per μg of NPs. These NPs enhanced the stability of the DNA protecting it from DNase I-derived degradation. Furthermore, in an *in vitro* setting, plasmid DNA encoding green fluorescent protein (GFP-pDNA) coated NPs were able to induce robust transfection in HeLa cells contrariwise to naked GFP-pDNA. This way, the authors have proved that the use of NPs enhanced both DNA stability and its transfection efficiency. The PVA/PVP dMNs were prepared using a micromolding method by the sequential casting of a PVA solution (containing, or not, either EboDNA/NPs or naked EboDNA) followed by casting of a PVA/PVP solution to form the backing layer. Casting solutions with higher concentrations of NPs and DNA led to an increment in the amount of NPs and DNA within the MNs, but reduced their encapsulation efficiency. This result was attributed to a higher viscosity observed at higher concentrations of DNA and NPs which hindered the payloads to flow to the MNs from the bases. Additionally, MNs prepared by casting of EboDNA/NPs solution had a 3.2-fold higher EboDNA encapsulation when compared to MNs prepared with naked EboDNA (*ca*. 48 μg and 14 μg, respectively). The authors suggested that the observed difference can derive from the lower viscosity observed for EboDNA/NPs solu-



Please cite this article in press as: T. Bauleth-Ramos et al., Materials Today, (2023), https://doi.org/10.1016/j.mattod.2022.12.007

tion compared to naked EboDNA solution, at the same EboDNA concentration. Compression studies showed that while the produced MNs had adequate mechanical properties for skin insertion, MNs with EboDNA/NPs had higher failure force than the ones produced with naked EboDNA. After the dissolution of MNs loaded with either naked EboDNA or EboDNA/NPs, it was observed that contrariwise to naked EboDNA, the EboDNA / NPs transfection efficiency in HeLa cells was similar to the one produced by EboDNA stock solution and also retained its supercoiled structure. Furthermore, MNs were able to enhance the long-term stability of EboDNA at 37 °C for 6 weeks, compared to naked EboDNA and EboDNA NPs solutions. *In vivo* studies in mice treated with naked EboDNA or EboDNA NPs by either IM administration or with MNs, have shown similar total antigen-specific IgG titers for EboDNA/NPs, by both administration methods, to IM naked EboDNA (positive control), and significantly lower titers for naked EboDNA using MNs. Moreover, vaccination with EboDNA/NPs loaded MNs induced a higher neutralization activity against GP-pseudovirions. This study represents a valuable example of the important contribution NPs can have to improving the loading of DNA into MNs, while enhancing its stability and its efficacy.

NPs can also be used to improve RNA loading and delivery using MNs. Wang *et al*. [161] loaded small interfering RNA (siRNA) into mesoporous silica-coated upconversion NPs (UCNPs@m$SiO_2$) to be delivered by HA dMNs. The NPs used in this study were chosen due to their ability to load and protect siRNA in the mesoporous silica shell, and to simultaneously monitor their diffusion due to the optical properties of the UCNPS. The NP-loaded MNs, prepared by a micromolding approach, had an average length of 800 μm and encapsulated 200 μg of NPs. These MNs were successfully inserted, *ex vivo,* in mouse ears and pig skin to a depth of *ca*. 235 μm. Silencing the expression of transforming growth factor-beta type 1 receptor (TGF-βRI) with siRNA suppresses connective tissue growth factor (CTGF) mRNA expression. Thus, to analyze the delivery of siRNA by the developing system, HA-MNs encapsulating NPs co-loaded with siRNA TGF-βRI (0.17 nmol/mg of NPs) and the molecular beacon for CTGF (0.31 nmol/mg of NPs), were inserted into 3D agarose gel with hypertrophic scar fibroblasts (which overexpress CTGF) (Fig. 16). MNs loaded with NPs without siRNA were used as control. After administration of the system with siRNA, it was observed a 44% decreased fluorescent intensity, by confocal microscopy, and a 50 % decreased expression of CTGF mRNA, by reverse transcription-quantitative polymerase chain reaction (RT-qPCR) analysis, in comparison to the control. These results suggested the successful delivery of siRNA by the NPs loaded MNs.

*Complexes/Polyplexes*Another strategy to protect genetic material from degradation and enhance its loading and transfection efficiency, is mixing DNA/RNA with cationic polymers to form polyplexes, or with acid cationic peptides to form cationic NPs [162–164]. Ali *et al*. [165] have applied this strategy using a 30 amino acid cationic peptide delivery sequence (RALA), developed by their group, to produce RALA-DNA NPs and load them into dMNs for vaccination purposes. By mixing HPV16 E6 or E7 (E6/E7) DNA with RALA, RALA-E6/E7 NPs were produced due to electrostatic interactions. This method produced highly stable NPs with a size below 100 nm, a surface charge of *ca*. 30 mV, and capable of preserving DNA integrity when exposed to serum or heparin. PVP MNs loaded with RALA-E6/E7 NPs were produced by a micromolding technique. After being released from freshly prepared or 28 days stored MNs, RALA-E6/E7 NPs successfully transfected NCTC-929 cells, *in vitro*, while naked E6/E7 DNA did not. This indicated that the formed complex with RALA was crucial to keep the DNA stability within the PVP matrix. The same observation was also obtained by other studies from the same research group [166,167]. *In vivo* experiments, in which mice were immunized with naked E6/E7 DNA or RALA- E6/E7 NPs either by IM injection or using MNs, have shown higher antibody titers for the RALA-E6/E7 NPs groups. Furthermore, mice immunized with RALA-E6/E7 NPs loaded MNs induced higher TC-1 cytotoxic response and enhanced IFN-γ secretion, indicating a more robust cytotoxic T cell-mediated immune response. In a prophylactic setting, RALA-E6/E7 NPs loaded MNs delayed tumor growth in comparison with other groups and 44% of the vaccinated mice from this group never developed tumors, compared to only 22% and 11%, after RALA-E6/E7 NPs IM vaccination and naked DNA vaccination, respectively. In a therapeutic setting, RALA-E6/E7 NPs loaded MNs induced complete regression of tumors in two out of nine mice, while RALA-E6/E7 NPs by IM and naked DNA-loaded MNs induced complete regression of tumors in one out of nine mice. The other strategies did not affect tumor growth. This study showed the importance of the RALA-DNA complex to preserve the DNA stability within MNs and increase its efficacy. A follow-up study by the same group, in which four different polymeric matrices (PVA 9–10 kDa, PVA 13–23 kDa, PVP 58 kDa, and PVP 360 kDa) were used to prepare the MNs loaded with RALA-DNA, has shown that the matrix critically affects the DNA stability and its loading [166]. In this study, transfection efficacies of RALA-DNA released from PVP MNs (*ca*. 13%) were lower than the ones released from PVA MNs (*ca*. 40%), which is explained by a greater loss of the supercoiled DNA conformation within the PVP matrices. Moreover, MNs made of PVA 9–10 kDa had higher amounts of DNA in the baseplate and needles and were able to deliver more DNA *in vivo* (12.5 μg) compared to PVP 58 kDa (10.9 μg), PVP 360 kDa (9.6 μg) and PVA 13–23 kDa (8.6 μg). Nonetheless, the amount of DNA per MN was still considered deficient. Thus, another approach employed by Cole *et al*. [168], was to lyophilize the RALA-DNA NPs in order to increase its loading within the PVA 9–10 kDa matrix of the MNs. Prior to MNs formation, lyophilization of RALA-DNA without using a cryoprotectant led to DNA damage with observed loss of the supercoiled conformation, seen by gel electrophoresis, and consequent significant loss of transfection efficacy *in vitro*. By adding 5% (w/v) trehalose prior to lyophilization, the transfection efficacy was maintained. Nevertheless, when loaded into PVA MNs, an approximately 25% loss of transfection efficacy was still observed, which was attributed to the manufacturing process (*e.g.*, drying conditions). The use of lyophilized NPs led to a 3.2-fold higher loading of DNA (57.3 μg of DNA/MN), compared to fresh NPs (17.7 μg of DNA/MN). When applied to mice, *in vivo*, the produced MNs loaded with lyophilized NPs delivered approximately 50 μg of DNA. These results showed an improvement of the loading and approximately 4-fold higher delivery capacity (~52 μg *vs*.



Please cite this article in press as: T. Bauleth-Ramos et al., Materials Today, (2023), https://doi.org/10.1016/j.mattod.2022.12.007

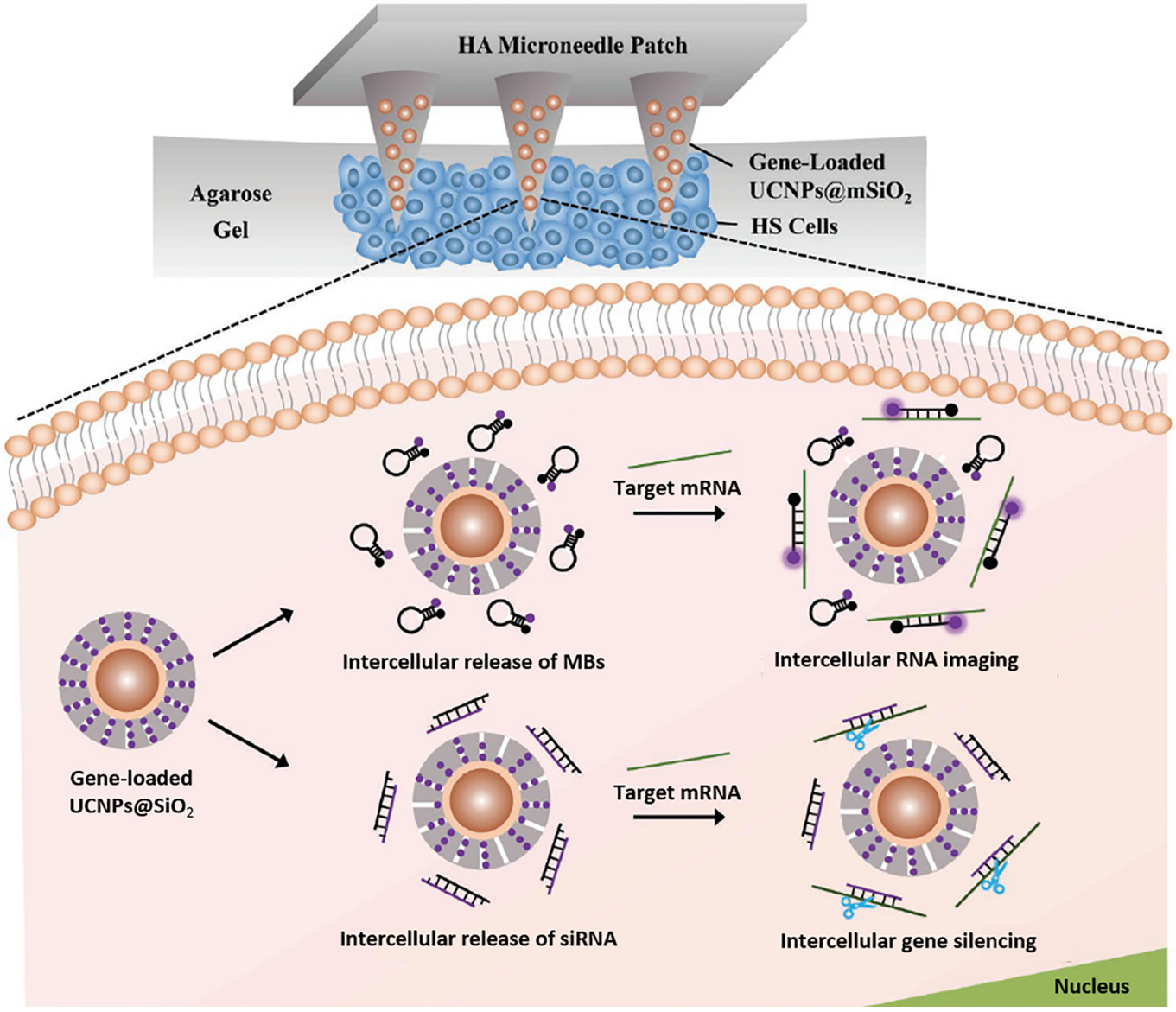


**FIGURE 16**

Schematic of the delivery of siRNA by HA-MNs loaded with UCNPs@mSiO$_2$ containing siRNA and molecular beacon. Adapted and reprinted with permission from ref. [161]; Copyright 2020, John Wiley & Sons, Inc.

~12 μg) of this formulation, compared to the previous studies from the same group. Furthermore, as observed in previous studies, NPs loaded MNs were able to evoke an antigen-specific humoral response and were capable of reducing tumor burden in a mouse tumor model.

One interesting one-step strategy to concentrate the loading of DNA in the needle's region and increase its stability and efficacy was designed by Liao *et al*. [169]. In this study, MNs were formed by micromolding technique, casting firstly a solution of PVA and branched polyethylenimine (bPEI), followed by centrifugation and vacuum to produce a thin positively charged layer in the needle's region (Fig. 17**A**). After, DNA solution was casted into the molds under vacuum, forming 56 nm polyplexes with the positively charged bPEI. Finally, a PVA (30%)/PVP (10%) backing layer was added by casting this solution into the molds under vacuum and pressure with a roller. MNs without bPEI pre-coating were also prepared to serve as control. The produced MNs with height of 860 μm (560 μm needle + 300 μm tapered base), were mechanically robust to penetrate the skin and had a quick dissolution profile (~90 % after 30 sec and total dissolution within 6 min). The bPEI pre-coating of the MNs led to higher localization of the DNA in the needles and *ca*. 1.5-fold higher encapsulation amount, compared to non bPEI pre-coated MNs (Fig. 17**B**). Moreover, bPEI also increased the encapsulation efficiency, specially at higher casting doses of DNA. When loaded within the MNs, DNA stability increased as after 60 days at 45 °C, despite partial transformation into nicked-circle form, transfection efficiency remained the same. Contrariwise, naked DNA was completely degraded and lost its activity after 7 days under the same conditions. *In vivo* studies in mice have shown higher administration of DNA from bPEI pre-coated MNs (*ca*. 93%) compared to non-coated (*ca*. 76%). Additionally, bPEI pre-coated MNs induced stronger immune response than non-coated MNs, even after 1 month storage at



Please cite this article in press as: T. Bauleth-Ramos et al., Materials Today, (2023), https://doi.org/10.1016/j.mattod.2022.12.007

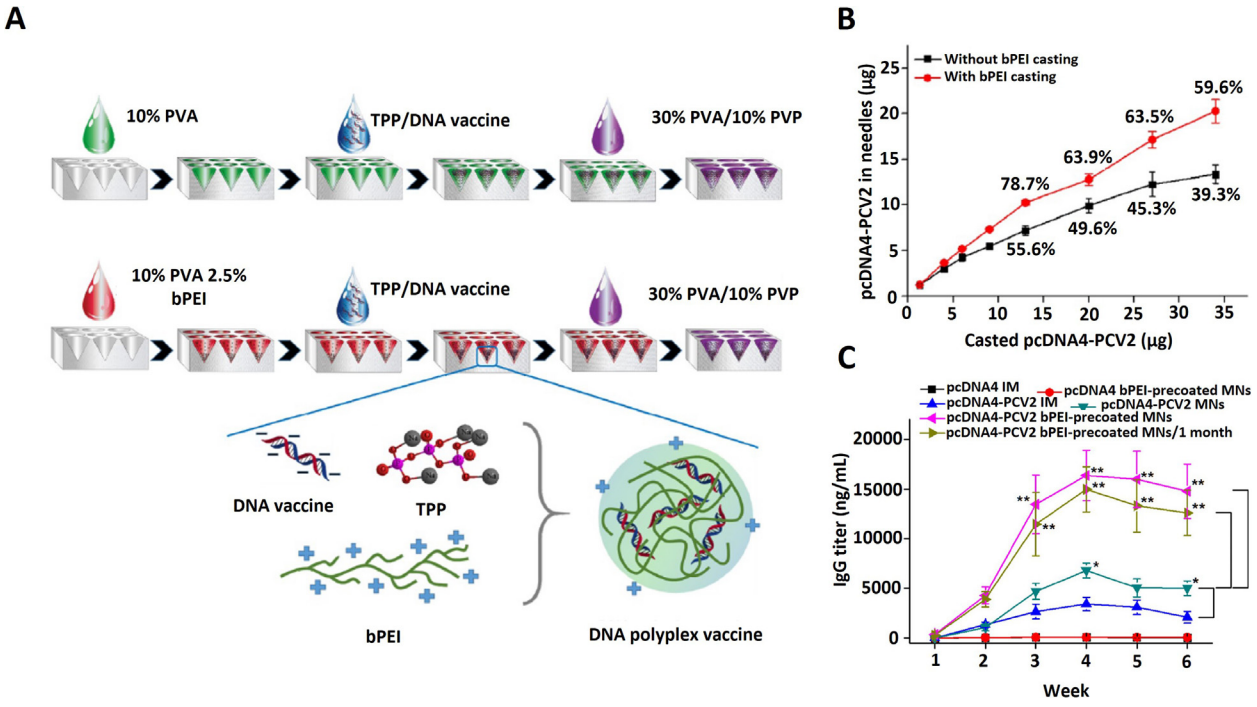


**FIGURE 17**

(A) Scheme of DNA-loaded MN production with and without bPEI pre-coating. (B) DNA amount in the needle region of the MNs with or without bPEI pre-coating, after casted in different concentrations. (C) Serum Immunoglobulin G responses after vaccination with different treatments. Adapted and reprinted with permission from ref. [169], Copyright 2017, Ivyspring International Publisher.

45 °C (Fig. 17**C**). These results show the ability of polyplexes to increase the loading and stability of DNA in MNs, and to increase their transfection efficacies.

Taking into consideration the temperature-sensitive nature of the mRNA, recently, Yu *et al.* [170], have designed cryoMNs loaded with mRNA (either complexed with PEI or loaded in liposomes) to surpass this hurdle. In this study, the MNs were prepared by micromolding by casting a solution of HA mixed with mRNA (mRNA:HA mass ratio of 1:100) into PDMS molds, followed by centrifugation and freezing at −80 °C for 15 min. Afterwards, the MNs were demolded and kept at −80 °C until further use. The produced MNs had pyramidal shape, a height of *ca.* 900 μm, and were able to be inserted into skin up to a depth of 386 μm. However, the MNs were only able to keep their structure up to 1.5 min when at RT, which allows their administration within 1 min after removal of the freezer. Through gel electrophoresis, the authors were able to confirm the stability of the mRNA after MN production, as the restored mRNA did not show any differences in terms of size and concentration compared to the original one. When applied in mice *in vivo*, cryoMNs loaded with PEI-mRNA luciferase, produced significantly higher luminescent signals up to 48 h when compared to vehicle controls and cryoMNs loaded with liposome-mRNA luciferase. The authors explain this difference due to possible structural changes in the liposomes when frozen, while the same is not expected in PEI-mRNA complexes.

*Matrix interaction*Usually, NPs are the most common carrier for mRNA delivery. However, several reports have shown that naked mRNA can be effectively delivered subcutaneously and efficiently translate its encoded protein [171–173]. Taking this into account, Koh *et al.* [46] have developed a proof of concept mRNA-loaded PVP dMN for immunotherapy. In this study, PVP (10 kDa) MNs were prepared by a micromolding technique, casting a mRNA/PVP mixed solution into PDMS molds of different sizes (400 μm, 800 μm, and 1000 μm), followed by centrifugation and drying. The mRNA loading amount was found to be limited by its solubility in the highly concentrated PVP solution as, for concentrations above 5 μg/μL, a gel was formed which prevented its diffusion into the molds. After loading into the dMNs, mRNA remained stable for up to 15 days as the recovered mRNA kept its physical integrity, observed by gel electrophoresis, and induced comparable levels of luciferase expression after subcutaneous injection. Moreover, the loading of mRNA did not significantly affect the MNs mechanical strength as the force–displacement profile remained the same in the presence of variable loadings of mRNA. While the produced MNs could successfully penetrate mouse and human cadaver skin, confocal microscopy images have shown that MNs with higher size were able to deliver the mRNA to greater depths. Further, *in vivo* transfection studies have also shown higher transfection efficiencies and expression kinetics associated with MNs with bigger sizes. Using MNs with height of 800 μm and loaded with OVA mRNA, the authors have shown that the developed mRNA patch was able to delay tumor progression and induce anti-OVA antibodies in the same level as an OVA mRNA subcutaneous injection in a E.G7-OVA mouse tumor model.

*Extracellular Vesicles.* Extracellular vesicles (EVs) despite being promising therapeutics and drug delivery systems, their clinical application is still limited due to stability issues, loss of biological



Please cite this article in press as: T. Bauleth-Ramos et al., Materials Today, (2023), https://doi.org/10.1016/j.mattod.2022.12.007

functions and delivery to the target site of action. In a recent study, EVs from human adipose stem cells (hASC-EVs) were loaded in HA-based MNs to increase their stability and enhance their transdermal delivery for skincare applications [174]. In this study, the MNs were formed by micromolding method, by casting a solution containing 7.5% (w/v) HA and hASC-EVs ($1.1 \times 10^{10}$ particles/mL) into silicone molds under vacuum, followed by addition of a second layer with 20% (w/v) HA and drying at 25 °C. The formed MNs had pyramidal shape and a height of *ca*. 600 μm. Confocal microscopy imaging showed concentration of the EVs in the tips of the needles. Moreover, using nanoparticle tracking analysis, the authors observed that the EVs retained their structure after dissolution of the MNs, and calculated a loading of $2 \times 10^7$ particles/patch. Furthermore, when loaded in the MNs and stored at 4 °C, there was only a decrease of less than 15% of particle concentration, in comparison with over 65% decrease when stored in PBS solution. By performing *in vitro* studies, it was shown that the EVs loaded in the HA MNs retain their bioactivity over 6 months of storage at 4 °C, as they induced fibroblast proliferation, migration and collagen generation equivalent to fresh EVs, while EVs stored in PBS lost their activity within 2 months. The produced MNs were able to be inserted into mouse skin, dissolving completely in 20 min. Also, when administered in mice, EVs administered by MNs were released for 7 days comparably to only 4 days when administered through intradermal injection. Moreover, after administration in the dorsal skin of mice, EVs administered by MNs significantly increased both the thickness of the dermis layer and the expression of collagen type I, and enhanced fibroblast proliferation in comparison with intradermal injection and topical administration. These results have shown the capacity of MNs to increase the stability of EVs and also to enhance their administration.

## Modification of drug release

Conventionally, dMNs are formulated with water-soluble polymers such as HA, PVP, gelatin, starch, or sugars [4]. Thereby, they are usually presenting a burst release profile due to the complete dissolution of the polymeric structure in MNs within seconds to minutes [190]. This type of bolus administration is useful when a rapid onset of action is demanded (*e.g.*, when treating migraine or for pain relief) [191,192]. However, a sustained payload release profile is desired to reduce the side effects, the frequency of MN administration and for better therapeutic efficacy, as in the case of vaccines or insulin [190]. In this section, we will analyze the conventional strategies proposed to extend the payloads' release from dissolving MNs, as well as the use of state-of-the-art stimuli-responsive materials.

### *Controlling the release rate*

The conventional strategies to control the release rate in dissolving MNs focus on the following 4 approaches, the selection of polymers with slower dissolution in water, the loading of micro/nano-particles, the use of hydrophobic polymers, or the cross-linking of hydrophilic polymers (Fig. 18) [193].

#### *Hydrophilic polymers with a slower dissolution rate*

Solutions of chitosan at high concentrations formulated into dMNs can sustain the release of the payload for up to 28 days [35,56,59]. To enable this prolonged release, the payload was added to a chitosan gel (9 wt-%). However, the mechanical properties of the chitosan gel are not optimal for the complete insertion of the MNs within the skin. Thereby, a supporting array patch of PVA/PVP was added to the design to improve the insertion: PVP/PVA dissolve within minutes in the skin, leaving the slowly dissolving chitosan gel tips in the skin (Fig. 19**A**) [59]. Interestingly, *in vitro* permeability studies on a previous formulation from the same research group showed sustained release for up to 7 days, with 40% or more of the payload released within the first day (Fig. 19**B**) [56]. However, confocal fluorescent images of histological sections showed the presence of the payload at the site of injection up to 14 or 28 days after administration, highlighting the difference between *in vitro* and *in vivo* models (Fig. 19**C**) [56,59].

A dual release profile can be achieved by combining a fast dissolving polymer like non-crosslinked HA with the chitosan gel MNs body (Fig. 20**A**). The fast dissolving tip will release the payload within 120 h, while the chitosan MNs body will continue the release up to 28 days, providing an initial bolus followed by a sustained release (Fig. 20**B**) [35]. The main challenge when formulating this type of MNs is the preparation of chitosan gel solution. The concentration of chitosan required is high (2%, w/v) and needs to be dissolved in acidic conditions (1%, v/v, acetic acid) [56]. Then, the excess of acid has to be removed via extensive dialysis, before filtering the solution and evaporating water to achieve the concentrated gel. The use of acids and the need to concentrate the gel by water evaporation may damage the payload. Thereby, fillers like trehalose and other molecules commonly used in the spray drying process can be added to stabilize the payload [56].

The dissolution rate of other hydrophilic polymers, such as hyaluronan, is dependent on their molecular weight. According to Leone *et al.*, an increase in the molecular weight from 20 kDa to 150 kDa decreases the dissolution rate of the MNs: 20 kDa MNs dissolve within 10 min, while 150 kDa MNs take up to 20 min to dissolve [194]. The balance between the dissolution rate of the polymer and the possibility to form the MNs is quite delicate: a solution of HA with 1.8 mDa MW did not form MNs following the same protocol used for the solutions with the other MW. Also, the polymer MW influences other formulation process parameters, such as the temperature for the drying of the MNs: for the lowest MW tested (4.8 kDa), HA-based MNs required drying at room temperature and did not tolerate drying at +37 °C [194].

Overall, a modulation in the payload's release rate is possible also when using unmodified hydrophilic polymers in the matrix of MNs. An increase in the MW of the polymer prolongs the dissolution rate in the order of minutes, while the choice of appropriate slow dissolving polymers at high concentrations can prolong the release for up to 1 month.

#### *Loading of Micro/Nano-particles*

Another strategy to prolong the dissolution rate of dMNs made of hydrophilic polymers is via the loading of micro/nano-particles within their structure. In this case, the drug release rate is not dependent anymore on the polymeric matrix of the MNs, but on the release rate from the particles [100,139,195]. Thereby,



Please cite this article in press as: T. Bauleth-Ramos et al., Materials Today, (2023), https://doi.org/10.1016/j.mattod.2022.12.007

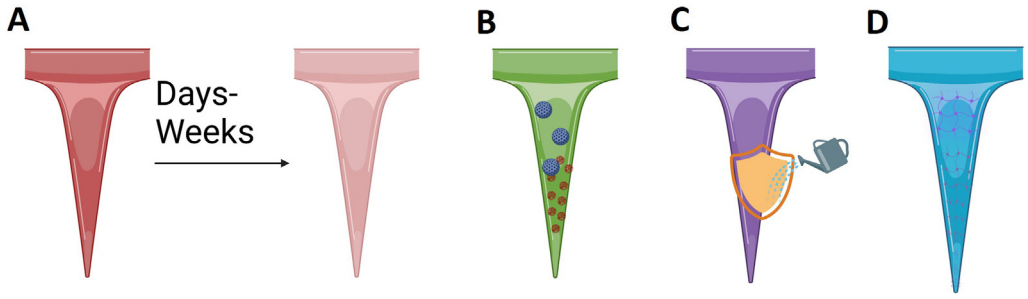


**FIGURE 18**

Schematic of the four main strategies to prolong the release of payloads from dMNs patches. (A) Formulating the MNs from hydrophilic polymers with a slower dissolution rate. (B) Adding micro/nano-particles in the MNs. The release rate of the drug will be determined by the particle and not by the microneedle. (C) Formulating the MNs with water-insoluble polymers. The release rate will be determined by the degradation of the polymers. (D) Formulating MNs by cross-linking of hydrophilic polymers. Created with Biorender.com.

the payload release rate can be fine-tuned to the proposed application by modulating the parameters of the particles. As an example, solid lipid NPs, cubosome-like liquid crystalline NPs, PLGA MPs can sustain the payload release for 2, 14, or up to 30 days respectively [101,196,197].

The formulation of this type of MNs can present some challenges related to the final morphology and strength of the MNs, as well as to the retention of structure from the particles. The distribution of the particles within the MNs depends on the density of the particles and the viscosity of the solution [96]. When the particles are dense, they tend to concentrate on the MNs tip region, particularly when the formulation protocol includes centrifugation (Fig. 21**A**). Furthermore, different microneedle shapes and a different density of the MNs in the array change the sedimentation of the particles. Consequently, the height of the particle layer is controlled by the concentration of the particles: a 50% dilution of PLGA particles resulted in a *ca.* 120 μm difference in the height of the layer containing the particles (Fig. 21**B**) [96]. Interestingly, the wide range of particle size resulted in a homogenous surface of the MNs, contributing to the mechanical strength of the whole structure (Fig. 21**C**) [96].

When formulating lighter and more delicate particles type like liposomes and micelles a strengthening of the particles' structure or changes in the production protocol (*e.g.*, keeping the temperature of the centrifugation at +4 °C to harden lipids) may be needed to maintain the integrity of the structure of the particles [198,199].

In summary, an alternative solution to sustain the release of payloads from dMNs made of hydrophilic polymer matrices is to embed micro- or nano-particles within the MNs structure. The release rate in this case is controlled exclusively by the particles.

*Hydrophobic polymers*

A sustained release of the payload is achievable also when the matrix of the MNs is composed of hydrophobic polymers that slowly degrade in the skin. Polymers like PLA and PLGA present adequate mechanical properties combined with a slow degradation rate, making them suitable for the formulation of MNs tips [193].

These MNs are suitable mainly for hydrophobic payloads which benefit from a slow and long-lasting release, such as hormones or contraceptives [200]. The payload and the polymer are usually dissolved in organic solvents (*e.g.*, N-methlypyrrolidone, dioxane, tetrahydrofuran) and casted in the molds by centrifugation or vacuum [200,201]. The full dMN is prepared by adding a rapidly dissolving backing layer [201]. Adding the dissolving backing layer to the dry MNs results in the formation of a bubble between the two layers which facilitates the detachment of the MNs from the base. The amount of backing layer solution added to the mold impacts the height of the bubble within the MN. Alternatively, to avoid the use of organic solvents, the MNs can be casted by melting the polymer. However, this production method is suitable only for payloads that can withstand heat [193].

The release profile of the payload (levonorgestrel) was controlled and sustained for more than 60 days *in vitro* and was dependent on the amount of ethanol contained in the release medium: if the release medium contained only PBS and Tween-80, the percentage of payload released at 60 days was just 20%; however, when ethanol constituted ¼ of the release medium, all the payload was released within the 60 days [201]. Nevertheless, when the same dMN was evaluated in rats, a higher plasma concentration was recorded in the first 10 days, followed by a decrease which resulted in plasma concentrations lower than the therapeutic level already around day 50. To homogenize the release profile, trehalose can be used as porogen in some of the MNs in the patch, resulting in a faster degradation rate compared to the conventional PLGA MNs [200]. However, this strategy increases the payload plasma concentration in the first days of release, while a slower degradation rate would be favorable to ensure a better therapeutic efficacy.

Overall, an extended-release can be achieved by formulating dMNs with hydrophobic polymers (*e.g.*, PLGA). However, the use of organic solvents or high temperatures in the casting process restricts the range of payloads. Further research is needed to finely tune the degradation profiles of the polymer.

*Postprocessing of hydrophilic polymers*

The postprocessing of hydrophilic polymers already casted in MNs sustains the release of the payloads by rendering the polymers water-insoluble. The crosslinking or the crystallization of the polymers can be achieved chemically or following physical treatment [193]. Polymers like PVA, HA, Gantrez, and alginate



Please cite this article in press as: T. Bauleth-Ramos et al., Materials Today, (2023), https://doi.org/10.1016/j.mattod.2022.12.007

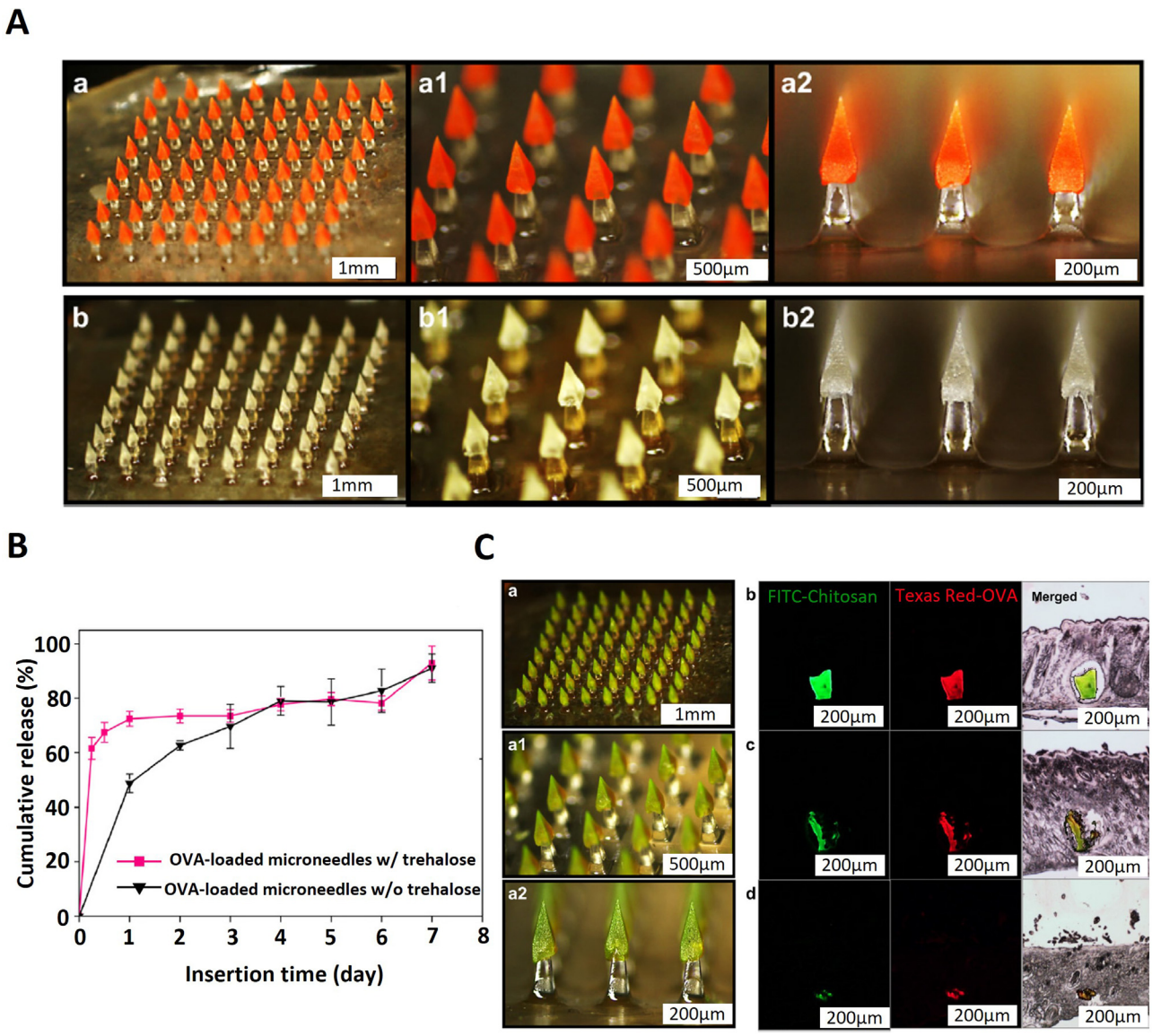


**FIGURE 19**

MN-patches based on slowly-dissolving chitosan tips. (A) Microscope images of (a) rhodamine-loaded chitosan tips and (b) ovalbumin-loaded chitosan tips on a PLGA support array. (B) Release profile of ovalbumin from MN-patches formulated with or without trehalose over 7 days. The release was performed on Franz cells. (C) Degradation of fluorescently-labeled microneedle patches *in vivo*. Chitosan was modified with fluorescein isothiocyanate (FITC, in green in the histological sections), while ovalbumin was conjugated with Texas Red: (a) Microscope images showing the array and the position of the fluorescent chitosan. (b-d) Histological sections at (b) day 1, (c) 1 week, (d) 2 weeks after administration of the MNs into the back of rats show the progressive degradation of the chitosan tip associated with a progressive release of the payload. Adapted and reprinted with permission from ref. [56]; Copyright 2013, Elsevier B.V.

can be chemically crosslinked, while other polymers such as silk fibroin can be crystallized. Importantly, the cross-linking process impacts also the mechanical properties of the polymers and not only their water solubility [193].

Silk fibroin was crystallized via an increase in the β-sheet fraction in the polymer by exposing it to methanol or 2-ethoxyethanol (Fig. 22**A**) [202]. An intermediate modulation in the release profile can be achieved by mixing silk fibroin with proline: adding proline can induce the formation of Silk I crystal structures, without the need to use any additional potentially toxic solvent (Fig. 22**B**) [26]. The release of a payload from fibroin MNs treated with 90% methanol was sustained for more than 96 h; only *ca*. 40% of the loaded insulin was released within 96 h, compared to a complete release from untreated MNs within 24 h (Fig. 22**C**) [26].

In the case of chemical cross-linking, the addiction of the cross-linker forms bonds between polymer chains. The cross-linkers added present functional groups that can react with the polymer chains. Polyethylene glycol (PEG) is commonly used for the cross-linking of Gantrez, while genipin is added to gelatin-based MNs [203]. The concentration of cross-linking agents added determines the degree of cross-linking and the payload release rate [204]. For example, when the degree of cross-linking increases from 35% to 60%, the release time for 100% of the insulin loaded in the MNs increases from 4 h to 14 h [204].



Please cite this article in press as: T. Bauleth-Ramos et al., Materials Today, (2023), https://doi.org/10.1016/j.mattod.2022.12.007

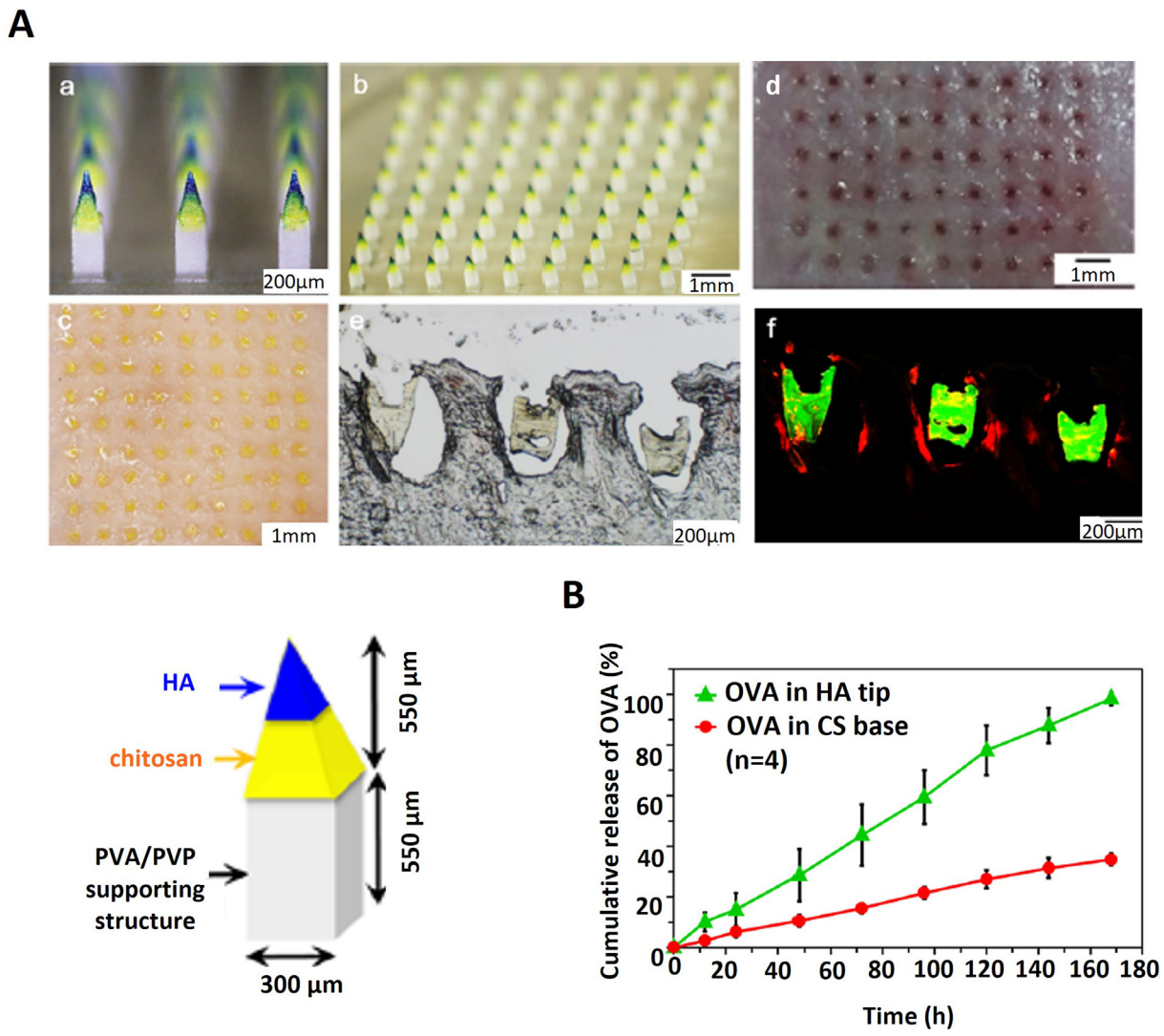


**FIGURE 20**

MN-patch design to achieve fast and prolonged release. (A) The MN-patch was designed to have a rapidly dissolving tip composed of hyaluronic acid, followed by a larger section of chitosan to ensure prolonged release. The structure is then supported by a PVA/PVP structure: (a-b) Microscope images of the MN-patch showing the two different layers on the tips; (c) Efficacy of penetration in porcine skin; (d) Efficacy of penetration in rat skin; (e-f) Histological images of the MNs after application in rat skin; The fluorescent image in figure (f) shows the layer of red HA and the layer of green chitosan both within the skin structure. (B) Release profile of the model payload, ovalbumin, from the HA layer (green) and from the chitosan layer (red). The release from the HA-layer is complete within 170 h, while only 30% of the payload is released from the chitosan layer in the same time frame. Adapted and reprinted with permission from ref. [35]; Copyright 2018, American Chemical Society.

Hydrophilic polymers can be chemically or physically cross-linked into water-insoluble, swellable, structures. The release of payloads is slower compared to the initial polymers, but it is in the time frame of days and not months as for the MNs prepared from hydrophobic polymers and can be adjusted based on the degree of cross-linking or crystallinity.

### *Stimuli-responsive release*

Rapid bolus or sustained release profiles, both achievable with the conventional matrix formulations described above in *Section "Controlling the release rate"*, may not appropriately fit therapeutic indications that require pulsatile payload delivery or a rapidly adapting release rate. The use of bioresponsive/stimuli-responsive polymers in the matrix of dissolving MNs enables the MNs to release the payloads according to changes in the environmental conditions or after external stimuli (Fig. 23).

#### *pH-Responsive release*

The first example of pH-responsive MNs has been developed to promote a faster release of the layer-by-layer films from MNs structures for immunotherapy [205]. The ultrarapid separation of the layers was promoted by the use of a pH-induced charge-invertible polymer, poly(2-(diisopropylamino) ethyl methacrylate-b-methacrylic acid). The charge inversion when shifting from the acidic pH used for the production to the pH of the skin induced a strong repulsion between the different layers composing the MNs, with a complete separation of the structure within 1 min of application (Fig. 24**A**). However, the actual release of antigen and adjuvants continued for *ca.* 3 days after



Please cite this article in press as: T. Bauleth-Ramos et al., Materials Today, (2023), https://doi.org/10.1016/j.mattod.2022.12.007

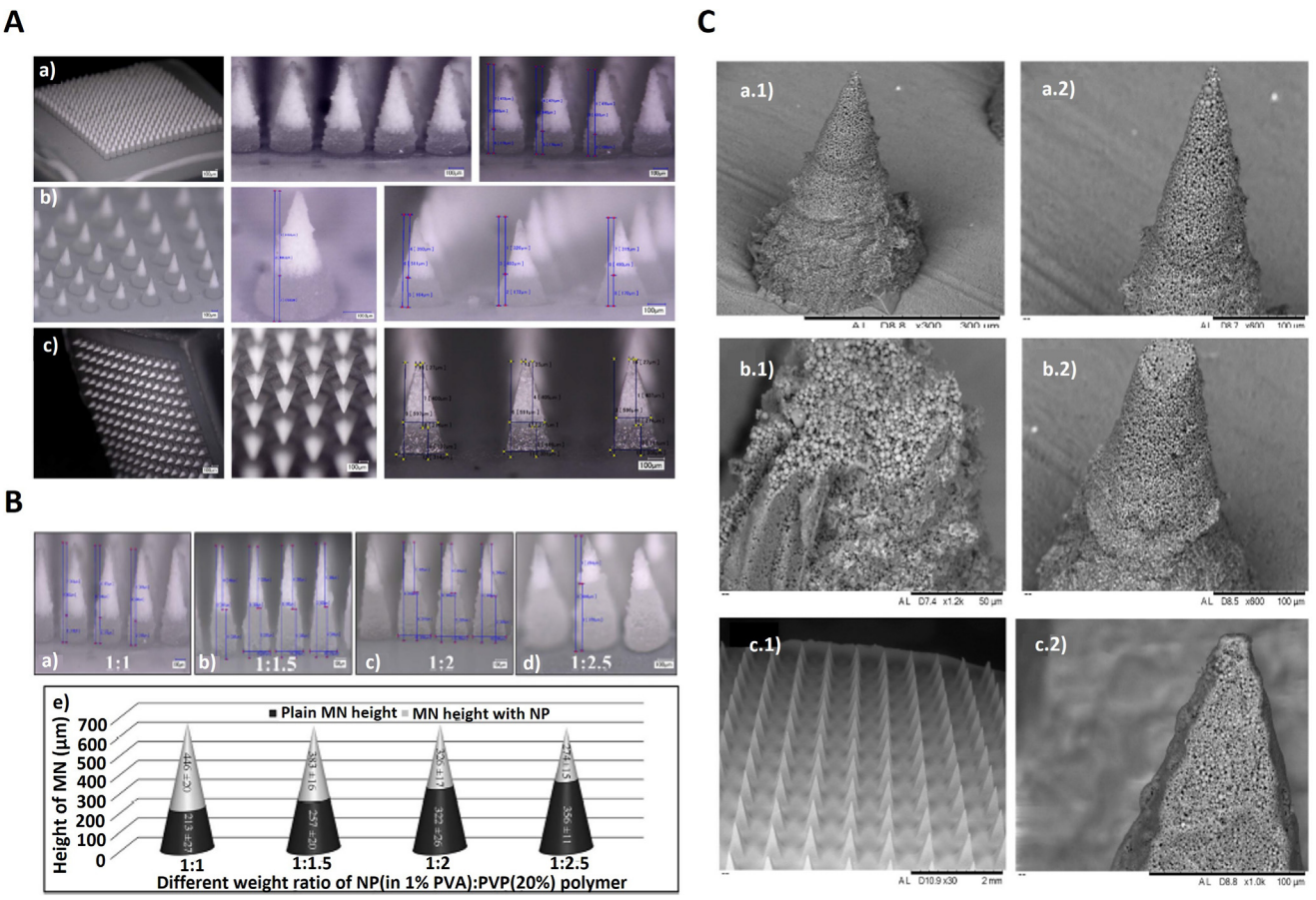


**FIGURE 21**

Formulating MN-patches with solid polymeric NPs. (A) How the different shape of the MN-mold and the density of the MNs in the patch impacts the accumulation of the particles in the tips: (a) conical 19x19 arrays; (b) conical 12 × 12 arrays; (c) pyramidal 14 × 14 arrays. (B) How the different ratio between NPs and polymer influences the height of the nanoparticle deposition layer at the tip of the needle; (a-d) Microscope images of formulations prepared with ratio NPs:PVP between 1:1 and 1:2.5; (e) 3D graph analyzing the differences in the height of the two layers. (C) SEM images of MNs loaded with PLGA NPs. The particles are visible on the surface of the needles, independently from the shape of the needle or the density of the arrays (a) conical 19 × 19, (b) conical 12 × 12, (c) pyramidal 14 × 14. Adapted and reprinted with permission from ref. [96]; Copyright 2017, Elsevier B.V.

administration to mice [205]. Other change-reversing polymers are dimethylmaleic anhydride-modified polylysine and oligo sulfamethazine conjugated poly(β-amino ester urethane) [206,207]. In the case of the modified polylysine, the release of a model DNA molecule was evaluated *in vitro* at pH 5.5, with 30% of the payload released within 3 h, while a control MN presenting only the layers of payload, released only 4% in the same timeframe (Fig. 24**B**) [206]. As for the poly(β-amino ester urethane), 80% of the payload was released within 10 minutes at pH 7.4, with a complete release within 1 h, while at pH 4.0, only 20% of the payload was released in the same timeframe [207].

The pH-responsive release features are provided by pH-induced charged-invertible polymers, which are assembled layer-by-layer with the payload, usually on top of a MNP template (*e.g.*, PCL). The release rate achieved upon pH change is usually quite rapid, in the order of minutes to hours. However, the payload permanence time in the skin may be longer, up to 3 days.

*Light-responsive release*

The light-responsive release is initiated by the shining of a near-infrared (NIR) laser over the MN-patch or the MNs. The matrix of the MNs is composed of hydrophobic polymers with low melting temperatures (*e.g.*, PCL) (Fig. 25**A**) [209]. The light-heat conversion is promoted by the presence of photothermal agents (*e.g.*, NPs, nanocrystals, melanin, plasmonic material) [210]. Thus, the payload release is pulsatile, controlled by laser irradiation and by the duration of laser irradiation. A complete release is achieved in 12 h for MNs irradiated for 2 mins every 2 h, while the whole payload is released within 6 h when the MNs are irradiated for 4 min every 2 h (Fig. 25**B**) [211]. A similar release profile was shown by Chen *et al.*, with a laser-dependent, pulsatile release, in the time frame of hours for the complete payload release [212].

Alternatively, the MNs can serve as a platform to contain photothermal agents in the tumor site, further allowing the combination between immunotherapy and photothermal therapy [213]. The matrix of the MNs was made of crosslinked HA, which maintained the structure for *ca.* 5 days, allowing for repeated laser treatments. Using NIR lasers and photothermal agents, the payload release can be controlled, pulsatile, and on-demand due to the precise control over the polymer matrix melting through the photothermal effect.



Please cite this article in press as: T. Bauleth-Ramos et al., Materials Today, (2023), https://doi.org/10.1016/j.mattod.2022.12.007

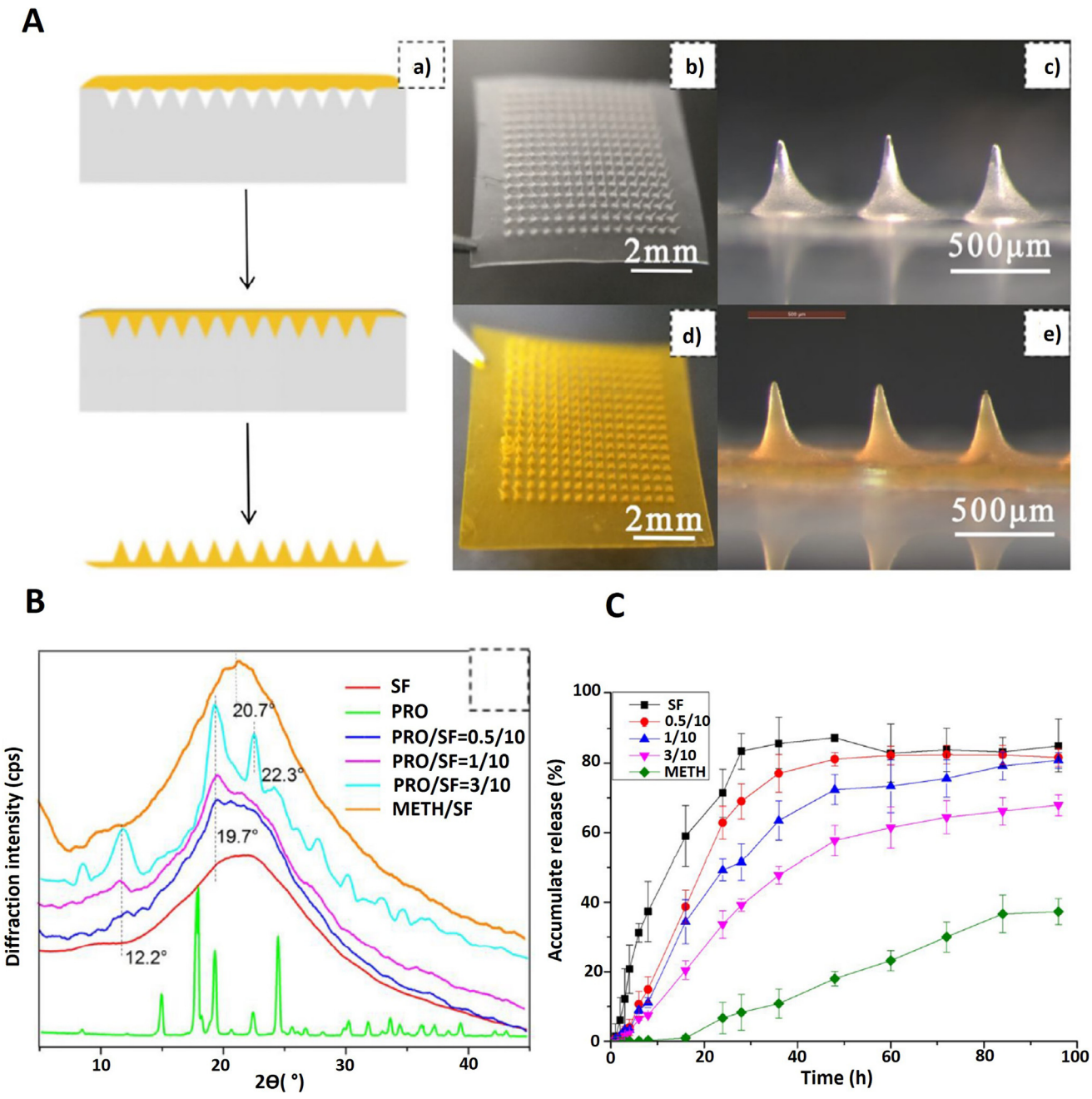


**FIGURE 22**

Crystallization of silk fibroin and its effects on the release profile of a model drug, insulin. (A) Schematic of the preparation process (a) and microscope images of (b-c) silk fibroin MN-patches and (d-e) FITC-insulin-loaded silk fibroin microneedle patches. (B) X-ray powder diffraction spectrum of silk fibroin compared to silk fibroin treated with proline in different ratios or methanol. The ratio 3/10 proline/fibroin presents distinctive crystallization peaks (light blue line). (C) Insulin release profiles from silk fibroin MNs patches before and after modification with proline or methanol. MN-patches formulated with unmodified fibroin complete the release of insulin within 24 h, reaching a plateau. By increasing concentrations of proline, the release rate can be decreased, with formulations in the ratio 3/10 proline/fibroin able to release only 60% of the loaded insulin in 100 h. Finally, the crystallization induced by methanol determines the biggest reduction in the release rate; only 30% of insulin is released within 100 h. Adapted and reprinted with permission from ref. [26]; Copyright 2019, American Chemical Society.

*Temperature and mechanical-responsive release*

The use of photothermal materials, as described in the section above, enables a temperature-responsive release determined by the melting of the polymeric matrix of the MNs. However, the repeated application of laser to induce a pulsatile release may cause undesired skin burns [210]. Alternatively, the temperature-responsive release *via* melting of PCL MNs can be achieved by heating the skin with an electric heating pad [214]. The precision in the pulsatile release recorded with NIR laser was less accurate with a different heating source; nevertheless, the complete release profile was achieved gradually over 12 h [214].

Temperature is the stimuli involved in the release of payload from cryoMNs. CryoMNs are prepared by freezing buffer and



Please cite this article in press as: T. Bauleth-Ramos et al., Materials Today, (2023), https://doi.org/10.1016/j.mattod.2022.12.007

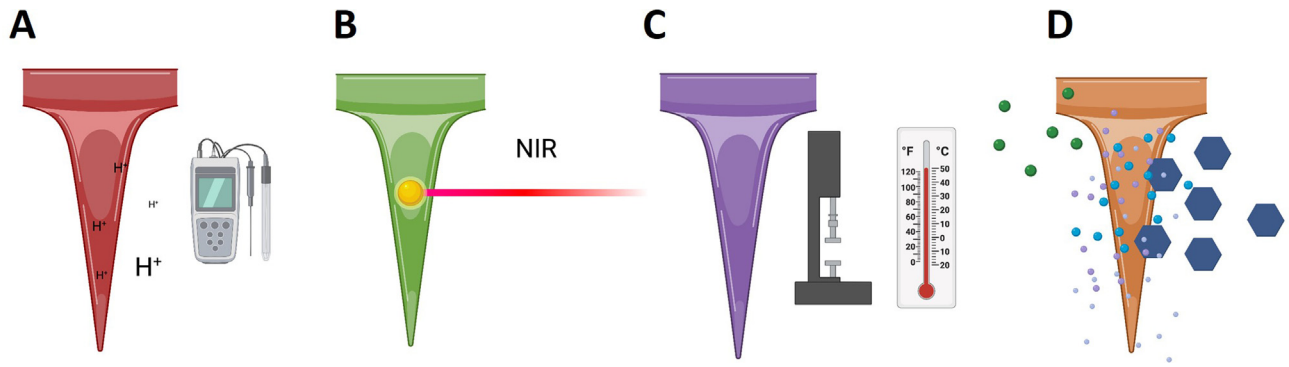


**FIGURE 23**

Stimuli-responsive release from MNs. (A) pH-responsive release. (B) Light-sensitive release. (C) Temperature- or mechanical-responsive release. (D) Glucose-responsive or active release. Created with Biorender.com.

payload and storing them in liquid nitrogen once demolded [215]. The cryo-MNs dissolved within 60 sec in the skin, releasing instantaneously the payload.

The skin mechanical resistance can be exploited to promote the detachment of MNs tips from the body of the patch, allowing for rapid dissolution of the skin-embedded HA tips [216]. This type of fast-detaching, fast-releasing MNs is useful for routine vaccination of pets, for the rapid administration and rapid release of the vaccine. The release is however controlled by the composition of the MNs' tips and not by the mechanical pressure imparted to the patch.

Ultrasounds have been researched to improve the skin delivery of drugs to minimize the effect of inter- and intra-individual differences in the skin of patients, as well as possible difference in the application [217]. The thermal effect and non-thermal effects associated with the application of ultrasounds on the skin increases skin permeability, as well as induces cavitation phenomena with an increase in the amount of payload permeating the skin [218,219]. MNs and ultrasounds are usually applied to the skin in sequence before the drug solution is added on the treated area: this approach can increase the delivery of triamcinolone acetonide within skin keloids, while the treatment with MNs is not effective in reaching the dermis to deliver the drug in the site of action [219]. The application of ultrasounds directly on a MNs patch accelerates the dissolution of MNs (*e.g.*, HA-MNs), increasing the release rate of the payload, due to cavitation-induced microjets in proximity of the needle [220]. The treatment with ultrasounds doubles the amount of payload released from the MNs within 10 min (500 ng vs 250 ng of rhodamine) [220].

The combination of ultrasounds with microneedles is useful to accelerate the release rate of the payloads, as well as improve the skin permeability, resulting in a more homogeneous diffusion of the payload, able to compensate for inter-individual differences in the skin. Further studies are needed to evaluate the duration and intensity of ultrasound treatments to maintain an excellent safety profile while providing improved efficacy of the MNs.

*Glucose-responsive release*

Systems provided with a glucose-responsive feature are particularly useful for the delivery of insulin in diabetes; this type of system allows for a real-time on-demand release based on the tissue glucose concentration [221]. The glucose sensitivity is provided by the encapsulation of glucose oxidase, an enzyme that converts glucose into gluconic acid and hydrogen peroxide. The matrix of the MNs or the insulin-loaded particles are either pH-responsive (*e.g.*, NPs made of dextran derivatives, which dissolves at acidic pH) (), hypoxia-sensitive (responding to a sharp decrease in the concentration of $O_2$) or ROS-sensitive (responding to the concentration of $H_2O_2$) [210]. When pH-responsive particles were used, the responsiveness to the changes in glucose levels was slow because of the buffered environment the MNs were administered into [221]. When comparing the recovery time between pH-sensitive MNs and hypoxia-sensitive MNs, the hypoxia-sensitive can return to basal delivery of insulin within 20 min, while pH-responsive MNs need at least 30 min [221,222]. However, the release profile for both the types of glucose-responsive systems was similar when the glucose concentration was kept at 400 mg/dL, with a complete release of the payload within 20–24 h, as well as in normoglycemic conditions (100 mg/dL) [221,222]. The ROS-responsive MNs showed the slowest reaction time to changes in the glucose concentration, with 40 min needed to return to basal levels [223]. Furthermore, this type of MNs was the fastest in releasing all the insulin when incubated with 400 mg/dL with a complete release in 18 h. All the glucose-responsive systems described above released insulin within 24 h due to MNs loading limitations. A longer release can be achieved by introducing pancreatic β-cells in capsules contained in the backing of the MNs; the glucose oxidase enzyme contained in the MNs acidifies the environment, dissolving the MNs matrix and allowing influx of glucose in the backing layer containing the β-cells, inducing the secretion of insulin for up to 120 h [224].

The concern with using glucose oxidase-based MNs is the possible release of enzymes and ROS in the skin surrounding the site of administration. The enzyme can be easily trapped within the polymeric network or within NPs insensitive to pH, $O_2$, or ROS variation [221,223]. More problematic is limiting the amount of ROS released in the tissue; the enzyme catalase is deputed to $H_2O_2$ purification and has been co-encapsulated within the MNs [222,223]. When catalase was encapsulated in NPs dispersed within the MNs matrix, the efficacy of detoxification was lower than when the enzyme was restricted to a shell layer



Please cite this article in press as: T. Bauleth-Ramos et al., Materials Today, (2023), https://doi.org/10.1016/j.mattod.2022.12.007

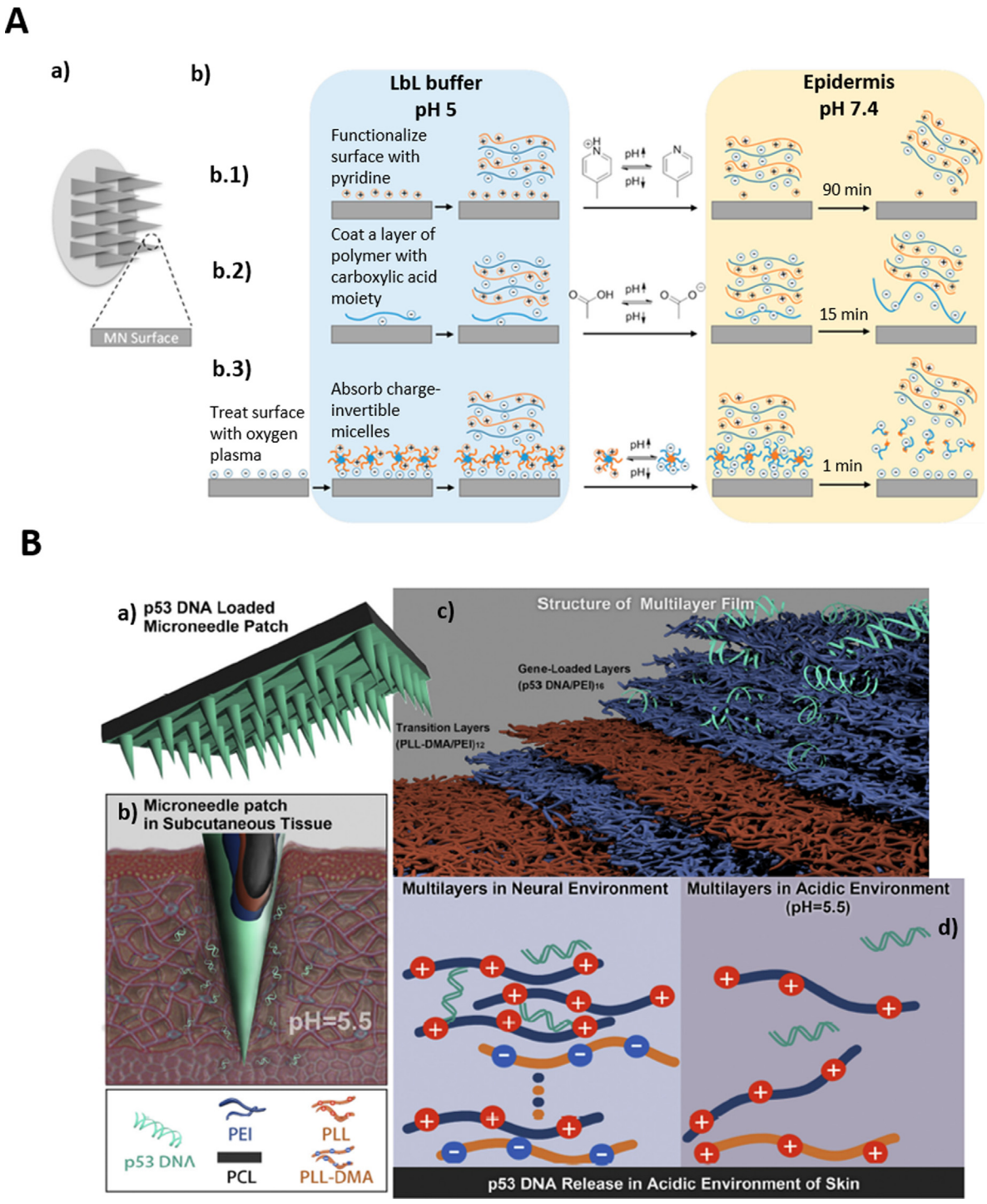


**FIGURE 24**

pH-Responsive MN-patches. (A) Layer-by-layer assembly of the polymer at acid (5.1) pH with fast release at neutral pH (7.4) in the epidermis. The fast release (within 1 min) is promoted by the presence of micelles adsorbed on the surface of the MN that change conformation when changing the pH, promoting the disassembly of the other layers. Adapted and reprinted with permission from ref. [208]; Copyright 2018, American Chemical Society. (B) Tumor microenvironment-responsive MN-patches for the delivery of p53. The MNs are formulated by layer-by-layer deposition of poly L-lyisine (PLL), dimethylmaleic anhydride-modified poly L-lysine (PLL-DMA), and polyethyleneimine (PEI) on PCL structure. The DMA moieties on PLL present a negative charge at neutral pH, with electrostatic interaction with PEI, while at pH 5.5 DMA becomes positively charged, repulsing PEI and determining the release of the payload. Adapted and reprinted with permission from ref. [206]; Copyright 2019, Elsevier B.V.

that $H_2O_2$ molecules needed to cross to diffuse out from the MNs.

To improve the lag-time between the increase in the concentration of glucose and the release of insulin, as well as to avoid the presence of enzymes and the formation of ROS as a byproduct of the reaction, glucose responsiveness was achieved also with the inclusion of boronic acid in the hydrogel (Fig. 26**A**-**B**) [225]. Boronic acid binds glucose releasing as byproduct water



Please cite this article in press as: T. Bauleth-Ramos et al., Materials Today, (2023), https://doi.org/10.1016/j.mattod.2022.12.007

molecules. The binding and subsequent change in the osmolarity of the gel modified the hydration of the hydrogel, promoting the release of insulin for up to 78 h before having to refill the insulin reservoir in the back of the MNs (Fig. 26**C**). Furthermore, the lag-time between glucose challenge and insulin release was in the order of tens of seconds.

The majority of the glucose-sensitive MNs developed so far focus on exploiting the enzyme glucose oxidase to achieve pH-,

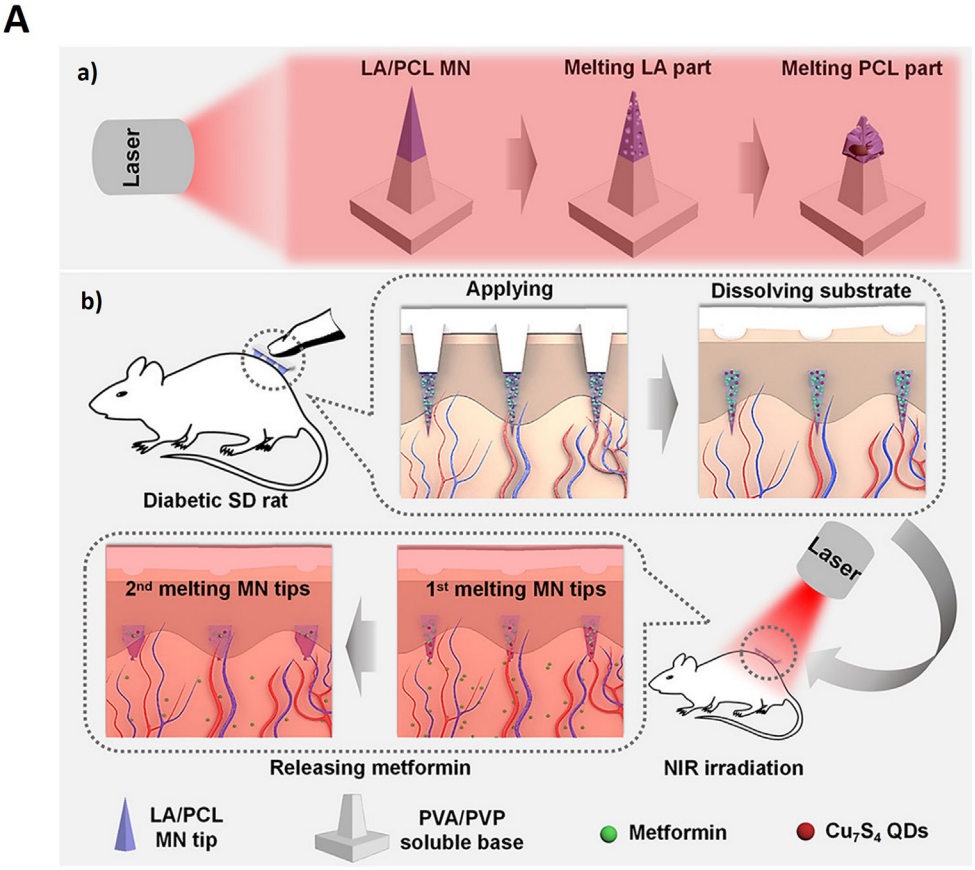


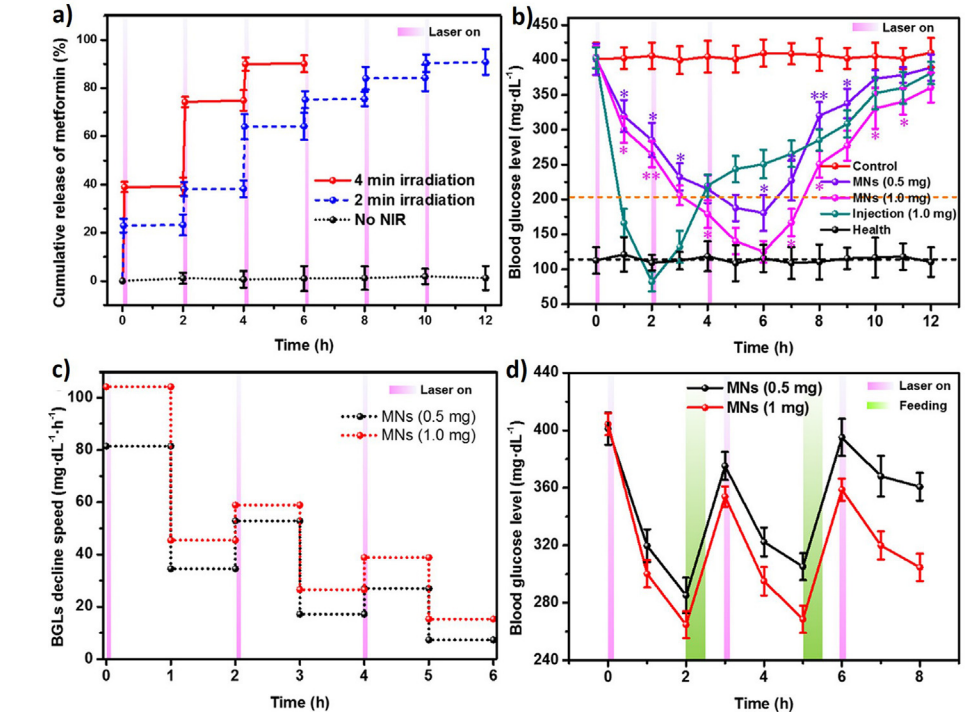




Please cite this article in press as: T. Bauleth-Ramos et al., Materials Today, (2023), https://doi.org/10.1016/j.mattod.2022.12.007

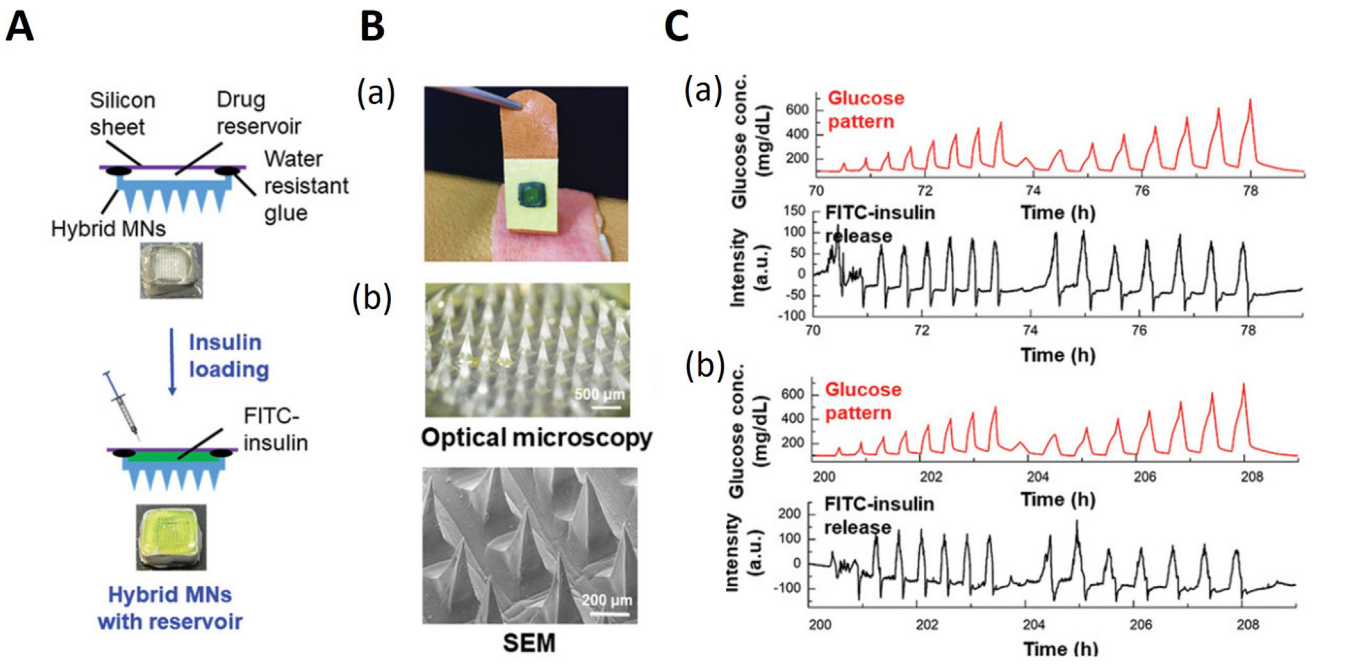


**FIGURE 26**

Glucose responsive MN patches for the delivery of insulin. (C) (A) Schematic of the system and how to reload it with insulin. (B) Image of the loaded patch ready to be administered; (c) Optical microscope image of the MN-array; (C) Glucose-responsive release of insulin: (a) over 76 h, with multiple fluctuations in the glucose concentration (between 100 and 400 mg/dL); (b) The glucose responsiveness is maintained also after reloading the patch with insulin, for a prolonged time frame (8 days). Adapted with permission from ref. [225]; Copyright 2019, John Wiley & Sons, Inc.

hypoxia-, or ROS-responsive release from the MNs. However, the systems developed so far are still suboptimal in the lag-time to respond to changes in glucose concentration, as well as the release of ROS at the site of injection. Boronic acid is a non-enzymatic alternative with excellent responsiveness to glucose concentration without releasing any toxic byproduct.

*Active/autonomous release*

The slow dermal diffusion of drugs after administration of MNs represents a hurdle for therapeutic regimens where a fast bolus administration of the payload is needed. On top of choosing a rapidly dissolving hydrophilic polymer as PVP, magnesium MPs can be added to the matrix of the MNs [226]. The magnesium MPs released $H_2$ bubbles when they entered into contact with the interstitial fluid, creating bubbles that helped pushing the payload through the dermis and achieving a complete release in 20 min, 15 min earlier than for a conventional PVP MNs. This superfast release can be combined with a slower sustained release through the engineering of customized molds preventing the mixing of solutions [226].

## Conclusions, challenges, translation to the clinics, and future perspectives

dMNs have gained significant attention due to the wide range of applications combined with painless application and the environmental compatibility of these devices. The formulation of dMNs needs to be carefully optimized in terms of materials and patch characteristics to achieve the target loading, stability, release rate and therapeutic application of the payload. The nature of the payload (*e.g.*, proteins and peptides or nucleic acids) strongly impacts the choice of materials available for the formulation, to ensure the conservation of the payload structure as well as long term stability in challenging storing conditions. The geometry of the needles should be tailored to the application, in terms of tissue and need for interlocking to prevent the incom-

**FIGURE 25**

Light-sensitive release of metformin from melting MNs. (A) The tips of the MNs are formulated with lauric acid (LA) and PCL. When the needles are irradiated with a NIR laser, the tips of the needles undergo a sequential melting with LA melting first, followed by PCL. The tips of the MNs are supported by a soluble PVA/PVP base. When administered to rats, the PVA/PVP base dissolves, leaving only the tips in the skin. The drug is then released by applying an NIR laser. Quantum dots (CU7S4 QD) are added to the formulation as photothermal agents to improve the conversion of light into heat and to ensure a homogeneous distribution of the heat in all the tips. (B) Laser irradiation-dependent pulsatile release of metformin from the MN-patches: (a) *In vitro* pulsatile release profile of metformin. The duration of the NIR irradiation at each pulse determines the time needed for the complete release of the drug and the amount of drug released after each pulse; (b) A blood glucose level of diabetic rats treated with MNs patches with two different dosages of metformin (0.5 or 1 mg), compared to hypodermic injection of the highest dose (1 mg) and in healthy rats. Each animal underwent three cycles of NIR irradiation for 4 min each; (c) Correlation between the decrease in the blood glucose levels associated with the release of metformin and the pulsatile release of the drug from the MNs; (d) The pulsatile release of the drug after the laser is able to counteract the increase in blood glucose levels determined by the feeding. Adapted and reprinted with permission from ref. [211]; Copyright 2018, American Chemical Society.



Please cite this article in press as: T. Bauleth-Ramos et al., Materials Today, (2023), https://doi.org/10.1016/j.mattod.2022.12.007

plete retention of the MNs in the tissue in problematic set of patients (*e.g.*, children). A patient compliant formulation requires easy and rapid administration and detachment of the MNs from the patch, with the optimization of the materials chosen for the backing layer or strategies to introduce fractures lines. Finally, the therapeutic mode of action of the payload requires tailored release rates, as in the case of glucose-responsive dMNs for the delivery of insulin. The release rate can be controlled through the choice of materials used for the fabrication of the dMNs or through resorting to stimuli-responsive features (*e.g.*, thermosensitive polymers, magnesium particles for burst release and diffusion in the epidermis).

The research on dMNs is expected to focus on the development of 3D-printed patches, with the possibility of experimenting with innovative geometries to achieve skin interlocking and the loading of the payload in precise regions of the MNs. Further development on the materials is expected to bring along increased options for the loading of sensible payloads and the control over the release rate.

dMNs have been successfully formulated for the delivery of vaccines, hormones, insulin, nano/microparticles, amongst others, with some patches evaluated in clinical trials. The lack of regulatory requirements is hindering the approval of any of these formulations. Donnelly analyzed the potential list of requirements from regulatory agencies for dMNs: the administration of microneedles will likely be regulated as injection and not as transdermal patch, thereby requiring sterility of the final product [227]. Further, the uniformity of dose and content needs to be tested at patch level and could be required also for the single microneedles, together with the analysis on the proposed package, its influence on the stability and storability of the MNs, and possible leakage of the packaging materials in the drug delivery system [228]. dMNs are considered as environment-friendly formulation because they are dissolvable and biodegradable; regulatory entities may require proofs of the easy disposal of the MNs, as well as data confirming the impossibility of reuse of the same patch by the same person or by different individuals [82,227,229]. Surveys of potential users, both patients and physicians, have brought forward the need for detailed instructions to be provided in the package for an easy and reliable self-application, as well as the need for an indicator to visually inform whether the administration has been successful [230,231]. Finally, the safety of repeated administrations of dMNs, the possible effects on the immune system, as well as the effects deriving from the deposition of polymer in the skin will need to be carefully evaluated in preclinical and clinical studies[227]: a transient erythema has been observed after administration of the microneedles with a complete resolution within 1 h after the administration [231]. dMNs are fabricated from polymers with high molecular weight to achieve the best mechanical properties while foregoing biocompatibility: such formulations may be accepted sporadically for use in vaccination, but may pose risks for more frequent dosing with more severe erythema, foreign body response, or accumulation of the polymer in the lymph nodes or at liver level [179,232]. Nevertheless, given the high demand for easy and patient friendly formulations, we expect to see a dMNs formulation on the market within the next 5 years.

## Data availability

Data will be made available on request.

## Declaration of Competing Interest

The authors declare that they have no known competing financial interests or personal relationships that could have appeared to influence the work reported in this paper.

## Acknowledgments

Dr. T. Bauleth-Ramos acknowledges financial from European Union's Horizon 2020 research and innovation program under the Marie Skłodowska-Curie grant agreement No 892758. Prof. H. A. Santos acknowledges financial support from the Academy of Finland (Decision no. 331151), Business Finland (Decision no. 1179/31/2020), and the UMCG Research Funds.

### References

[1] A. Tröls et al., Microfluid. Nanofluidics. 23 (2019) 1–5, https://doi.org/10.1007/s10404-019-2257-3.
[2] R.R. Wickett, M.O. Visscher, Am. J. Infect. Control 34 (2006) 98–110, https://doi.org/10.1016/j.ajic.2006.05.295.
[3] M. Schneider et al., Dermatoendocrinol. 1 (2009) 197–206.
[4] K. Ita, Biomed. Pharmacother. 93 (2017) 1116–1127, https://doi.org/10.1016/j.biopha.2017.07.019.
[5] A. Kumar, R. Bharti, S. Agarwal, J. Am. Acad. Dermatol. 81 (2019) e67–e69, https://doi.org/10.1016/j.jaad.2018.12.066.
[6] M. El-Domyati, H. Abdel-Wahab, A. Hossam, Int. J. Dermatol. 57 (2018) 1324–1334, https://doi.org/10.1111/ijd.14172.
[7] Y.C. Kim et al., J. Control. Release 142 (2010) 187–195, https://doi.org/10.1016/j.jconrel.2009.10.013.
[8] W. Martanto et al., Pharm. Res. 21 (2004) 947–952, https://doi.org/10.1023/B:PHAM.0000029282.44140.2e.
[9] R. Wang, W. Wang, Z. Li, Sensors (Switzerland) 16 (2016), https://doi.org/10.3390/s16101628.
[10] O. Khandan et al., Int. Conf. IEEE Eng. Med. Biol. Soc. 80045 (2012) 6572–6575.
[11] X. He et al., Dose-Response 17 (2019), https://doi.org/10.1177/1559325819878585.
[12] L.Y. Chu, S.O. Choi, M.R. Prausnitz, J. Pharm. Sci. 99 (2010) 4228–4238, https://doi.org/10.1002/jps.22140.
[13] E. Larrañeta et al., Mater. Sci. Eng. R Rep. 104 (2016) 1–32, https://doi.org/10.1016/j.mser.2016.03.001.
[14] J. Gupta et al., J. Control. Release 154 (2011) 148–155, https://doi.org/10.1016/j.jconrel.2011.05.021.
[15] K. Ita, Pharmaceutics. 7 (2015) 90–105, https://doi.org/10.3390/pharmaceutics7030090.
[16] R.R.S. Thakur et al., Transl. Res. 6 (2016) 800–815, https://doi.org/10.1007/s13346-016-0332-9.
[17] Y. Li et al., Eur. J. Pharm. Sci. 151 (2020), https://doi.org/10.1016/j.ejps.2020.105361 105361.
[18] P. Loaded et al., Viruses (2022).
[19] N. El-Sayed, L. Vaut, M. Schneider, Eur. J. Pharm. Biopharm. 154 (2020) 166–174, https://doi.org/10.1016/j.ejpb.2020.07.005.
[20] B. Bediz et al., Pharm. Res. 31 (2014) 117–135, https://doi.org/10.1007/s11095-013-1137-x.
[21] A. Hou et al., Adv. Healthc. Mater. 8 (2019) 1–11, https://doi.org/10.1002/adhm.201900898.
[22] S. Fakhraei Lahiji et al., Sci. Rep. 9 (2019) 1–9, https://doi.org/10.1038/s41598-019-44418-6.
[23] L.Y. Chu, M.R. Prausnitz, J. Control. Release 149 (2011) 242–249, https://doi.org/10.1016/j.jconrel.2010.10.033.
[24] C.R. Jung et al., Pharmaceutics. 12 (2020) 1–11, https://doi.org/10.3390/pharmaceutics12060581.
[25] H. Jun et al., RSC Adv. 8 (2018) 17786–17796, https://doi.org/10.1039/c8ra02334d.
[26] S. Wang et al., ACS Biomater Sci. Eng. 5 (2019) 1887–1894, https://doi.org/10.1021/acsbiomaterials.9b00229.
[27] G. Bonfante et al., Micro Nano Syst. Lett. 8 (2020), https://doi.org/10.1186/s40486-020-00113-0.



Please cite this article in press as: T. Bauleth-Ramos et al., Materials Today, (2023), https://doi.org/10.1016/j.mattod.2022.12.007

[28] S.A. Shah et al., Front. Immunol. 13 (2022) 1–12, https://doi.org/10.3389/fimmu.2022.843355.
[29] S.P. Davis et al., J. Biomech. 37 (2004) 1155–1163, https://doi.org/10.1016/j.jbiomech.2003.12.010.
[30] Y. Kim et al., Biomed. Microdevices 21 (2019) 1–9, https://doi.org/10.1007/s10544-019-0455-0.
[31] H. Du et al., ACS Appl. Mater. Interfaces 11 (2019) 43588–43598, https://doi.org/10.1021/acsami.9b15668.
[32] D.F.S. Fonseca et al., Mater. Sci. Eng. C 118 (2021), https://doi.org/10.1016/j.msec.2020.111350 111350.
[33] S.Y. Park et al., Mater. Sci. Eng. C 42 (2014) 757–762, https://doi.org/10.1016/j.msec.2014.06.021.
[34] M. Jang et al., Int. J. Cosmet. Sci. 42 (2020) 302–309, https://doi.org/10.1111/ics.12617.
[35] Y.H. Chiu, M.C. Chen, S.W. Wan, Biomacromolecules 19 (2018) 2278–2285, https://doi.org/10.1021/acs.biomac.8b00441.
[36] Z. Cheng et al., Transl. Res. 10 (2020) 1520–1530, https://doi.org/10.1007/s13346-020-00735-2.
[37] S. Liu et al., J. Control. Release 161 (2012) 933–941, https://doi.org/10.1016/j.jconrel.2012.05.030.
[38] Y. Hao et al., Adv. Ther. 1 (2018) 1–14, https://doi.org/10.1002/adtp.201800008.
[39] J. Zhu et al., Adv. Healthc. Mater. 8 (2019) 1–10, https://doi.org/10.1002/adhm.201900896.
[40] D. Wu et al., Biol. Pharm. Bull. 38 (2015) 365–373, https://doi.org/10.1248/bpb.b14-00502.
[41] P. González-Vázquez et al., J. Control. Release 265 (2017) 30–40, https://doi.org/10.1016/j.jconrel.2017.07.032.
[42] W. Yu et al., Mater. Sci. Eng. C 80 (2017) 187–196, https://doi.org/10.1016/j.msec.2017.05.143.
[43] I.C. Lee et al., RSC Adv. 7 (2017) 5067–5075, https://doi.org/10.1039/c6ra27476e.
[44] J. Mönkäre et al., J. Control. Release 218 (2015) 53–62, https://doi.org/10.1016/j.jconrel.2015.10.002.
[45] L.G. Tran, W.T. Park, Micro Nano Syst. Lett. 8 (2020) 4, https://doi.org/10.1186/s40486-020-00114-z.
[46] K.J. Koh et al., Sci. Rep. 8 (2018) 1–11, https://doi.org/10.1038/s41598-018-30290-3.
[47] Z. Shu et al., Drug Deliv. 27 (2020) 642–651, https://doi.org/10.1080/10717544.2020.1754524.
[48] Z. Li et al., J. Mater. Chem. B 8 (2020) 216–225, https://doi.org/10.1039/c9tb02061f.
[49] A. Ono et al., Pharmaceutics. 9 (2017) 1–13, https://doi.org/10.3390/pharmaceutics9030027.
[50] B.M. Lee et al., Pharmaceutics. 12 (2020), https://doi.org/10.3390/pharmaceutics12040366.
[51] S. Kim et al., J. Control. Release 316 (2019) 1–11, https://doi.org/10.1016/j.jconrel.2019.11.002.
[52] H.R. Jeong et al., Eur. J. Pharm. Biopharm. 127 (2018) 237–243, https://doi.org/10.1016/j.ejpb.2018.02.014.
[53] N.N. Aung et al., AAPS PharmSciTech 21 (2020) 1–13, https://doi.org/10.1208/s12249-019-1599-1.
[54] M.C. Chen et al., Biomacromolecules 13 (2012) 4022–4031, https://doi.org/10.1021/bm301293d.
[55] J. Chi et al., Bioact. Mater. 5 (2020) 253–259, https://doi.org/10.1016/j.bioactmat.2020.02.004.
[56] M.C. Chen et al., Biomaterials 34 (2013) 3077–3086, https://doi.org/10.1016/j.biomaterials.2012.12.041.
[57] Z. Ahmad et al., AAPS PharmSciTech 21 (2020) 1–12, https://doi.org/10.1208/s12249-019-1611-9.
[58] D.A. Castilla-Casadiego et al., Mater. Sci. Eng. C 118 (2021), https://doi.org/10.1016/j.msec.2020.111544 111544.
[59] M.C. Chen et al., Acta Biomater. 65 (2018) 66–75, https://doi.org/10.1016/j.actbio.2017.11.004.
[60] M.Y. Chen et al., Anticancer Res. 37 (2017) 6791–6797, https://doi.org/10.21873/anticanres.12139.
[61] Y. Zhang et al., Mater. Sci. Eng. C 85 (2018) 18–26, https://doi.org/10.1016/j.msec.2017.12.006.
[62] Y.K. Demir, Z. Akan, O. Kerimoglu, PLoS One 8 (2013), https://doi.org/10.1371/journal.pone.0063819.
[63] Y. Zhang et al., ACS Appl. Bio Mater. 3 (2020) 8640–8649, https://doi.org/10.1021/acsabm.0c01042.
[64] M. Zhu et al., ACS Biomater. Sci. Eng. 6 (2020) 3422–3429, https://doi.org/10.1021/acsbiomaterials.0c00273.
[65] Z. Wang et al., Adv. Mater. 34 (2022), https://doi.org/10.1002/adma.202106606.
[66] J.A. Stinson et al., Vaccine 39 (2021) 5410–5421, https://doi.org/10.1016/j.vaccine.2021.07.064.
[67] H.X. Nguyen et al., Eur. J. Pharm. Biopharm. 129 (2018) 88–103, https://doi.org/10.1016/j.ejpb.2018.05.017.
[68] I.C. Lee et al., J. Mater. Chem. B 3 (2015) 276–285, https://doi.org/10.1039/c4tb01555j.
[69] J. Zhao et al., J. Innov. Opt. Health Sci. 11 (2018) 1–12, https://doi.org/10.1142/S1793545818500323.
[70] L.K. Vora et al., J. Interdiscip. Nanomedicine. 3 (2018) 89–101, https://doi.org/10.1002/jin2.41.
[71] Y. Cao et al., J. Drug Deliv. Sci. Technol. 35 (2016) 1–7, https://doi.org/10.1016/j.jddst.2016.06.007.
[72] M.R. Prausnitz, Annu. Rev. Chem. Biomol. Eng. 8 (2017) 177–200, https://doi.org/10.1146/annurev-chembioeng.
[73] H. Amani et al., J. Control. Release 330 (2021) 185–217, https://doi.org/10.1016/j.jconrel.2020.12.019.
[74] G. Yao et al., Int. J. Pharm. 534 (2017) 378–386, https://doi.org/10.1016/j.ijpharm.2017.10.035.
[75] M.R. Prausnitz, Annu. Rev. Chem. Biomol. Eng. 8 (2017) 177–200, https://doi.org/10.1146/annurev-chembioeng-060816-101514.
[76] Q.L. Wang et al., Sci. Rep. 6 (2016) 1–11, https://doi.org/10.1038/srep38755.
[77] P. Yang et al., Acta Biomater. 104 (2020) 147–157, https://doi.org/10.1016/j.actbio.2019.12.037.
[78] A.H. Sabri et al., Adv. Drug Deliv. Rev. 153 (2020) 195–215, https://doi.org/10.1016/j.addr.2019.10.004.
[79] R.F. Donnelly et al., Drug Dev. Ind. Pharm. 35 (2009) 1242–1254, https://doi.org/10.1080/03639040902882280.
[80] L.Y. Chu et al., Pharm. Res. 33 (2016) 868–878, https://doi.org/10.1007/s11095-015-1833-9.
[81] M.J. Mistilis, A.S. Bommarius, M.R. Prausnitz, J. Pharm. Sci. 104 (2015) 740–749, https://doi.org/10.1002/jps.24283.
[82] A.J. Paredes et al., Adv. Funct. Mater. 31 (2021), https://doi.org/10.1002/adfm.202005792.
[83] H.D. Williams et al., Pharmacol. Rev. 65 (2013) 315–499, https://doi.org/10.1124/pr.112.005660.
[84] A. Fahr, X. Liu, Expert Opin. Drug Deliv. 4 (2007) 403–416, https://doi.org/10.1517/17425247.4.4.403.
[85] M.W. Shaw, Annu. Rev. Med. 21 (1970) 409–432, https://doi.org/10.1146/annurev.me.21.020170.002205.
[86] M. Dangol et al., J. Control. Release 223 (2016) 118–125, https://doi.org/10.1016/j.jconrel.2015.12.038.
[87] M. Chen et al., J. Control. Release 325 (2020) 163–175, https://doi.org/10.1016/j.jconrel.2020.06.039.
[88] F. Fontana et al., Small Methods 2 (2018) 1700347, https://doi.org/10.1002/smtd.201700347.
[89] T. Bauleth-Ramos et al., Adv. Funct. Mater. 27 (2017), https://doi.org/10.1002/adfm.201703303.
[90] M. Fusciello et al., Nat. Commun. 10 (2019) 1–13, https://doi.org/10.1038/s41467-019-13744-8.
[91] P. Figueiredo et al., The emerging role of multifunctional theranostic materials in cancer nanomedicine, Elsevier Inc., 2018. https://doi.org/10.1016/B978-0-12-813339-2.00001-3.
[92] L. Sercombe et al., Front. Pharmacol. 6 (2015) 1–13, https://doi.org/10.3389/fphar.2015.00286.
[93] B. García-Pinel et al., Nanomaterials 9 (2019) 1–23, https://doi.org/10.3390/nano9040638.
[94] B. Ozpolat, A.K. Sood, G. Lopez-Berestein, Adv. Drug Deliv. Rev. 66 (2014) 110–116, https://doi.org/10.1016/j.addr.2013.12.008.
[95] C. Vauthier, K. Bouchemal, Pharm. Res. 26 (2009) 1025–1058, https://doi.org/10.1007/s11095-008-9800-3.
[96] L.K. Vora et al., J. Control. Release 265 (2017) 93–101, https://doi.org/10.1016/j.jconrel.2017.10.005.
[97] E. Larrañeta et al., Int. J. Pharm. 472 (2014) 65–73, https://doi.org/10.1016/j.ijpharm.2014.05.042.
[98] C. Bao et al., Adv. Funct. Mater. 31 (2021), https://doi.org/10.1002/adfm.202011130.
[99] Q. Jing et al., Biomaterials 278 (2021), https://doi.org/10.1016/j.biomaterials.2021.121142 121142.



Please cite this article in press as: T. Bauleth-Ramos et al., Materials Today, (2023), https://doi.org/10.1016/j.mattod.2022.12.007

[100] W. Qin et al., Theranostics. 10 (2020) 8179–8196, https://doi.org/10.7150/thno.44194.
[101] A.D. Permana et al., J. Control. Release 316 (2019) 34–52, https://doi.org/10.1016/j.jconrel.2019.10.004.
[102] X. Lan et al., ACS Appl. Mater. Interfaces 10 (2018) 33060–33069, https://doi.org/10.1021/acsami.8b12926.
[103] J. Zhang et al., Nanosuspension drug delivery system: preparation, characterization, postproduction processing, dosage form, and application, Elsevier Inc., 2017. https://doi.org/10.1016/b978-0-323-46143-6.00013-0.
[104] R.H. Müller, K. Peters, Int. J. Pharm. 160 (1998) 229–237, https://doi.org/10.1016/S0378-5173(97)00311-6.
[105] B.E. Rabinow, Nat. Rev. Drug Discov. 3 (2004) 785–796, https://doi.org/10.1038/nrd1494.
[106] M.M. Chogale, V.N. Ghodake, V.B. Patravale, Pharmaceutics. 8 (2016), https://doi.org/10.3390/pharmaceutics8030026.
[107] R.F. Donnelly, E. Larrañeta, Drug Discov. Today 23 (2018) 1026–1033, https://doi.org/10.1016/j.drudis.2017.10.013.
[108] M.T.C. Mc Crudden et al., Adv. Healthc. Mater. 8 (2019), https://doi.org/10.1002/adhm.201801510.
[109] A.D. Permana et al., Eur. J. Pharm. Biopharm. 154 (2020) 50–61, https://doi.org/10.1016/j.ejpb.2020.06.025.
[110] G.B. Romero, C.M. Keck, R.H. Müller, Int. J. Pharm. 501 (2016) 236–244, https://doi.org/10.1016/j.ijpharm.2015.11.047.
[111] F. Volpe-Zanutto et al., J. Control. Release 333 (2021) 298–315, https://doi.org/10.1016/j.jconrel.2021.03.036.
[112] A.D. Permana, M.T.C. McCrudden, R.F. Donnelly, Pharmaceutics. 11 (2019) 1–22, https://doi.org/10.3390/pharmaceutics11070346.
[113] I.A. Tekko et al., Eur. J. Pharm. Sci. 152 (2020), https://doi.org/10.1016/j.ejps.2020.105469 105469.
[114] S. Abdelghany et al., Pharmaceutics. 11 (2019), https://doi.org/10.3390/pharmaceutics11070308.
[115] P.S. Giffen et al., J. Pharm. Sci. 109 (2020) 1303–1311, https://doi.org/10.1016/j.xphs.2019.11.012.
[116] E.M.M. Del Valle, Process Biochem. 39 (2004) 1033–1046, https://doi.org/10.1016/S0032-9592(03)00258-9.
[117] J. Szejtli, J. Mater. Chem. 7 (1997) 575–587, https://doi.org/10.1039/a605235e.
[118] à. Haimhoffer et al., Sci. Pharm. 87 (2019), https://doi.org/10.3390/scipharm87040033.
[119] C. Muankaew, T. Loftsson, Basic Clin. Paharmacol. Toxicol. 122 (2018) 46–55, https://doi.org/10.1111/bcpt.12917.
[120] S. Lin et al., J. Control. Release 306 (2019) 69–82, https://doi.org/10.1016/j.jconrel.2019.05.038.
[121] X. Zhou et al., Adv. Healthc. Mater. 9 (2020) 1–12, https://doi.org/10.1002/adhm.202000527.
[122] H. Zhan et al., Eur. J. Pharm. Sci. 121 (2018) 330–337, https://doi.org/10.1016/j.ejps.2018.06.014.
[123] H. Yang et al., Pharmaceutics. 12 (2020) 1–13, https://doi.org/10.3390/pharmaceutics12111067.
[124] Y. Huang et al., J. Control. Release 343 (2022) 408–419, https://doi.org/10.1016/j.jconrel.2022.01.043.
[125] G. Du et al., J. Control. Release 336 (2021) 537–548, https://doi.org/10.1016/j.jconrel.2021.07.005.
[126] M. Abbasi et al., Pharmaceutics. 14 (2022), https://doi.org/10.3390/pharmaceutics14040879.
[127] S.F. Lahiji, M. Dangol, H. Jung, Sci. Rep. 5 (2015) 1–7, https://doi.org/10.1038/srep07914.
[128] C. Lee et al., Adv. Healthc. Mater. 7 (2018) 1–8, https://doi.org/10.1002/adhm.201701381.
[129] L. Zhang et al., Int. J. Pharm. 604 (2021), https://doi.org/10.1016/j.ijpharm.2021.120749 120749.
[130] D.S. Dimitrov, Methods Mol. Biol. 899 (2012) 1–26, https://doi.org/10.1007/978-1-61779-921-1.
[131] P.J. Carter, Exp. Cell Res. 317 (2011) 1261–1269, https://doi.org/10.1016/j.yexcr.2011.02.013.
[132] A. Panda et al., Int. J. Pharm. 593 (2021), https://doi.org/10.1016/j.ijpharm.2020.120104 120104.
[133] Y. Li et al., J. Mater. Chem. B 7 (2019) 6604–6611, https://doi.org/10.1039/c9tb01449g.
[134] Y. Wu et al., Drug Deliv. Transl. Res. (2022), https://doi.org/10.1007/s13346-022-01190-x.
[135] S. Liu et al., Vaccine 37 (2019) 3810–3819, https://doi.org/10.1016/j.vaccine.2019.05.055.
[136] L.R. Pires, I.R. Amado, J. Gaspar, Int. J. Pharm. 586 (2020), https://doi.org/10.1016/j.ijpharm.2020.119590 119590.
[137] S.J. Lee et al., PLoS One 14 (2019) 1–24, https://doi.org/10.1371/journal.pone.0220382.
[138] S. Hirobe et al., Biomaterials 57 (2015) 50–58, https://doi.org/10.1016/j.biomaterials.2015.04.007.
[139] C. Wang et al., Nano Lett. 16 (2016) 2334–2340, https://doi.org/10.1021/acs.nanolett.5b05030.
[140] Y. Ye et al., ACS Nano 10 (2016) 8956–8963, https://doi.org/10.1021/acsnano.6b04989.
[141] M. Zaric et al., ACS Nano 7 (2013) 2042–2055, https://doi.org/10.1021/nn304235j.
[142] A.F. Lima, I.R. Amado, L.R. Pires, New Administration Route (2020).
[143] J. Mönkäre et al., Eur. J. Pharm. Biopharm. 129 (2018) 111–121, https://doi.org/10.1016/j.ejpb.2018.05.031.
[144] Q. Guo et al., Appl. Mater. Today 24 (2021), https://doi.org/10.1016/j.apmt.2021.101110 101110.
[145] M.L. Crichton et al., Acta Biomater. 36 (2016) 186–194, https://doi.org/10.1016/j.actbio.2016.02.039.
[146] F. Chen et al., J. Control. Release 255 (2017) 36–44, https://doi.org/10.1016/j.jconrel.2017.03.397.
[147] S. Kim et al., Biomaterials 232 (2020), https://doi.org/10.1016/j.biomaterials.2019.119733 119733.
[148] J.P. Amorij et al., Vaccine 25 (2007) 6447–6457, https://doi.org/10.1016/j.vaccine.2007.06.054.
[149] Y.C. Kim et al., Pharm. Res. 28 (2011) 135–144, https://doi.org/10.1007/s11095-010-0134-6.
[150] H.K. Kim et al., Biomater. Sci. 6 (2018) 2566–2570, https://doi.org/10.1039/c8bm00768c.
[151] M.J. Mistilis et al., Transl. Res. 7 (2017) 195–205, https://doi.org/10.1007/s13346-016-0282-2.
[152] T. Waghule et al., Biomed. Pharmacother. 109 (2019) 1249–1258, https://doi.org/10.1016/j.biopha.2018.10.078.
[153] N.G. Rouphael et al., Lancet 390 (2017) (2015) 649–658, https://doi.org/10.1016/S0140-6736(17)30575-5.
[154] F.E. Pearson et al., PLoS One 8 (2013) 1–10, https://doi.org/10.1371/journal.pone.0067888.
[155] P.R. Lowenstein et al., Biochem. Soc. Trans. 27 (1999) 873–881, https://doi.org/10.1042/bst0270873.
[156] A. Fire et al., Nature 391 (1998) 806–811. https://www.nature.com/articles/35888.pdf.
[157] J. McCaffrey, R.F. Donnelly, H.O. McCarthy, Transl. Res. 5 (2015) 424–437, https://doi.org/10.1007/s13346-015-0243-1.
[158] T. Wang, J.R. Upponi, V.P. Torchilin, Int. J. Pharm. 427 (2012) 3–20, https://doi.org/10.1016/j.ijpharm.2011.07.013.
[159] M.K. Riley, W. Vermerris, Nanomaterials 7 (2017) 1–19, https://doi.org/10.3390/nano7050094.
[160] H.W. Yang et al., Adv. Healthc. Mater. 6 (2017) 1–7, https://doi.org/10.1002/adhm.201600750.
[161] M. Wang et al., Adv. Healthc. Mater. 9 (2020) 1–11, https://doi.org/10.1002/adhm.201900635.
[162] N.W. Kim et al., J. Control. Release 179 (2014) 11–17, https://doi.org/10.1016/j.jconrel.2014.01.016.
[163] H.O. Mccarthy et al., J. Control. Release 189 (2014) 141–149, https://doi.org/10.1016/j.jconrel.2014.06.048.
[164] R. Bennett et al., Nanomedicine 10 (2015) 2989–3001, https://doi.org/10.2217/nnm.15.115.
[165] A.A. Ali et al., Biol. Med. 13 (2017) 921–932, https://doi.org/10.1016/j.nano.2016.11.019.
[166] G. Cole et al., Hum. Vaccines Immunother. 13 (2017) 50–62, https://doi.org/10.1080/21645515.2016.1248008.
[167] J. McCaffrey et al., J. Control. Release 226 (2016) 238–247, https://doi.org/10.1016/j.jconrel.2016.02.023.
[168] G. Cole et al., Eur. J. Pharm. Biopharm. 127 (2018) 288–297, https://doi.org/10.1016/j.ejpb.2018.02.029.
[169] J.F. Liao et al., Theranostics. 7 (2017) 2593–2605, https://doi.org/10.7150/thno.19894.
[170] J. Yu et al., Acta Biomater. 148 (2022) 133–141, https://doi.org/10.1016/j.actbio.2022.06.015.



Please cite this article in press as: T. Bauleth-Ramos et al., Materials Today, (2023), https://doi.org/10.1016/j.mattod.2022.12.007

[171] K.K.L. Phua, K.W. Leong, S.K. Nair, J. Control. Release 166 (2013) 227–233, https://doi.org/10.1016/j.jconrel.2012.12.029.
[172] N. Sultana et al., Mol. Ther. 25 (2017) 1306–1315, https://doi.org/10.1016/j.ymthe.2017.03.016.
[173] S. Van Lint et al., Cancer Res. 72 (2012) 1661–1671, https://doi.org/10.1158/0008-5472.CAN-11-2957.
[174] V.D. Bui et al., Biomaterials 287 (2022), https://doi.org/10.1016/j.biomaterials.2022.121644 121644.
[175] X. Lan et al., Nanoscale 12 (2020) 18885–18898, https://doi.org/10.1039/d0nr04213g.
[176] M. Qu et al., Nanoscale 12 (2020) 16724–16729, https://doi.org/10.1039/d0nr02759f.
[177] Y. Wu et al., Biomater. Adv. 137 (2022), https://doi.org/10.1016/j.bioadv.2022.212767.
[178] Y. Ito et al., Int. J. Pharm. 407 (2011) 126–131, https://doi.org/10.1016/j.ijpharm.2011.01.039.
[179] H.L. Quinn et al., J. Pharm. Sci. 104 (2015) 3490–3500, https://doi.org/10.1002/jps.24563.
[180] S. Cao et al., J. Control. Release 329 (2021) 1–15, https://doi.org/10.1016/j.jconrel.2020.11.038.
[181] Q. Jing et al., Biomaterials 278 (2021), https://doi.org/10.1016/j.biomaterials.2021.121142 121142.
[182] I.C. Lee et al., J. Biomed. Mater. Res. - Part A 105 (2017) 84–93, https://doi.org/10.1002/jbm.a.35869.
[183] M.C. Chen, M.H. Ling, S.J. Kusuma, Acta Biomater. 24 (2015) 106–116, https://doi.org/10.1016/j.actbio.2015.06.021.
[184] S. Zhu et al., J. Drug Deliv. Sci. Technol. 62 (2021), https://doi.org/10.1016/j.jddst.2021.102336 102336.
[185] K. Braz Gomes et al., Int. J. Pharm. 613 (2022), https://doi.org/10.1016/j.ijpharm.2021.121393 121393.
[186] L. Long et al., Nanoscale 14 (2022) 1285–1295, https://doi.org/10.1039/D1NR07708B.
[187] Y. Chen et al., Biomater. Sci. 10 (2022) 2409–2416, https://doi.org/10.1039/D2BM00281G.
[188] Q. Yan et al., Vaccine 36 (2018) 4471–4476, https://doi.org/10.1016/j.vaccine.2018.06.025.
[189] J. Coyne et al., ACS Biomater Sci. Eng. 3 (2017) 3395–3403, https://doi.org/10.1021/acsbiomaterials.7b00718.
[190] R. Jamaledin et al., Adv. Ther. 3 (2020) 1–27, https://doi.org/10.1002/adtp.202000171.
[191] J. Chen et al., AAPS PharmSciTech 19 (2018) 1141–1151, https://doi.org/10.1208/s12249-017-0926-7.
[192] C. Tas et al., J. Control. Release 268 (2017) 159–165, https://doi.org/10.1016/j.jconrel.2017.10.021.
[193] G. Du, X. Sun, Pharm. Front. 02 (2020) e11–e22, https://doi.org/10.1055/s-0040-1701435.
[194] M. Leone et al., Eur. J. Pharm. Sci. 146 (2020), https://doi.org/10.1016/j.ejps.2020.105269 105269.
[195] M. Mir et al., Eur. J. Pharm. Biopharm. 147 (2020) 57–68, https://doi.org/10.1016/j.ejpb.2019.12.008.
[196] A. Ramalheiro et al., Int. J. Pharm. 591 (2020), https://doi.org/10.1016/j.ijpharm.2020.119942 119942.
[197] J.M. Mazzara et al., Bioeng. Transl. Med. 4 (2019) 116–128, https://doi.org/10.1002/btm2.10103.
[198] P.K. Srivastava, H.P. Thakkar, Eur. J. Pharm. Biopharm. 156 (2020) 176–190, https://doi.org/10.1016/j.ejpb.2020.09.006.
[199] N.W. Kim et al., ACS Nano 12 (2018) 9702–9713, https://doi.org/10.1021/acsnano.8b04146.
[200] X. Zhao et al., Polymers (Basel) 12 (2020), https://doi.org/10.3390/polym12010059.
[201] W. Li et al., Nat. Biomed. Eng. 3 (2019) 220–229, https://doi.org/10.1038/s41551-018-0337-4.
[202] Z. Yin et al., Int. J. Biol. Macromol. 106 (2018) 48–56, https://doi.org/10.1016/j.ijbiomac.2017.07.178.
[203] M.C. Kearney et al., Eur. J. Pharm. Biopharm. 103 (2016) 43–50, https://doi.org/10.1016/j.ejpb.2016.03.026.
[204] B.Z. Chen et al., Macromol. Rapid Commun. 39 (2018) 1–6, https://doi.org/10.1002/marc.201800075.
[205] Y. He et al., Physiol. Behav. 176 (2017) 139–148, https://doi.org/10.1021/acsnano.8b05373.Synthetic.
[206] X. Li et al., J. Control. Release 314 (2019) 72–80, https://doi.org/10.1016/j.jconrel.2019.10.016.
[207] H.T.T. Duong et al., Biomaterials 185 (2018) 13–24, https://doi.org/10.1016/j.biomaterials.2018.09.008.
[208] Y. He et al., ACS Nano 12 (2018) 10272–10280, https://doi.org/10.1021/acsnano.8b05373.
[209] Y. Hao et al., ACS Appl. Mater. Interfaces 9 (2017) 15317–15327, https://doi.org/10.1021/acsami.7b03604.
[210] J. Yang et al., Chem. Eng. J. 426 (2021), https://doi.org/10.1016/j.cej.2021.130561 130561.
[211] Y. Zhang et al., ACS Biomater Sci. Eng. 4 (2018) 2879–2888, https://doi.org/10.1021/acsbiomaterials.8b00642.
[212] M.C. Chen, Z.W. Lin, M.H. Ling, ACS Nano 10 (2016) 93–101, https://doi.org/10.1021/acsnano.5b05043.
[213] Y. Ye et al., Sci. Immunol. 2 (2017) 1–13. http://immunology.sciencemag.org/content/immunology/suppl/2017/11/07/2.17.eaan5692.DC1/aan5692_SM.pdf.
[214] Y. Zhang et al., Int. J. Polym. Mater. Polym. Biomater. 68 (2019) 850–858, https://doi.org/10.1080/00914037.2018.1517347.
[215] H. Chang et al., Nat. Biomed. Eng. 5 (2021) 1008–1018, https://doi.org/10.1038/s41551-021-00720-1.
[216] I.J. Choi et al., J. Control. Release 286 (2018) 460–466, https://doi.org/10.1016/j.jconrel.2018.08.017.
[217] X. Ning et al., ACS Appl. Polym. Mater. 3 (2021) 6502–6512, https://doi.org/10.1021/acsapm.1c01219.
[218] P. Wei, E.J. Cornel, J. Du, Transl. Res. 11 (2021) 1323–1339, https://doi.org/10.1007/s13346-021-00963-0.
[219] Y. Yang et al., SLAS Technol. 26 (2021) 660–666, https://doi.org/10.1177/24726303211024568.
[220] M. Bok et al., Sci. Rep. 10 (2020) 1–10, https://doi.org/10.1038/s41598-020-58822-w.
[221] J. Yu et al., PNAS 112 (2015) 8260–8265, https://doi.org/10.1073/pnas.1505405112.
[222] F.Q. Luo et al., Nano Res. 14 (2021) 2689–2696, https://doi.org/10.1007/s12274-020-3273-z.
[223] J. Wang et al., ACS Nano 12 (2018) 2466–2473, https://doi.org/10.1021/acsnano.7b08152.
[224] Y. Ye et al., Adv. Mater. 28 (2016) 3115–3121, https://doi.org/10.1002/adma.201506025.
[225] S. Chen et al., Adv. Funct. Mater. 29 (2019), https://doi.org/10.1002/adfm.201807369.
[226] M.A. Lopez-Ramirez et al., Adv. Mater. 32 (2020), https://doi.org/10.1002/adma.201905740.
[227] R.F. Donnelly, in: Microneedles Drug Vaccine Deliv. Patient Monit., 2018, pp. 307–322. https://doi.org/10.1002/9781119305101.ch11.
[228] E. McAlister et al., Transl. Res. 11 (2021) 2169–2185, https://doi.org/10.1007/s13346-020-00883-5.
[229] A.R.J. Hutton et al., J. Pharm. Sci. 000 (2022) 1–15, https://doi.org/10.1016/j.xphs.2022.08.027.
[230] K. Moffatt et al., Transl. Res. 11 (2021) 1199–1217, https://doi.org/10.1007/s13346-020-00848-8.
[231] A. Ripolin et al., Int. J. Pharm. 521 (2017) 92–101, https://doi.org/10.1016/j.ijpharm.2017.02.011.
[232] L.K. Vora et al., Int. J. Biol. Macromol. 146 (2020) 290–298, https://doi.org/10.1016/j.ijbiomac.2019.12.184.



Please cite this article in press as: T. Bauleth-Ramos et al., Materials Today, (2023), https://doi.org/10.1016/j.mattod.2022.12.007